



**Calhoun: The NPS Institutional Archive**  
**DSpace Repository**

---

Theses and Dissertations

1. Thesis and Dissertation Collection, all items

---

1970

## Impact resistance of ferro-cement plates.

Key, William H.

Massachusetts Institute of Technology

---

<http://hdl.handle.net/10945/15034>

---

*Downloaded from NPS Archive: Calhoun*



Calhoun is the Naval Postgraduate School's public access digital repository for research materials and institutional publications created by the NPS community. Calhoun is named for Professor of Mathematics Guy K. Calhoun, NPS's first appointed -- and published -- scholarly author.

**Dudley Knox Library / Naval Postgraduate School**  
**411 Dyer Road / 1 University Circle**  
**Monterey, California USA 93943**

<http://www.nps.edu/library>

IMPACT RESISTANCE OF FERRO-CEMENT  
PLATES

William H. Key



IMPACT RESISTANCE OF FERRO-CEMENT PLATES

By

LT. WILLIAM H. KEY, JR., USN

Submitted in Partial Fulfillment of the Requirements  
For the Degree of Naval Engineer and For the Degree  
of Master of Science in Marine Engineering

at the

Massachusetts Institute of Technology

May 1970



Handwritten text at the top of the page, possibly a title or header.

A horizontal line spanning the width of the page, likely a section separator.

TITLE: Impact Resistance of Ferro-cement Plates

AUTHOR: Lt. William H. Key, Jr., USN

Submitted to the Department of Naval  
Architecture and Marine Engineering on  
May 21, 1970 in partial fulfillment of  
the requirements for the degrees of Naval  
Engineer and Master of Science in Marine  
Engineering.

The experimental findings for impact resistance of square ferro-cement plates 0.5 inches thick are related to experimental findings for tensile tests of identically composed rectangular tensile specimens. The mechanism of failure of ferro-cement in tension is explored in depth considering research now in progress. Conclusions are obtained from tensile investigation, and are compared with the results of impact tests to determine if a correlation can be made between the performance of ferro-cement under both types of loadings.

Thesis Supervisor: Surendra P. Shah, Visiting Associate Professor  
of Civil Engineering, Massachusetts Institute  
of Technology.



ACKNOWLEDGMENT

The author is indebted to Professor S.P. Shah for his guidance, which made this project possible. The author further wishes to thank Arthur Rudolph for his helpful advice, without which the project could not have been completed.



## TABLE OF CONTENTS

	Page
Title Page	1
Abstract	2
Acknowledgment	3
Contents	4
List of Figures	6
List of Tables	9
I. Introduction	10
II. Characteristics of Ferro-cement	19
A. Cost	19
B. Construction Techniques	21
C. Maintenance	22
D. Durability	23
E. Disadvantages	23
F. Design Information	24
III. Characteristics of Reinforcement	25
IV. Present Concepts	28
V. Impact	33
A. Background	33
B. Impact Failure Criteria	43
C. Impact Mechanism in Plates	45
D. Impact Spalling	47
VI. Scope of the Present Investigation	48
VII. Experimental Procedure	50
A. Tensile Phase	50



	Page
B. Impact Phase	55
C. Composition of the Samples	58
D. Designation of Samples	59
VIII. Apparatus	60
A. Tensile Tests	60
B. Impact Tests	63
IX. Testing Procedures	77
A. Tensile Tests	77
B. Impact Tests	81
X. Experimental Results	83
XI. Discussion of Results	84
A. Tensile Tests	84
B. Impact Tests	103
XII. Conclusions	116
XIII. Recommendations	117
Selected Bibliography	118
Appendix A	126
Appendix B	146
Appendix C	182
Appendix D	189





## LIST OF FIGURES

- Figure 1. Lambot's original boat
2. Translation of notice
  3. Zeemeeuw at Amsterdam Zoo
  4. First Ferro-cement Vessel in U.S.
  5. Ocean Going Concrete Vessel
  6. Effect of Specific Surface on Stress at first crack by Naaman
  13. Permanent Deflection Curves by Kluge
  14. Crack Width resulting from impact loads by Kudrysevtsev
  15. Tensile Specimen
  16. Tensile Specimen mold
  17. Impact Specimen
  18. Impact Specimen mold
  19. Impact Testing Machine
  20. Impact Testing Machine
  21. Impact Striker
  22. Impact Receiver
  23. Spark Arc Schematic
  24. Striker Calibration Curve
  25. Receiver Calibration Curve



Figure 26. Aid to Determination of Energy

27. Water Test Device
28. Photograph of Water Test Device
29. Instron Error
30. Effect of Sand Surface Area on Ultimate composite load.
31. Effect of Sand/cement ratio on ultimate composite load.
32. Effect of light weight sand on ultimate composite load.
33. Effect of Specific Surface on Number of Cracks
34. Effect of Specific Surface on composite stress
35. Observed and Calculated Ultimate Stress of composite
36. Observed and Calculated Modulus of Elasticity of Reinforcement
37. Effect of Ultimate Load of Reinforcement on crack width after fracture
38. Effect of Ultimate Load of Reinforcement on composite stress at first crack.



## LIST OF TABLES

- Table 1. Comparative Cost of 100-ft. Scallop
2. Bare Hull Costs 100-ft Scallop
  3. Impact Test Results - Kluge
  4. Characteristics of Reinforced Concrete and  
Ferro-concrete Plates During the Impact Tests.
  5. Composition of Kelly and Mouat Samples.
  6. Panel Test - Impact - Kelly and Mouat
  7. Impact Damage Data - Collins
  8. Reinforcement Schedule
  9. Composition of Series 6-0-X
  10. Modulus of Elasticity of Tensile Specimens



## I. INTRODUCTION

### Historical Background

Ferro-cement in the general sense of the word indicates a material with a high percentage of reinforcement, imbedded in a cementuous matrix. The material usually contains by volume between five and eight percent steel.

This hybrid reinforced concrete has become increasingly important in the construction of small boats, with several firms producing boats at this time. The reasons for the increased importance of ferro-cement are numerous: the apparent low cost, apparent ease of fabrication, lack of maintenance, and durability. These factors immediately make the material desirable for the manufacture of small boats.

Ferro-cement is not new, although it has had other names; it is approximately the same material that was introduced in 1848 by a Frenchman, Joseph Louis Lambot. The ferro-cement boats that he built in 1848 and 1849 were still afloat in 1901. They were rediscovered in 1955 in the silt of a Provencal pond in France. Lambot's original boat is on display at Brignoles and the second boat is boxed in a warehouse in Paris.<sup>4</sup>





Experiments and tests over five years  
Bateau-Ciment  
Invented  
by M. LAMBOT-MIRAVAL  
owner of the Miraval Estate near Brignoles (Var).

This construction is eminently applicable for mill-boats, swimming schools, boats for washerwomen, barges, buoys, boats for coastal traffic, water cisterns, cellar doors, tubs for orange trees . . . in other words this is most applicable for all structures which tend to deteriorate where they stand whether in or out of water.

All kinds of cements can be used indiscriminately either separately or at the same time, depending on whether one wishes to obtain structures of great durability or lightness of elasticity or incombustibility.

Please apply to the inventor for more details.

N.B. One can see on the little lake of the Miraval Estate (Var), a cement boat built five years ago which has resisted violent shocks and needed no kind of repair nor maintenance. Also one can see water cisterns and orange-tree boxes which fulfil the conditions of the earlier notice.



those made today about ferro-cement. The translation of the notice which he exhibited beside his boat at the Paris International Exhibition in 1855 shows his line of reasoning and provides interesting reading.<sup>50</sup> See figure 2.

In 1887, A.A. Boon constructed in Holland a similar boat of wire mesh and mortar construction. His scow Zeemeeuw has been in regular service since constructed and reportedly is still in regular use at the Amsterdam Zoo. Figure 3 is a photograph of the Zeemeeuw as taken

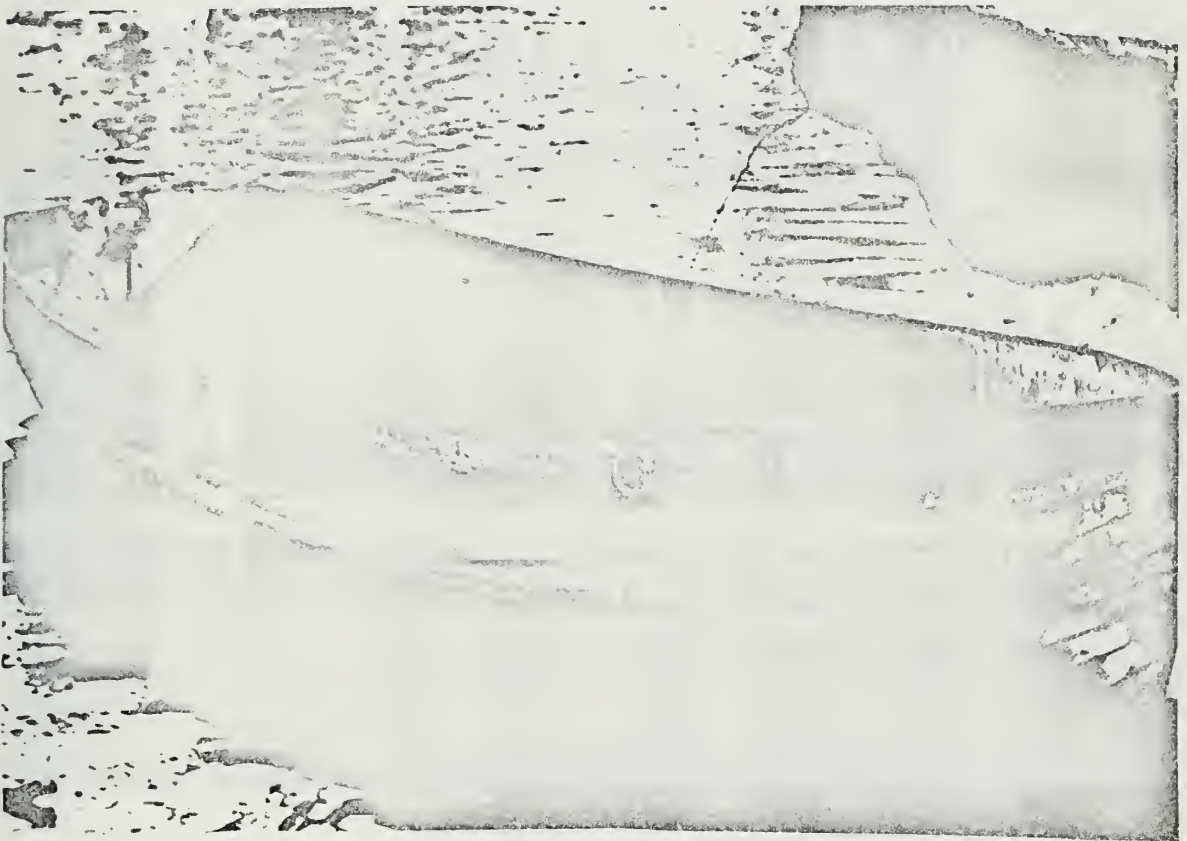


FIGURE 3



at the Amsterdam Zoo in 1966 by B.J. de Ruiker.<sup>49</sup>

In Italy in 1943, Pier Luigi Nervi started what can be considered modern day ferro-cement when he built three 150-ton transport vessels for the Italian Navy. He also built a 400-ton mortar vessel with a reinforced concrete frame and a ferro-cement hull. Nervi used anywhere up to eight layers of mesh reinforcement, with diameters ranging from 0.02 to 0.06 inches in a 3/8 inch square mesh with weight ranging between 0.4 and 0.1 lb/ft<sup>2</sup>.

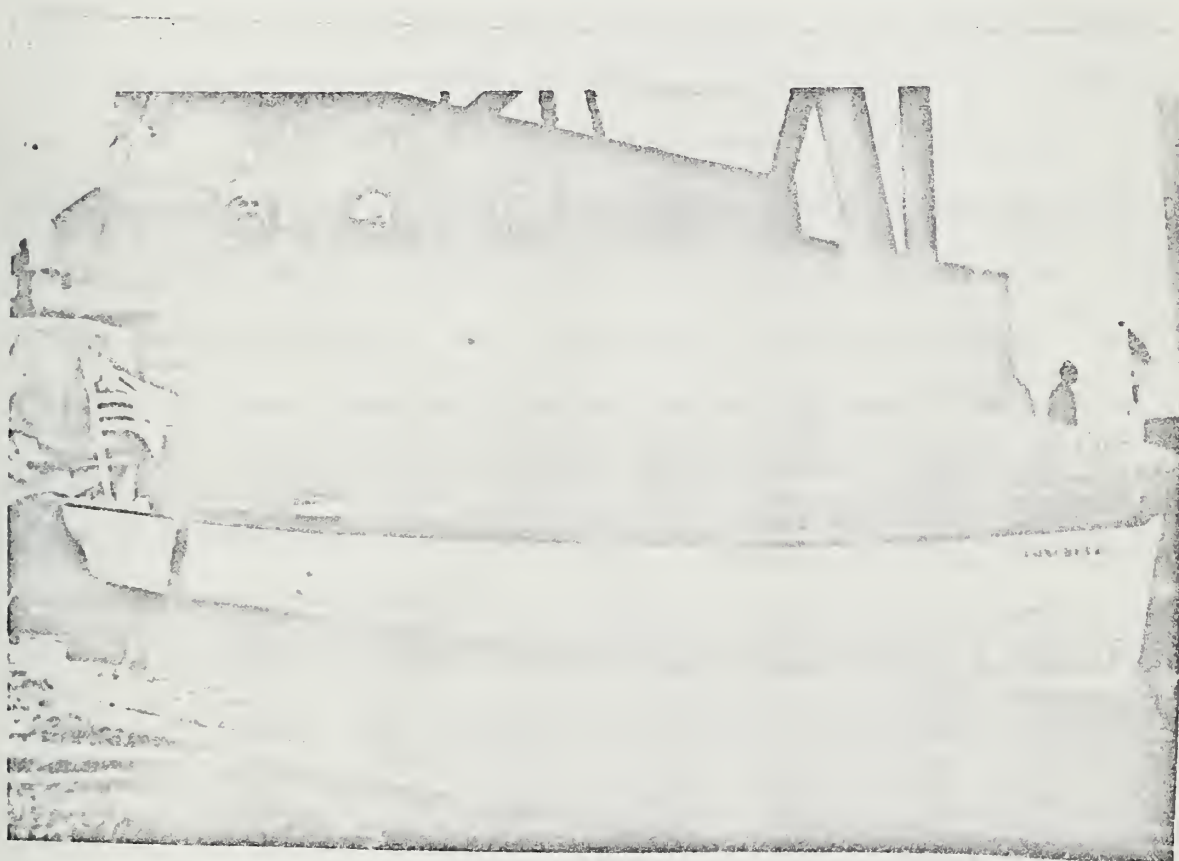


FIGURE 4



He placed between the layers of mesh one or more layers of 1/4 inch to 3/8 inch diameter reinforcing bar. His own ketch, Nanelle, was constructed with a hull thickness of 1/2 to 5/8 inches throughout most of the hull. The hull reinforcement was composed of seven layers of mesh with 1/4 inch reinforcing bars on 2-inch centers placed in a longitudinal direction.<sup>29 30 62</sup>

Ferro-cement construction of vessels in the United States is considered to have begun in 1911 when some Naval Reservists constructed the boat shown in Figure 4. The boat was 18 feet, 6 inches long, 6 feet, 6 inches in beam, and 3 feet, 2 inches in depth, with a shell thickness of 3/4 inches. The reinforcement used was 1/4 inch square mesh covering ribs of 12-gauge steel flats. The ribs were riveted to the T-bar keel every 12 inches. Two layers of mesh were used below the waterline. The mortar was hand plastered in a single fifteen-hour operation. The boat was very successful and achieved 10 mph with a 6-horsepower engine.<sup>49</sup>

Many countries have experimented with reinforced concrete ships, the earliest reported reinforced concrete ship being the 356-ton Namsenfjord, launched in Norway in





August 1917. Great Britain launched in March 1919 the 1150-ton Armistice.<sup>28</sup>

The United States participated in reinforced concrete construction programs in both World War I and World War II. The Emergency Fleet Corporation in 1918 built approximately 16.7 million tons of seagoing reinforced concrete barges and ships. The Maritime Commission constructed 80 seagoing barges and 25

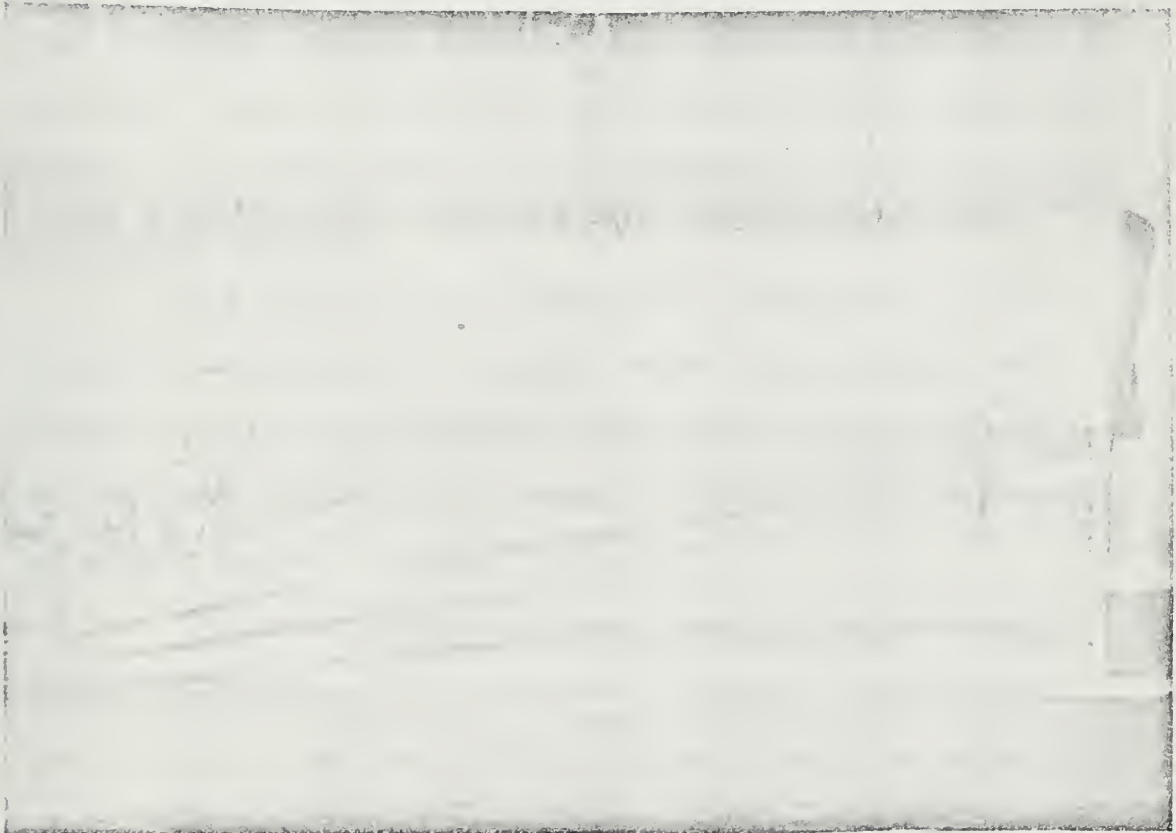


FIGURE 5



self-propelled reinforced concrete ships which were used throughout World War II. The deadweight tonnage available in concrete ships and barges constructed in World War II was roughly approximate to the capacity of 46 Liberty ships. The ships and barges were all approximately 365 feet long, 54 foot beam, and 35 feet in depth, displacing between 11,000 and 13,000 tons. Figure 5 shows one of the concrete ships underway.<sup>67</sup>

The decision to use concrete came as a result of growing world tension in 1941 and the realization that the available supply of steel plates and shapes would be severely taxed. Of the two alternate building materials, wood or concrete, concrete was considered more feasible for large vessels.

The program was considered successful, for the vessels performed as designed, with few problems. They showed little deterioration during the course of the war and several can still be found in the floating breakwater at Powell River, British Columbia.<sup>28</sup>

There is great interest today in ferro-cement, generally centered in Australia, England, New Zealand, the U.S.S.R., and the United States. With the exception of the U.S.S.R., most countries have focused their interest upon small boats, generally under 60 feet. The



Soviets, who have continually been interested in reinforced concrete vessels for their inland waters, have also investigated the use of ferro-cement in larger commercial vessels. They have done considerable research into the performance of ferro-cement in regard to load capacity and cracking.



## II. CHARACTERISTICS OF FERRO-CEMENT

Ferro-cement, although hailed as everything imaginable depending upon who is trying to sell what, does have limitations. The advantages and limitations must be skilfully balanced as the design requires to give the optimum possible performance.

### A. COST

The universal claim that ferro-cement saves 20-40% in cost is inaccurate. When all costs, labor, material, etc., are considered, savings are generally in the 3 to 5% range. The materials prove to be more expensive than anticipated at first glance. Wire mesh screening when purchased from a wholesale agent costs generally in the vicinity of \$1.00 a pound. Purchased directly from the factory, the cost runs about \$.50 a pound. Compare this to structural steel or rolled plate at \$.08 to \$.14 a pound. Table I compares costs of five different building materials: <sup>19</sup>

Steel	\$122,400
Aluminum	165,202
Wood	129,821
Fiber reinforced plastic	175,379
Ferro-cement	108,075
Comparative Cost of 100-foot scalloper (includes 10% profit)	

Table I





Construction of ferro-cement vessels does not require expensive building equipment. The construction procedure is relatively simple and can be handled by amateurs. Any high quality production of ferro-cement hulls will, however, require at least as much equipment as for a plastic hull.

Fabrication of ferro-cement vessels will remain a critical area until a fabrication technique is developed which is applicable to production methods. High labor requirements will prevent ferro-cement from being substantially more competitive than other materials. In Table II, which shows the cost breakdown for a hand laid-up ferro-cement basic hull, it can be seen that direct labor cost is approximately 1/3 the total cost of the hull.<sup>31</sup>

Material	\$ 22,352
Direct labor	33,030
Miscellaneous	11,010
Overhead	30,828
Subtotal	97,220
Total cost (including 10% profit)	104,000

Bare Hull Costs 100-foot scalloper in ferro-cement  
Hand application of mortar

Table II



## B. CONSTRUCTION TECHNIQUES

Construction techniques in use today fall into three classes. The first, the "free-standing" or bent pipe frame method, utilizes iron pipe frames bent to shape with longitudinal steel rods run on the outside of the frames. Wire mesh is laid over the framework and the concrete is plastered on from both sides. The advantage of this method is that it enables one to plaster from both sides, eliminating the possibility of voids in the concrete.

The second, or wood mold method, employs a wooden mold in the form of the vessel's hull. The reinforcing rods and mesh are laid over the mold and the mortar applied. There are two variations of this method, one in which the mold is completely removed upon completion, and the second in which planking is laid on temporary frames with the reinforcing rod and mesh placed over the planking. The wooden hull liner remains after completion of the vessel. The main disadvantage of both these methods is that it is impossible to plaster from both sides. The removable mold method allows filling of voids after the removal of the mold, but the wooden liner method prevents the filling of the voids. In some cases, builders have had to rip out the wooden liner in order to stop leakage.

A corporation in California uses a unique variation of the above methods. A female mold is utilized and the concrete lay-up proceeds in similar fashion to that of fiberglass. An initial coat of cement is sprayed on to the mold and a layer of reinforcing laid



on top of it. The first layer is followed by successive layers of concrete and reinforcing until the desired wall thickness is achieved.

Of the methods described, only the last, which approaches fiberglass technique, is at all applicable to production methods. The main disadvantage of this method is that optimum wall thickness is difficult to achieve. The other methods use some variation of manually joining or tying the reinforcement together. It is the fabrication of the reinforcement which consumes a majority of the direct labor requirement. Variations of methods of hand tying or welding the reinforcement together include stapling or nailing to the mold or using a hand crimping tool in the free-standing method.

#### C. MAINTENANCE

Maintenance is necessary for any vessel regardless of its construction material. When compared with steel or wood, ferro-cement has low maintenance requirements. However, when compared to reinforced plastics, ferro-cement is about equal. There is little data on the long-term effect of low maintenance and there could possibly be adverse results from a lack of maintenance. Literature recommends sealing the surface with epoxy to prevent seepage and corrosion. If this is necessary to prevent corrosion and is not done, the light mesh used in the hull may corrode to a low level of strength, with ensuing failure.



#### D. DURABILITY

Lambot's boats, over 100 years old, still exist and the Zeemeauw is still in use in Amsterdam,<sup>4</sup> having been built in 1878. However, it must be realized that all such quoted cases are isolated instances, and sufficient data does not exist to show conclusively the durability of this type of vessel.

Available literature does not indicate excessive deterioration on vessels built within ten to fifteen years. The author personally inspected a 30-foot ferro-cement sailboat which has been weathering on a cradle since 1960, after one year of use, and other than minor cracks on the flat transom caused by vandals, the hull is in perfect condition. The wooden deckhouse is badly deteriorated, as would be expected.

#### E. DISADVANTAGES

The principal disadvantage of cement is the low strength to weight ratio for a vessel of equal strength capacity. Excessive use of concrete over the minimum required causes the strength to weight ratio to decrease greatly. Ferro-cement, if properly constructed, has a competitive strength to weight ratio when considering vessels over fifty feet.

A second disadvantage is that once the vessel is completed, modifications are difficult, if not impossible, to accomplish. It is generally extremely difficult to predict the nature of future use of a vessel over its lifetime, so a limitation of this type will impose





stringent design requirements on the Naval Architect.

Production quality control will be difficult and expensive, but necessary because of the catastrophic nature of a hull failure.

#### F. DESIGN INFORMATION

Information on the design of ferro-cement is not accessible, if indeed it exists, and there is no evidence of understanding the mechanisms involved with ferro-cement. To date there has been little systematic investigation into the problem, with the result that most information available is unreliable and unreproducible. There are several companies which specialize in ferro-cement construction, but which have not shown a clear understanding of the mechanisms necessary for proper design. Information provided by these companies is sketchy and does not correlate well. Apparently, every boat-builder has his "secret" formula and design data which he is not willing to disclose for proprietary reasons.

Design techniques for ferro-cement have been hampered by this lack of accurate and reliable design information. In consequence, all design techniques have followed that of conventional reinforced concrete even though there are indications that ferro-cement performs in a different manner from that of reinforced concrete.

Vasta<sup>6</sup> indicates that on the 385-foot concrete ships built during World War II, using conventional reinforced concrete design techniques, the calculated stresses were conservative and the structures performed better than anticipated. To date, no one has analyzed



a ferro-cement hull and compared the predicted stresses with observed stresses to provide a basis for design. Muhler<sup>4,9</sup> analyzed ferro-cement in bending using conventional reinforced design techniques and compared the results to observed laboratory results. He concluded that the behavior of ferro-cement in bending follows the normal load deflection curve for reinforced concrete.

It appears that reinforced concrete design techniques will provide a conservative design basis for ferro-cement vessels. In the future, with further studies, there will come a better understanding from an advanced knowledge of the material and the application of shell theory.

### III. CHARACTERISTICS OF REINFORCEMENT

There are five types of reinforcement used with ferro-cement: woven wire mesh, welded wire mesh, hexagonal chicken mesh, hexagonal mesh with a longitudinal wire usually referred to as sparrow netting, and plasters lathing.

Recommendations for the use of a specific type of reinforcement appear to vary with the reference. It is not obvious why different types of meshes are recommended, so to achieve a better understanding of the performance of the reinforcement, Naaman<sup>5,2</sup>, Key<sup>3,6</sup> and Nelson<sup>5,6</sup> investigated the properties of woven mesh, hexagonal mesh, and sparrow netting. It was observed that certain mesh had peculiarities which, if not considered, could cause variations in observed results.



It was noted by Key<sup>36</sup> that woven wire mesh reinforcement has preferential directions of maximum strength as a result of the weaving process. The wire, which is longitudinal in the roll and is called the warp, is deformed in the weaving process to allow the shuttle to travel across with the woof or transverse wire. Both the woof and the warp take a permanent set, with the warp having the greater deformation. When tested in tension the warp failed at approximately ten to fifteen percent less stress than the woof, the apparent difference being a result of the excessive deformation of the warp caused by weaving.

Nagman<sup>52</sup> observed that the failure mechanism of the ferro-cement samples varied as a function of the angle,  $X$ , formed by the crossing of the woof and the warp. As the angle of the wire increases, and as uniaxial tension is applied, there is a perpendicular component of the normal force,  $T \sin X$ , which causes a splitting of the section into planes as determined by the layers of mesh. See Figure 6.



FIGURE 6

Consequently, for a constant mesh dimension, e.g., 1/4 inch by 1/4 inch, decreasing the gauge of the wire causes an increase in  $X$ , or alternately decreasing the mesh dimensions while holding the gauge constant also increases  $X$ . As was noted previously, the orientation of the woof and the warp in the sample affects the ultimate strength. It must





also be noted that there is a variation of  $X$  with the woof and the warp. In consequence of the weaving process,  $X$  was observed to be larger on the warp than on the woof.

Any investigation must take this into consideration because the 10-15% variance in ultimate strength and the splitting failure will not provide reproducible results.

Also noted by Key<sup>36</sup> and Naaman<sup>52</sup> was the effect of ultimate strength on the failure mode of tensile samples. Samples with low strength, ductile reinforcement showed a ductile failure where the mesh elongated and the mortar fell out. Samples with higher strength, low ductility reinforcement failed in a brittle fashion and all cracks observed before failure, except at the point of failure, closed up after failure so as to be almost invisible. Cracks that opened in the lower strength specimen remained open after failure.

It was observed additionally that wire mesh as is now obtained from manufacturers does not have constant properties. Normal usage of mesh does not require a knowledge of the properties of the mesh, so manufacturers do not attempt to produce mesh with known properties. Two rolls from the same manufacturer varied by 50,000 lb/in<sup>2</sup> in ultimate strength.

Nelson<sup>56</sup> noted that sparrow netting exhibited 2.5 times the ultimate strength of plain hexagonal netting. However, the types of mesh were from different manufacturers and it was impossible to test the wire used in the mesh, so no valid conclusions can be drawn from this investigation.





## IV. PRESENT CONCEPTS

The enthusiasm for ferro-cement appears to be based upon the fact that once the mean spacing between the reinforcing fibers approaches some critical distance  $d$ , the composite material exhibits properties other than those of reinforced concrete. Romualdi and Batson<sup>58</sup> claim that for the same volume of reinforcing steel, if the critical distance  $d$  is reduced to less than 0.4 inches, the stress to initiate cracking is greatly increased. Collins'<sup>11</sup>work appeared to substantiate the theory of Romualdi, as he achieved tensile strength far in excess of the sum of the tensile strength of the mortar and the reinforcing.

Romualdi based his work on the theory that the Griffith criteria for cracking can be applied to concrete. Griffith's formula:

$$\sigma^2 = G_c E / (1 - \mu^2) \pi a$$

$$\sigma = \text{tensile strength}$$

$$G_c = \text{critical energy release rate}$$

$$E = \text{modulus of elasticity}$$

$$\mu = \text{Poisson's Ratio}$$

$$a = \text{half length of critical flow}$$

By applying the Griffith criteria, he implied that once the length of critical flow at fracture is reduced by reducing the spacing between the reinforcing, the stress required to initiate a crack will be greatly increased.



In their experimental work with chopped wire fibers, Romualdi and Batson, in order to maintain the same volume of steel, varied the diameter of the wires for different spacings. Shah and Broms pointed out that for smaller spacings, wires with higher tensile strength were used. The ultimate resisting moment of the beams was recalculated taking this fact into consideration and the results indicated that wire spacing does not effect ultimate strength.

Romualdi and Mandel<sup>59</sup> tested with randomly distributed short steel fibers to circumvent the difficulty of close spacing with small wires. They claim to have obtained the same results as with continuous wires. However, Shah and Rangan<sup>64</sup> pointed out that Romualdi and Mandel achieved their spacing-strength relationship by using fibers of different volumes, using different mix proportions and using two different types of testing methods.

Shah and Rangan<sup>64</sup> investigated the effect of spacing of wire reinforcements by using three different geometrical arrangements, one wire, six wires, and aligned parallel fibers ( $L/d = 100$ ). The results obtained indicated that the spacing of the reinforcement does have an effect on the strength of the composite. However, the increase was not as significant as indicated by Romualdi and Mandel. The theoretical increase in strength as predicted by Romualdi and Mandel should have been in the range of 300% for a decrease of spacing from 1 inch to 0.1 inch, while actual observed increase was 25%.

Shah and Rangan also noted that the influence of spacing is



negligible for spacing less than 0.8 inches. The increase in tensile strength when reducing the spacing from 0.82 inches to 0.133 inches was observed to be less than 10% for mortar.

Collins,<sup>11</sup> in his experimental work with continuous wire reinforcement, obtained results which supported the theory of Romualdi and Mandel. He obtained on one series of samples, ultimate tensile strengths of 1.8 to 2.0 times the sum of the ultimate strengths of the components. He obtained these results on one series of six samples while his other series of samples broke near or slightly above the sum of the tensile strengths. He described the failures of the first series as being quite abrupt and as a brittle failure. Minor surface cracks were observed before failure, but closed up after failure. The second series was said to fail by elongation and spalling out of the mortar with the ultimate failure of the reinforcement in a ductile fashion. Collins was unable to reproduce the brittle mode of failure and was unable to explain the unusual results obtained other than with the theory of Romualdi et al.

Key<sup>36</sup> and Naaman<sup>52</sup> observed that the metallurgical properties of the reinforcement determine failure mode of the sample. Key used a high strength (160KSI), low ductility mesh and Naaman used a low strength (51KSI), high ductility mesh.





Naaman observed the ductile failure as observed by Collins while Key observed the brittle failure mode. As wire mesh does not have constant properties as obtained from the manufacturer, unless all experiments are done from the same batch, variations will occur. It is felt that Collins inadvertently used mesh from different batches and based his calculated results on the ultimate tensile strength of the lower strength, more ductile mesh.

Separate investigations by Bezukladov<sup>2</sup> and Naaman<sup>52</sup> have indicated that performance of the ferro-cement is a function of the surface area of the reinforcement. Bezukladov found that as the specific surface, i.e., surface area of reinforcement per cubic unit of material, increases, crack resistance increases, but ultimate breaking load is dependent upon the total reinforcement. Naaman also observed that the breaking load of the samples in tension depends only on the total amount of reinforcement present. He also noted that cracking resistance of the composite increases lineally with the specific surface. Naaman observed that the dissemination of the reinforcement inside the mass does not enhance the ultimate tensile strength, but does its elasticity, i.e., strain at the same ultimate load. Figure 7 shows the effect of specific surface as noted by Naaman.

Naaman carried out his investigations with both low





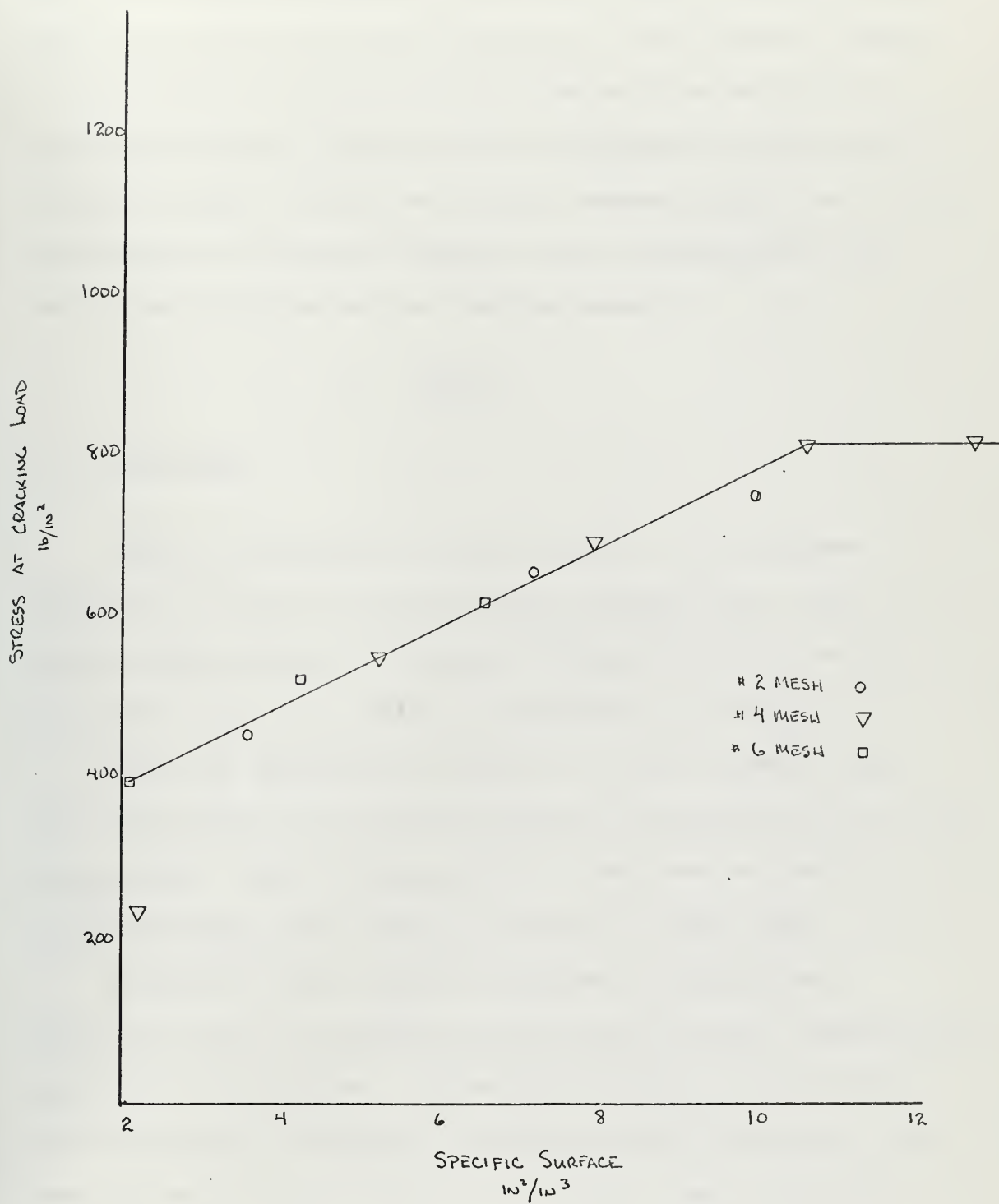


FIGURE 7 EFFECT OF SPECIFIC SURFACE ON  
STRESS AT FIRST CRACK



and high strength mesh and noted the effect of increasing specific surface in both instances. The relative effect of the specific surface on the samples made with high strength mesh was less than that observed with the low strength mesh. It must be noted, however, that the overall performance of the two samples varied considerably with the characteristics of the reinforcement.

## V. IMPACT

### A. BACKGROUND

Impact resistance of ferro-cement is of extreme interest to users of ferro-cement vessels due to the catastrophic effect of a brittle fracture of the hull resulting from a collision or undesired grounding.

The data presently available on ferro-cement impact resistance does not provide adequate information from which to proceed. Some of the work done has been extensive, but is unfortunately not easily related to other work.

Kluge,<sup>37</sup> in 1943, tested a series of reinforced concrete slabs in conjunction with the Maritime Commission's concrete ship program. He tested a series of 15 slabs at various loads by swinging a pendulum into the slabs. He investigated the behavior of the slabs when reinforced



normally as reinforced concrete and when supplemented with overlapping helices of large diameter wire. Table 3 gives the characteristics of the slabs and Figure 13 shows the performance as observed by Kluge. He concluded that the use of overlapping spirals as supplementary reinforcement increased the relative impact resistance of concrete slabs by from 1 1/2 to 3 times. The 7 1/2-inch thick slab with a volume of steel equal to 5.3% exhibited the greatest resistance to impact and its performance in relation to the quantity of steel used was the best of all the slabs tested. He also noted that a slab may be as high as 3 times as resistant to a single loading than to successive loads increasing uniformly in intensity. It is interesting to note that in 1943 Kluge approximated wire mesh ferro-cement and observed optimum results in the range of percentage volume of steel commonly used.

Kudryavtsev<sup>2</sup> conducted impact tests by dropping a 25 kg. weight onto a ferro-cement plate 90 cm by 50 cm to determine the relative difference between conventional reinforced concrete and ferro-cement. Table 4 lists the composition of the samples and Figure 14 shows the dependence of crack opening on number of blows.

Bezukladov<sup>2</sup> conducted a somewhat similar test using a 10 kg. weight and although no values are given, it was noted that a ferro-cement plate 25 cm. thick reinforced



# IMPACT TEST RESULTS

Slab designation	Thick-ness	Spiral Wire Dia.	% of reinforcement (Area)	Wt. of steel per sq.ft. of slab		Vertical Pendulum fall at failure	Relative Impact Resistance	Patios II		Control Cylinder Strength
				Main Spiral				Total wt. Steel	II	
				Long Trans	Spiral					
In.	In.	In.	Lb.	Lb.	Lb.	In.	lb/in <sup>2</sup>			
1-st	6 1/2	-	4.6	2.0	17.6	-	14	0.21	0.79	2840
1-sp4	6 1/2	1/4	4.6	2.0	17.6	4.4	32	0.45	1.45	2810
1-sp3	6 1/2	3/16	4.6	2.0	17.6	2.5	22	0.31	1.09	2760
2-st	4 1/4	-	4.7	3.1	13.5	-	14*	0.30	1.04	3400
2-sp3	4 1/4	3/16	4.7	3.1	13.5	2.3	18	0.37	1.14	3400
3-st	7 1/2	-	6.7	1.1	23.8	-	17	0.21	0.72	2760
3-sp4	7 1/2	1/4	6.7	1.1	23.8	5.1	48	0.56	1.66	2720
4-st	6	-	12.1	1.4	32.9	-	18	0.24	0.55	2800
4-sp4	6	1/4	12.1	1.4	32.9	4.1	38	0.48	1.03	2800
G4-st	6	-	12.1	1.4	32.9	-	-	-	-	6500
G4-sp4	6	1/4	12.1	1.4	32.9	4.1	-	-	-	6500
5-st	6 1/2	-	3.8	2.0	15.7	-	12	0.18	0.77	5220
5-sp3	6 1/2	3/16	3.8	2.0	15.7	2.6	21	0.31	1.15	5220
5-stx	6 1/2	-	3.8	2.0	15.7	-	-	-	-	4830
5-sp3x	6 1/2	3/16	3.8	2.0	15.7	2.6	-	-	-	4830

\* Not determined for permanent deflection.

TABLE 3





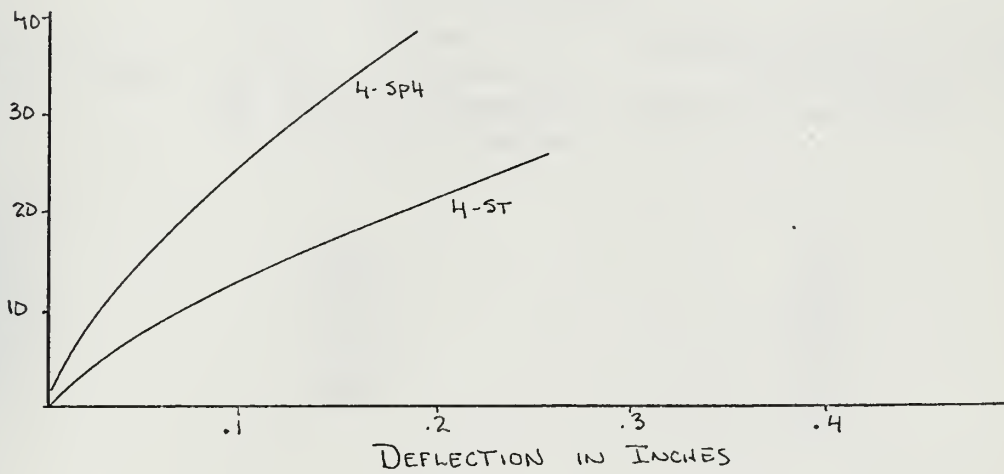
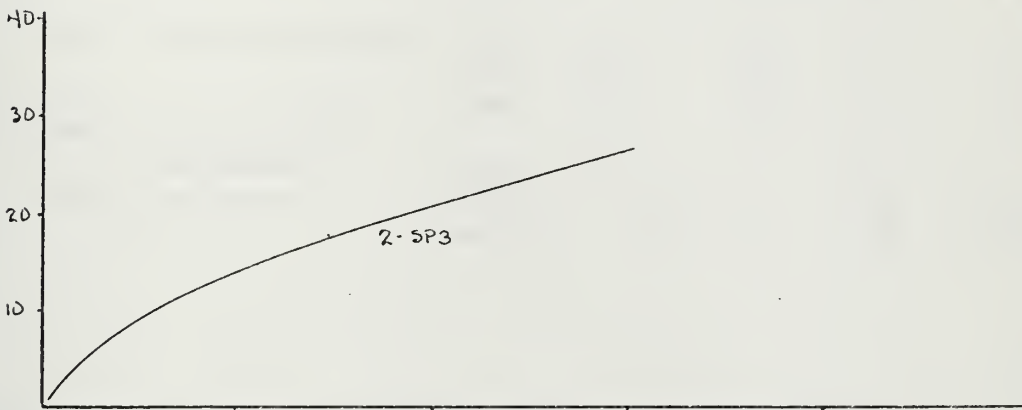
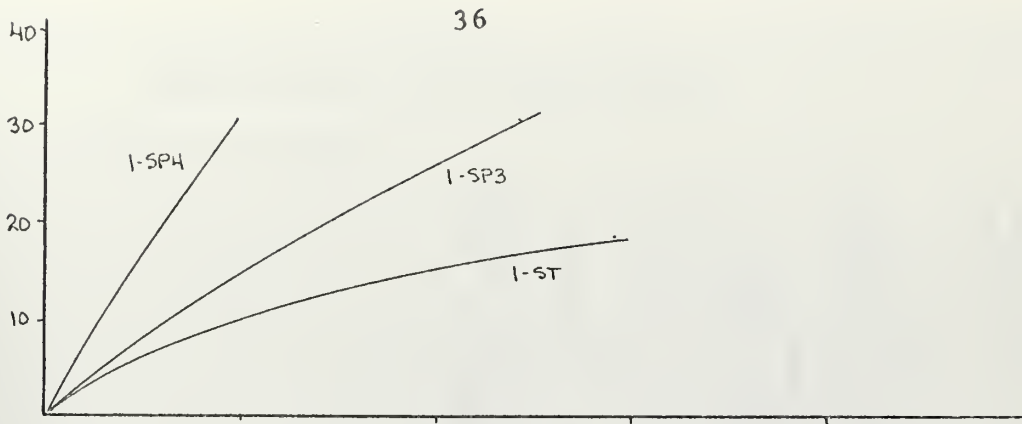


FIGURE 13 PERMANENT DEFLECTION CURVES  
By KULGE



Characteristics of Reinforced Concrete and Ferroconcrete  
Plates During the Impact Tests

Type of material

Index of sample	Type of material	Strength of con- crete $P_{28}$ , kg/cm <sup>2</sup>	Plate thickness cm	Number of meshes	Diameter (mm) of working rein- forcement	Spacing of work- ing reinforce- ment, mm	Use of steel per sq. m. of plate, kg
AU-3	Reinforced concrete	420	2,5	3	0,8	12	3,78
AU-5	"	400	2,5	5	0,8	12	5,43
AU-8	"	400	2,5	8	0,8	12	7,86
Wb-2,5	Reinforced sandy concrete	420	2,5	2	6	84	9,76
Wb-3	Ferroconcrete	470	3	2	4	50	5,38
Wb-5	"	405	5	2	6	84	9,76

Data on Impact Strength of Reinforced Concrete and  
Ferroconcrete Plates

Index of sample	Value of $\Sigma p H \eta$ in moment of appearance of first cleavages of concrete, kg/cm	In percentages of $\Sigma p H \eta$ for ferroconcrete plate 5 cm thick
-----------------	---	--

AU-3	8750	53
AU-5	15000	94
AU-8	18000	109
Wb-2,5	6750	41
Wb-3	7750	47
Wb-5	16500	100

TABLE 4



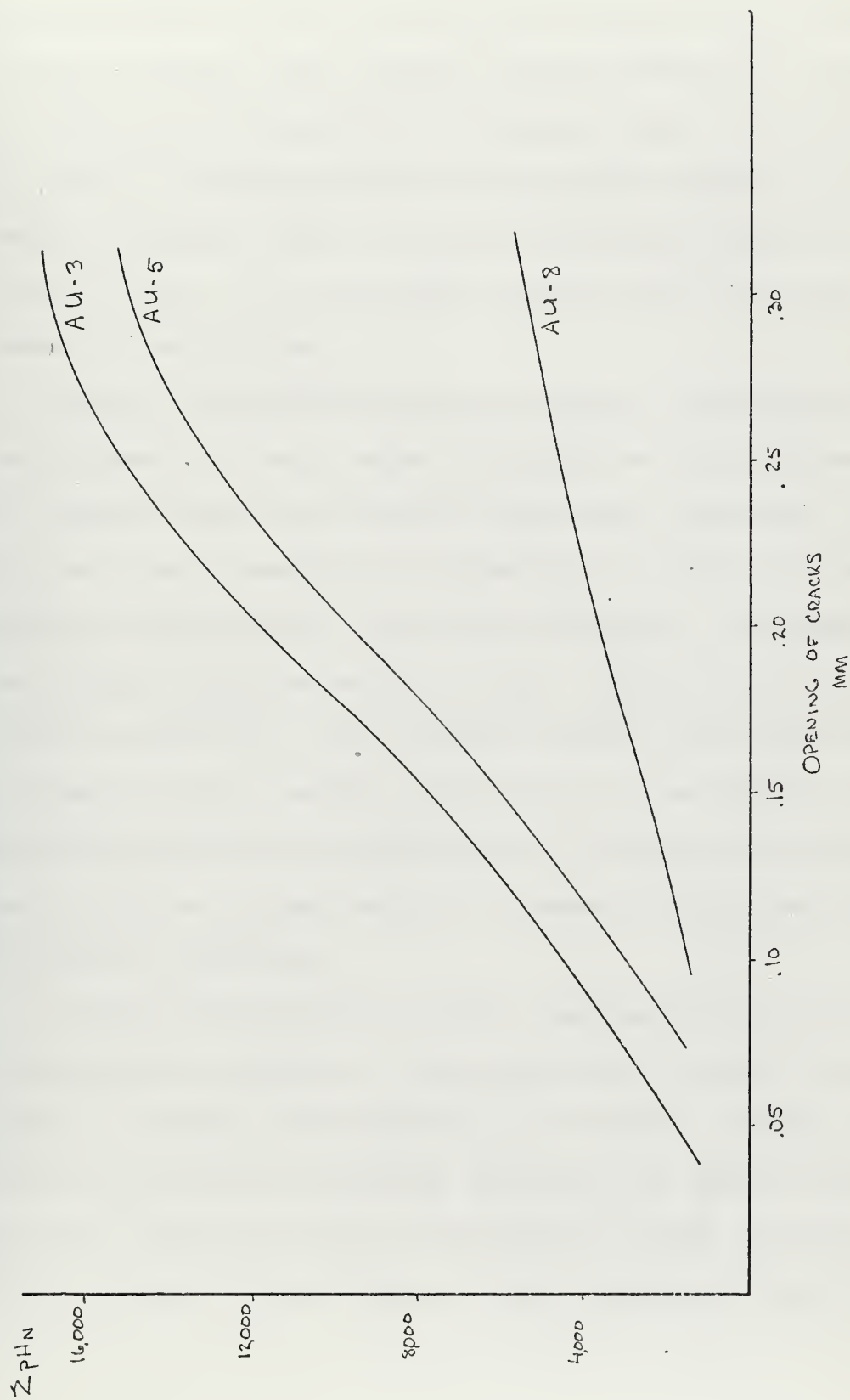


FIGURE 14 CRACK WIDTH BY KUDRYANTSEV



with six number 10 meshes (10 mm between wires), 1.0 mm in diameter, and an intermediate welded mesh of rods 5 mm in diameter, had the same impact strength in respect to cleavages as a reinforced concrete plate 5 cm thick.

Both of these men used an arbitrary standard of impact strength,  $\Sigma PHN$ , to relate the damage observed.  $P$  is the weight,  $H$  is the height of the fall,  $N$  is the number of repetitions.

Kelly and Mouat<sup>35</sup> investigated impact resistance of ferro-cement in their paper presented to the Conference on Fishing Vessel Construction Materials, Montreal, 1968. The tests were conducted by dropping a weight on a panel through progressively increasing distances. The panel was simply supported on four sides. Table 5 and Table 6 give descriptions of the samples and show the results of the tests, with a verbal description of the failure. Kelly and Mouat noted that variability in resistance to impact and in the nature and extent of damage made recognition of failure uncertain.

Collins<sup>14</sup> investigated impact loading with the same type of apparatus as Kluge, a swing pendulum. Collins did not make an extensive investigation into impact loading and only investigated sufficient specimens to assure himself that his vessel did have a reasonable margin of safety. Table 7 gives a description of his samples and the observed





Panel Numbers	1	2	3	4	5	6	7	8	9	10	11
	Weight of Material in Pounds										
Sand	184	200	210	211	195	190	204	199	189	195	195
Cement	92	92	92	92	92	92	92	92	92	92	92
Pozzolan	13 1/2	15	15	15	15	15	15	15	15	15	15
Water	40	49 1/2	49	56	64	36	52 1/2	53	52	56	56

# Reinforcement, Nature and Quantity

Number of layers	1	2	4	6	8	10	12	8	8	8	8
1/2-in galv. No.											
22 ga Hexagon mesh											
1-in pitch No. 14											
ga Hardware cloth											
See Note (a)								x			
1/4-in dia. mild											
steel rods on 2-in											
centers. See Note (b)									x	x	x

Notes: (a) 1 layer of hardware cloth, 1-inch square mesh, No. 14 ga wires with 4 layers of galv. mesh on each side.

(b) In central plane, lengthwise of panel, mild steel rods 1/4-in dia. on 2-in. centers, 4 layers of galv. mesh on each side.

TABLE 5



# PANEL TESTS - IMPACT

Specimen Code	Layers of Mesh	Impact on Trowelled Face	Back	Max. Impact Inch-Pounds	Remarks
160	1	x		-	Completely shattered by 30 ft.-lb.
161		x		-	Completely shattered by 8 ft.-lb.
162			x	20	Quartered; mesh intact
163			x	14	Halved; mesh intact
260	2	x		45	Halved; mesh intact
261		x		45	Quartered; mesh intact
262			x	36	Cracked in quarters to mesh
263			x	27	Cracked in quarters to mesh
360	4	x		205	Cracked in half to mesh
361		x		108	Quartered; mesh intact
362			x	27	Quartered; mesh intact
363			x	36	Quartered; mesh intact
460	6		x	73	Quartered; mesh intact
461		x		215	Quartered; cracks follow mesh
462		x		143	Center punched through; cracks
463			x	63	Punching shear-type failure
560	8	x		215	Halved; crack opened progressively
561			x	54	Punching shear; quartered
562		x		215	Quartered; cracks opened progressively
563			x	45	Cracks follow mesh
660	10	x		332	Quartered; parallel cracks showed
661			x	89	Cracks follow mesh; opened slowly
662		x		322	Quartered
663			x	90	Center punched through; spalled
760	12	x		36	Cracks center to 3 edges
761		x		322	Cracks opened somewhat; spalled
762			x	143	Center punched; mesh bulged; spalled
763			x	322	Cracks; center to 3 edges
					Center punched; mesh bulged; spalled

NOTES: Tensile, Compressive, Shear, Flexure and Panel tests were performed by Goldex, Brawner and Associates

TABLE 6



## Impact Damage Data

% steel (vol.)	(ft-lb) Impact Energy Absorbed	2/in. 19g Mesh (14) 2x2 14/14 wire- cloth #3 ReRod, Shells 1" thick.
6.45	918	Mortar crushed through over 10" dia. area
6.45	515	Same over 6" dia.
6.45	280	Outer surface only crushed over 4" dia. area

TABLE 7



results, with a verbal description of the failure.

Claman<sup>6</sup> observed an increase of 103% in impact energy/unit area when comparing fibrous reinforced samples with woven wire mesh samples. He used a standard Charpy Test on a 260 ft/lb capacity IZOD testing machine, which to obtain any reading must break the sample completely. It is doubtful whether this data would prove to be useful in this investigation because of the manner of obtaining the results.

#### B. IMPACT FAILURE CRITERIA

The choice of a criterion for impact loading of ferro-cement plates is extremely difficult. All of the investigators previously mentioned used either a subjective or an objective failure criterion. Kudravtsev and Bezukladov both used the criterion of crack width with the crack width being observed as a function of energy input. Kluge<sup>37</sup> used deformation of the rear surface and specified arbitrarily that 0.015 inches deflection was failure, while Kelly<sup>35</sup> and Collins<sup>14</sup> used verbal descriptions of the failure.

The selection of a physical characteristic such as crack width or first spall is not desirable when investigating the performance of structural members. The appearance of the first crack does not mean failure of the





member. In the case of ferro-cement, an obvious deviation of the  $\sigma$ - $\epsilon$  curve from linearity is observed at lower values of  $\sigma$  indicating formation of cracks. The material will continue to perform adequately until  $\sigma_u$ , so that selection of first crack or spall is not a valid indication of the capability of the material. Mavis and Greaves,<sup>25</sup> in their experimentation with impulse loading of reinforced concrete beams, loaded the beams until what could be considered failure. The beam's concrete compression side failed, but the steel deformed and did not fracture. Any comparison of energy absorbed in this sort of test would, to a large extent, reflect the ability of the reinforcement to absorb energy.

It is also felt that any classification of damage to the material based on crack width is inadequate to fully indicate the damage suffered by the material. Failure due to impact loads, as indicated by the literature,<sup>20 21 46 75</sup> occurs at some finite distance beneath the surface with the surface becoming visible at a distance  $r$  from the origin of the failure; the maximum distance  $r$  appears to be two diameters of the striking object. Cracks inside of



the spall will not be an indication of further damage because after the initial failure, if the spall does not fly off, it remains only by mechanical action of the mesh.

Deflection of the surface is a good criterion, but does not give an accurate indication of the damage suffered by the matrix.

What is required is a universal criterion which can be applied and which will give an accurate indication of the ability of the material to continue to perform with certain limits as designed.

#### C. IMPACT MECHANISM IN PLATES

A unique form of failure resulting from impact loading is the formation of spalls or cleavages on the opposite side from the point of impact, as a result of stress waves traveling through the plate and being reflected from all free surfaces.

A compression stress wave is generated at the point of contact and propagates spherically outward. It approaches the free surface at the opposite side of the plate and is reflected at normal incidence. The reflected wave will be of opposite sign or tensile. The tensile wave interferes with the remainder of the still-propagating



compressive wave with a resultant wave being the algebraic sum of the waves. The compressive wave and the tensile wave combine, with the resultant wave being decreasingly compressive, and then becoming increasingly tensile. When the resultant tensile wave builds to a sufficiently high level to exceed the tensile strength of the matrix, a fracture will occur. If the reflected wave is not sufficiently high to cause fracture, no damage will be visible. However, if the initial compressive wave is high enough, there can be a possibility of multiple spalls as each succeeding tensile wave is reflected from the free surface formed by the preceding fracture.

The visible surface fracture will be circular, as a result of the spherical stress wave and the diameter will be a function of the plate thickness and the radius of the striking object. Since the fracture is generally continuous beneath the surface within the visible fracture, cracks observed on the surface within the circular fracture will not be indicative of further damage to the sample, only further damage to the retained spall. As a result, any attempt to classify impact damage to plates on the basis of visible cracks would not give a valid indication of damage suffered by the sample.



## D. IMPACT SPALLING

Spalling is defined as the formation of a fracture and the subsequent separation of the fractured material from the parent material. If the plates under investigation have reinforcing material sufficiently close to the reflecting surface, so that the point at which the tensile wave exceeds the tensile strength of the matrix, is beneath the reinforcement, then the formation of a fracture will not cause spalling, due to the mechanical holding action of the reinforcement.

Mellinger<sup>46</sup> indicates in his work on fibrous reinforced concrete that fibrous reinforced concrete does not exhibit higher failure strength than plain concrete under dynamic loading. He does note that fibrous reinforced concrete does not spall as does plain concrete and infers that the reinforcement mechanically holds the concrete in place after the failure has occurred.





## VI. SCOPE OF THE PRESENT INVESTIGATION

As a result of the lack of basic knowledge of ferro-cement, this investigation was undertaken in two parts, the first part to investigate the basic performance of ferro-cement in tension, and the second to investigate the effects of impact loading on ferro-cement and to relate the impact performance to the tensile performance so as to provide a basis for knowledge of impact performance.

Proceeding in the first phase from the previous work of Naaman,<sup>52</sup> the investigation undertook first to investigate the influence of the matrix composition on the performance of tensile specimens, to acquire a basic knowledge of the material, then to correlate the findings of Naaman on specific surface, using, however, different mesh sizes which approximate those in common use today. In conjunction with the investigation of the variance of specific surface, the effect of the placement of small dimension mesh in outer layers of reinforcement and large dimension mesh in the inner layers was observed to determine whether there would be a beneficial effect. The use of large dimension mesh is more economical per pound than small dimension mesh and practical aspects of ferro-cement would benefit through the use of less expensive reinforcement if proven to be suitable. Also in conjunction with the above two investigations, the effect of the ultimate strength of



the reinforcement was investigated. Prior investigations have indicated that the performance of ferro-cement after cracking is dependent on the type of reinforcement used and indicates a possibility for enhanced performance through the use of higher strength reinforcements.

The second phase followed the first phase closely in procedure. The effect of the variation of specific surface on impact resistance was investigated, again using different sizes of mesh to simulate the material as it is currently constructed. The specific surface was varied up to the optimum as recommended by Naaman and the impact resistance was noted. In conjunction with the variance of the specific surface, the effect of small dimension mesh in the outer layers was observed. Bezukladov noted that concrete damaged by impact loadings was held in place by the mesh reinforcement and it is this effect which will be of interest. If the mesh does hold the crushed concrete in place, then the ingress of water is impeded, and this is desirable in ferro-cement vessels. In conjunction with both of the above investigations, the effect of the variance of the strength of the reinforcement was observed.

For comparison purposes, the second phase also investigated the impact resistance of fibrous-reinforced mortar plates.



## VII. EXPERIMENTAL PROCEDURE

## A. TENSILE PHASE

The tensile specimens were 12<sup>25</sup> inch long, 3 inches wide, and 0.5 inches thick with a 2.5-inch necked portion extending over the middle 6 inches. See Figure 15. All specimens used in this phase of the investigation were identical in composition with the exception of the reinforcement. Reinforcement used in Series X, L, M and H varied in yield and ultimate strengths as is indicated in the schedule of reinforcement seen in Table 8.

The volume of the reinforcement was held constant at approximately 5.4%. The volume of one layer of 1.0 inch by 1.0 inch welded mesh is approximately equal to that of two layers of 0.25 by 0.25 inch woven mesh so that with proper arrangement of the layers of mesh, an orderly variation of the desired factors could be achieved without varying the volume of steel.

As was noted previously, in woven mesh, the woof has shown 10 to 15% higher ultimate strength than the warp and has less of a woven angle X, so the preferential direction of the mesh for tensile tests should be in the direction of the woof. However, since the second phase of the investigation involves biaxial stresses and would indicate an orientation of the mesh so that there is no overall preferential direction, and the fact that the tensile test results are to be compared with impact test results, it was decided



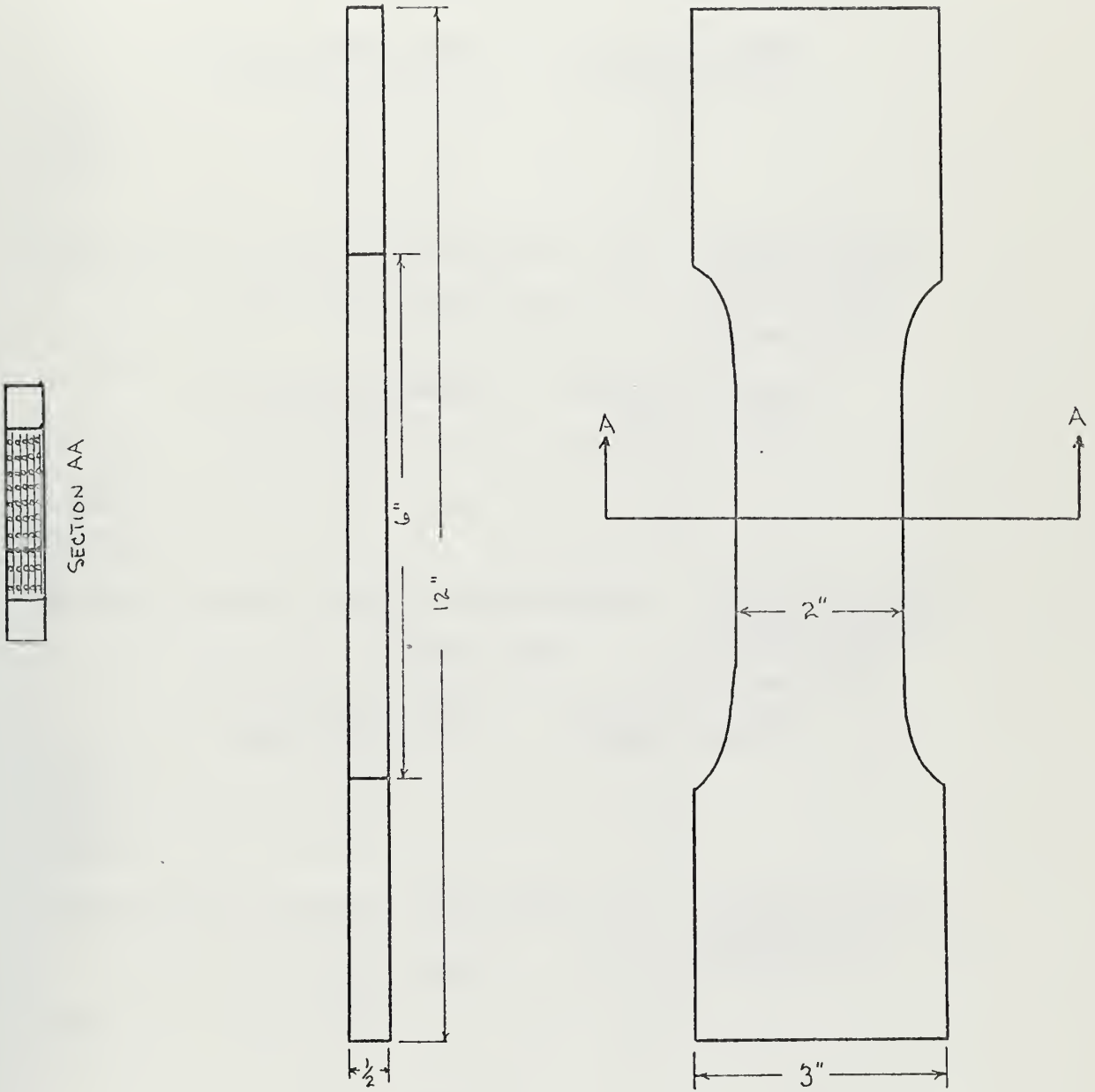


FIGURE 15 TENSILE SPECIMEN





## REINFORCEMENT SCHEDULE

Series L	0.25"x0.25" woven mesh $\sigma_u = 56,600 \text{ lb/in}^2$ (ungalvanized)	
	1.0"x1.0" welded mesh $\sigma_u = 57,700 \text{ lb/in}^2$ (galvanized)	
	0.25"x0.25" mesh outer layers	1.0"x1.0" mesh inner layers
0-3-L	0	3
2-2-L	2	2
4-1-L	4	1
6-0-L	6	0
Series M	0.25"x0.25" woven mesh $\sigma_u = 119,000 \text{ lb/in}^2$ (galvanized)	
	1.0"x1.0" welded mesh $\sigma_u = 57,700 \text{ lb/in}^2$ (galvanized)	
	0.25"x0.25" mesh outer layers	1.0"x1.0" mesh inner layers
0-3-M	0	3
2-2-M	2	2
4-1-M	4	1
6-0-M	6	0
Series H	0.25"x 0.25" woven mesh $\sigma_u = 161,000 \text{ lb/in}^2$ (ungalvanized)	
	1.0"x1.0" welded mesh $\sigma_u = 57,700 \text{ lb/in}^2$ (galvanized)	
	0.25"x0.25" mesh outer layers	1.0"x1.0" mesh inner layers
0-3-H	0	3
2-2-H	2	2
4-1-H	4	1
6-0-H	6	0
Series X	0.25"x0.25" woven mesh $\sigma_u = 131,000 \text{ lb/in}^2$ (galvanized)	
	0.25"x0.25" mesh	1.0"x1.0" mesh
6-0-X	6	0

TABLE 8



to orientate the mesh in the tensile specimens so that on adjoining layers, the woof was perpendicular. This orientation of the mesh reduced the ultimate strength and may possibly cause a premature splitting failure of the sample, but represented the reinforcement in the impact specimens and gives more accurate indication of any correlation.

The mesh was arranged in the desired orientation and bound lightly together with a loop of 19-gauge galvanized wire at each end. The bundle of mesh was then cut to the dog-bone shape on a metal-cutting bandsaw and fitted to the mold.

The mold for the tensile specimens was constructed of plexiglass as is seen in Figure 16. The mesh and the mortar were placed in from the top and the mortar troweled to the level of the sidewalls of the mold. The molds were oiled with mineral oil to assure easy release of the samples. In order to assure the maintenance of a proper cover of mortar over the mesh, spacer pieces consisting of 0.3 inch square portions of 0.25 by 0.25 inch mesh were laid on the floor of the mold before the mesh was laid in. This provided a constant cover of approximately .100 inches on the bottom surface of the specimen. The binding of the reinforcement together for shaping has a secondary effect of adding rigidity to the reinforcement so that when it was placed on the spacer pieces, it would not sag in the middle upon application of the mortar.







## B. IMPACT PHASE

The impact specimens were 9 inches square with a 0.5 inch thickness as is shown in Figure 17. All specimens used in this phase of the investigation were identical in composition with the exception of the reinforcement, which followed the tensile samples as noted in Table 8.

The impact specimens were identical to the tensile specimens except in size. All effort was made to keep the two series of samples standard to as to facilitate any correlation between the two series. The volume of steel was again maintained at 5.4% throughout the series with an orderly variation of the reinforcement.

As was noted, woven wire mesh shows preferential properties in direction of the woof and anticipating biaxial loading in impact testing, the layers of mesh were arranged so that in each succeeding layer the woof is orientated at 90 degrees to the preceding layer.

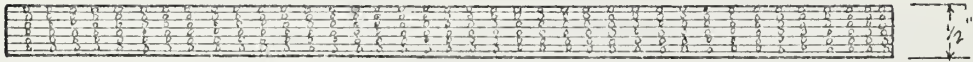
The mesh was bound lightly together with 19-gauge galvanized wire at four corners so as to facilitate the placing of the reinforcement in the molds. The mesh was cut out on a foot-operated shear before binding together.

The mold for the impact specimens was constructed of plywood with a formica top and 0.5 inch square oak side walls as seen in Figure 18. Strips of 0.25 by 0.25 inch galvanized woven mesh, 6 inches by 1 inch, were placed on the bottom of the mold along the





## MESH ARRANGEMENT FOR G-D SERIES



SECTION AA

NOTE:

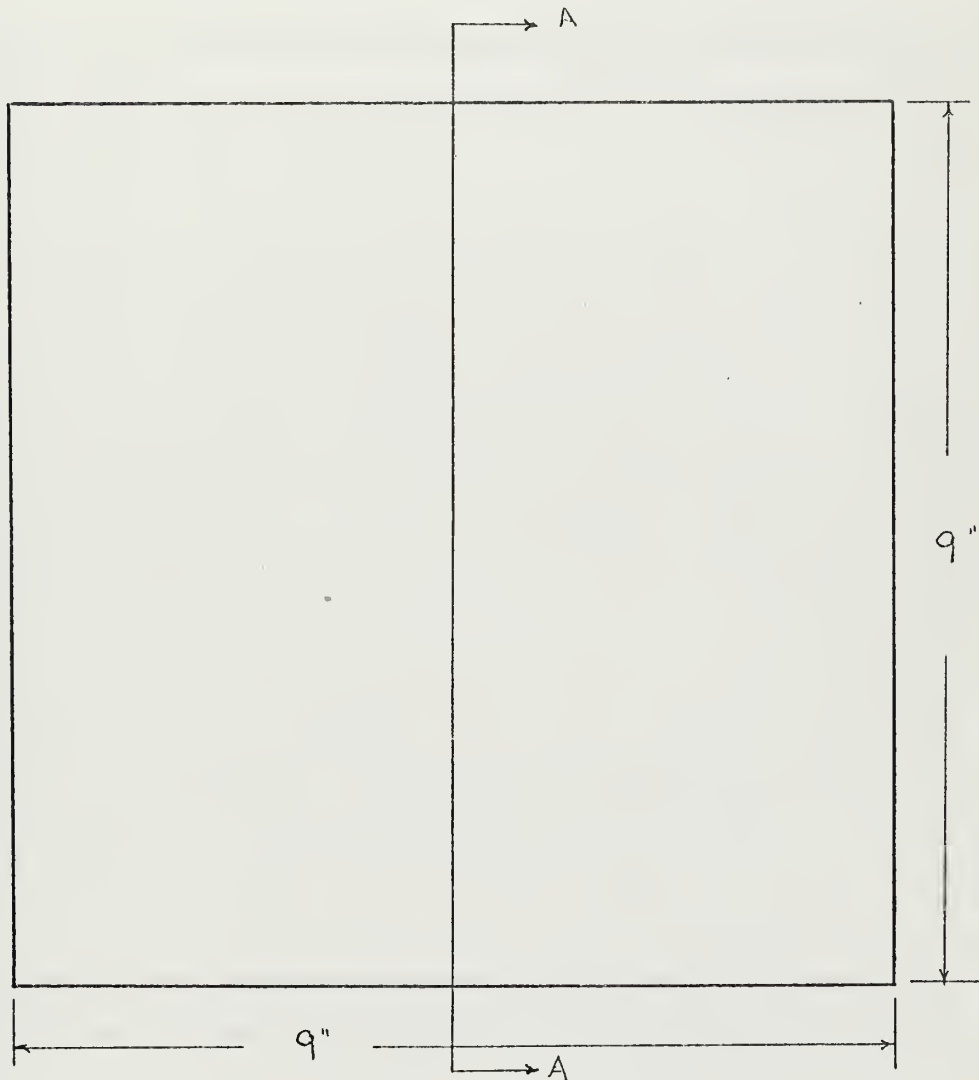
MESH SIZE, ARRANGEMENT, AND  
LOCATION NOT TO SCALE.

FIGURE 17 IMPACT SPECIMEN



57

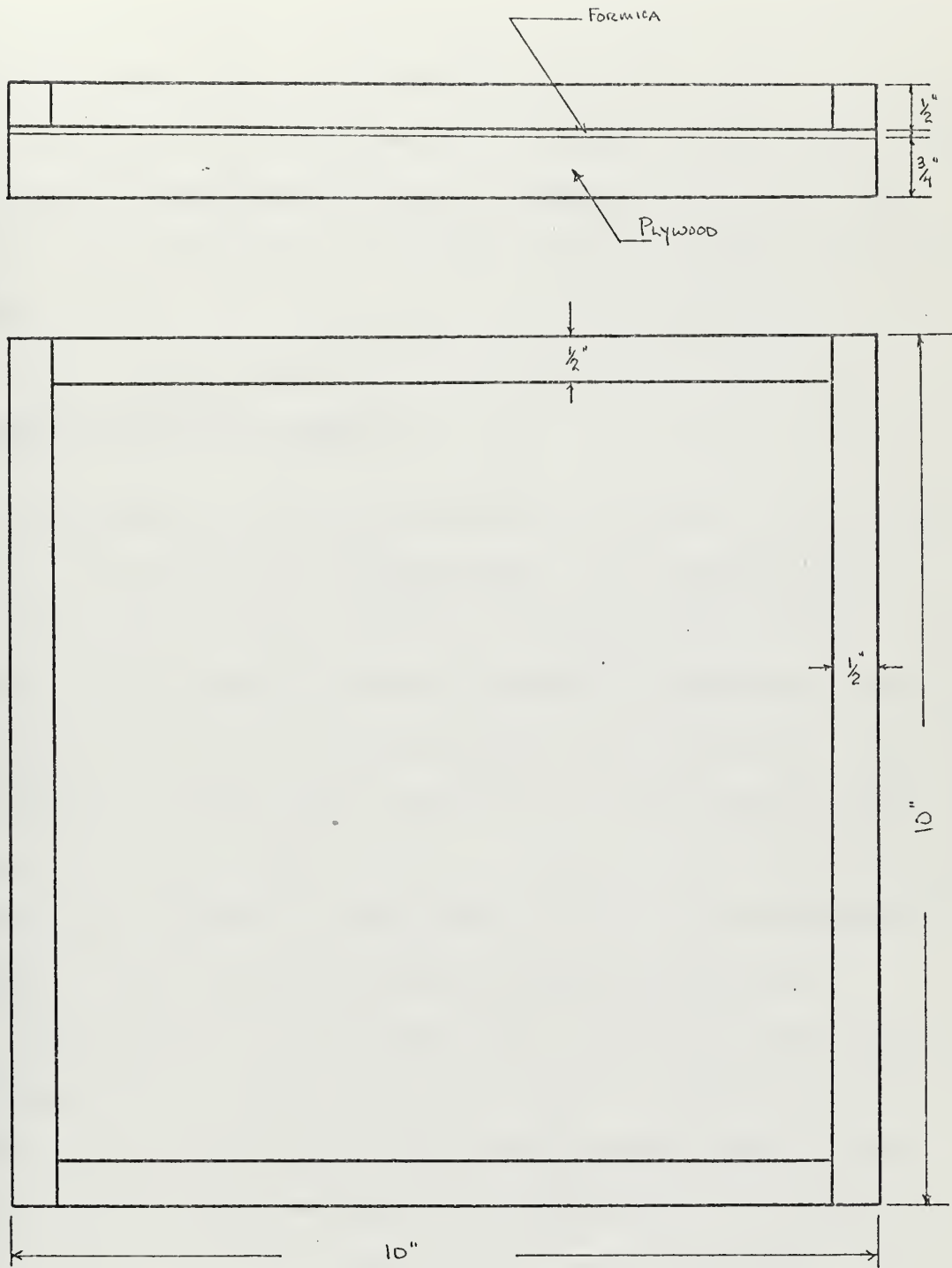


FIGURE 18 IMPACT SPECIMENS MOLD



side walls to provide a constant mortar cover of approximately .100 inches. The mesh was placed on the spacer pieces and the mortar poured on. The binding of the reinforcement again served the purpose of stiffening the mesh bundle, so that with the application of the mortar, the middle of the reinforcement would not sag.

### C. COMPOSITION OF THE SAMPLES

All samples, with the exception of Series X, were identically composed, except for the reinforcement. The reinforcement of Series X was held constant while the constituents varied. Reinforcement was as noted in Table 8 and was as purchased from the manufacturer, except the low-strength woven wire mesh. This mesh was obtained by heating the ungalvanized high-strength mesh in an annealing furnace at  $600^{\circ}$  C. for 45 minutes, then cooling in air. Annealing was required because there are no U.S. manufacturers who produce mesh with the desired strength properties.

Sand gradation, sand/cement ratio, and sand type were varied independently over a wide range in Series X. Optimum results as indicated by this section of the investigation were not used in the following sections in order to standardize all concurrent investigations at M.I.T. Water/cement and sand/cement ratios were maintained at 0.6 and 1.5 respectfully.

Hercules Type III High Early Cement was used throughout the



investigation. A graded common sand was utilized in Series X, while Ottawa fine graded sand, ASTM C109 was used in the other sections of the investigation. Gradation curves for both the Ottawa and the common sand are seen in Appendix D.

Each batch of mortar was mixed in a 10-quart Hobart food mixer for three minutes, poured, and then vibrated in the mold for thirty seconds. Each batch was sufficient to cast one series of specimens, so that identical specimens came from the same batch.

Each sample was cured one day in air under a polyurethane cover and then demolded. Then they were cured for six days under water. The samples were tested on the seventh day after a drying period of one hour.

#### D. DESIGNATION OF SAMPLES

The samples are designated in relation to the mesh arrangement and the strength of the mesh used, with the exception of Series X. The first number indicates the number of layers of 0.25 by 0.25 inch woven mesh used and the second number indicates the number of layers of 1.0 by 1.0 inch welded mesh used. The letter designates the strength of the 0.25 by 0.25 inch mesh used, L indicating  $56.6 \times 10^3$  lb/in<sup>2</sup>, M indicating  $119 \times 10^3$  lb/in<sup>2</sup>, and H indicating  $161 \times 10^3$  lb/in<sup>2</sup> ultimate strength.





The 1.0 by 1.0 inch welded mesh is constant throughout the investigation at  $57.7 \times 10^3 \text{ lb/in}^2$  ultimate strength. The reinforcement schedule, Table 8, explains the arrangement of the reinforcement and Figure 17 shows a typical arrangement. Series X has a suffix to indicate the test in the series, where a indicates the sand gradation, b sand/cement ratio, and c the sand type. Also with the suffix is a number indicating the composition of the sample as shown in Table 9.

## VIII. APPARATUS

### A. TENSILE TESTS

The INSTRON Universal Testing Machine was utilized in all tensile tests. Special grips were constructed to clamp to each end of the specimen for a distance of three inches or to the start of the dog-bone. The inner face of the grips had angular teeth cut into it so that adequate holding power could be developed without causing excessive compressive stresses on the sample by excessive tightening of the grips. Figure 18.5 shows the machine with the grips in place ready for testing.

Load-deflection information as generated by the INSTRON was recorded on a graphical pen recorder with a chart speed of 2.0 inches per minute. The loading rate during all tests was 0.5 inches per minute.



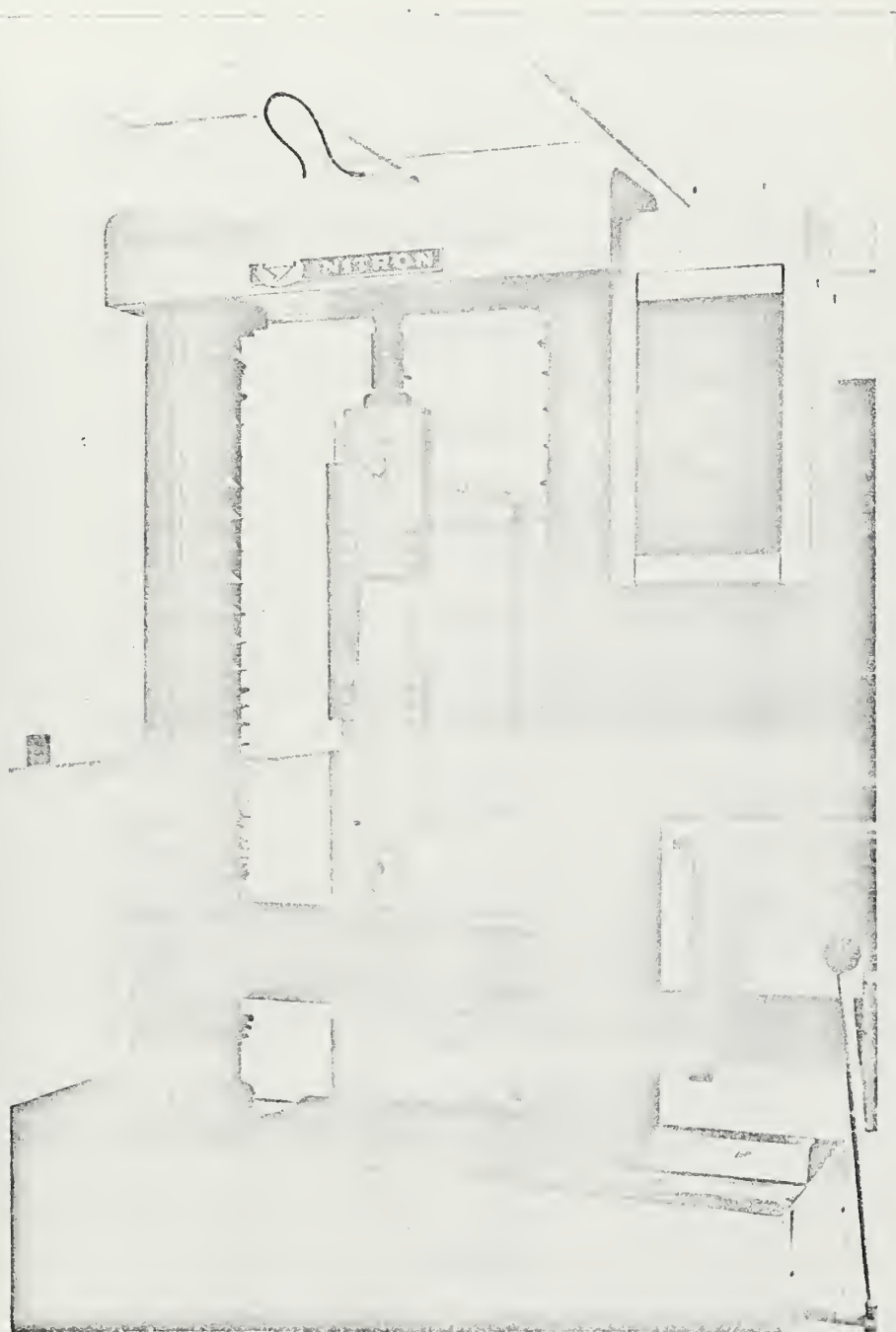


FIGURE 18.5



Sample	Sand Gradation	Sand Type	<u>Sand</u> <u>Cement</u>	<u>Water</u> <u>Cement</u>
XA1	#8> <#30	common	1.5	0.6
XA2	#16> <#50	common	1.5	0.6
XA3	#50> <#100	common	1.5	0.6
XA4	#100>	common	1.5	0.6
XA5	Mix 1	common	1.5	0.6
XA6	Mix 2	common	1.5	0.6
XA7	Mix 3	common	1.5	0.6
XB1	graded fine	Ottawa	0.75	0.6
XB2	graded fine	Ottawa	1.5	0.6
XB3	graded fine	Ottawa	3.0	0.6
XC1	16	Expanded shale	1.5	0.6
XC2	16	Vermiculite	1.5	0.6

TABLE 9



## B. IMPACT TESTS

A special testing machine was built for the impact tests, because of the lack of testing equipment suitable for testing specimens of the configuration used in this investigation.

The apparatus consisted of two ballistic pendulums swinging from parallel arms supported at a height of eight feet from the floor. The sample was mounted on a steel plate which was inserted in slots on the receiver pendulum. The striker pendulum was suspended at its maximum height by a solenoid-operated trigger. Both the swing of the receiver and the rebound of the striker were measured by a spark trace on Sanborn recorder paper. Figures 19 and 20 show the apparatus in the ready position and the swing-through position.

The striker pendulum consisted of a 4-inch diameter steel shaft, 6 inches long with a 7-inch rod, 1 1/2 inches in diameter, inserted in a hole bored in the forward face of the larger piece. The device was supported by 4 piano wires attached to the webs of 1-inch channel pieces, which were bolted to the top of the larger piece. The channels were located so that the points of suspension were equidistant from the center of mass of the section. See Figure 21. The receiver pendulum was an I-beam, 12 inches wide, 14 inches deep, and 18 inches long. The forward face of the receiver was machined flat and two 2-inch pieces of 1 1/2 inch angle were bolted







FIGURE 19



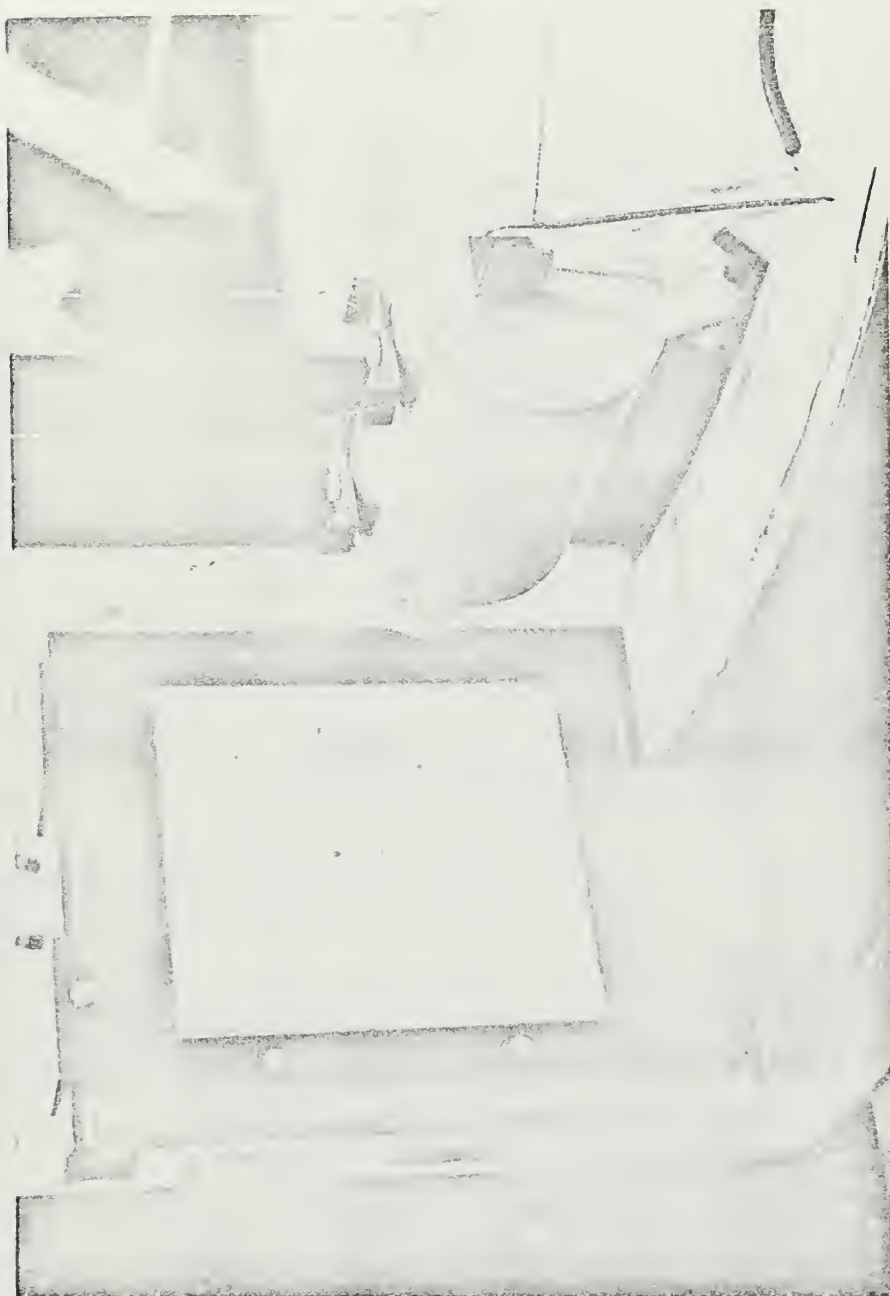
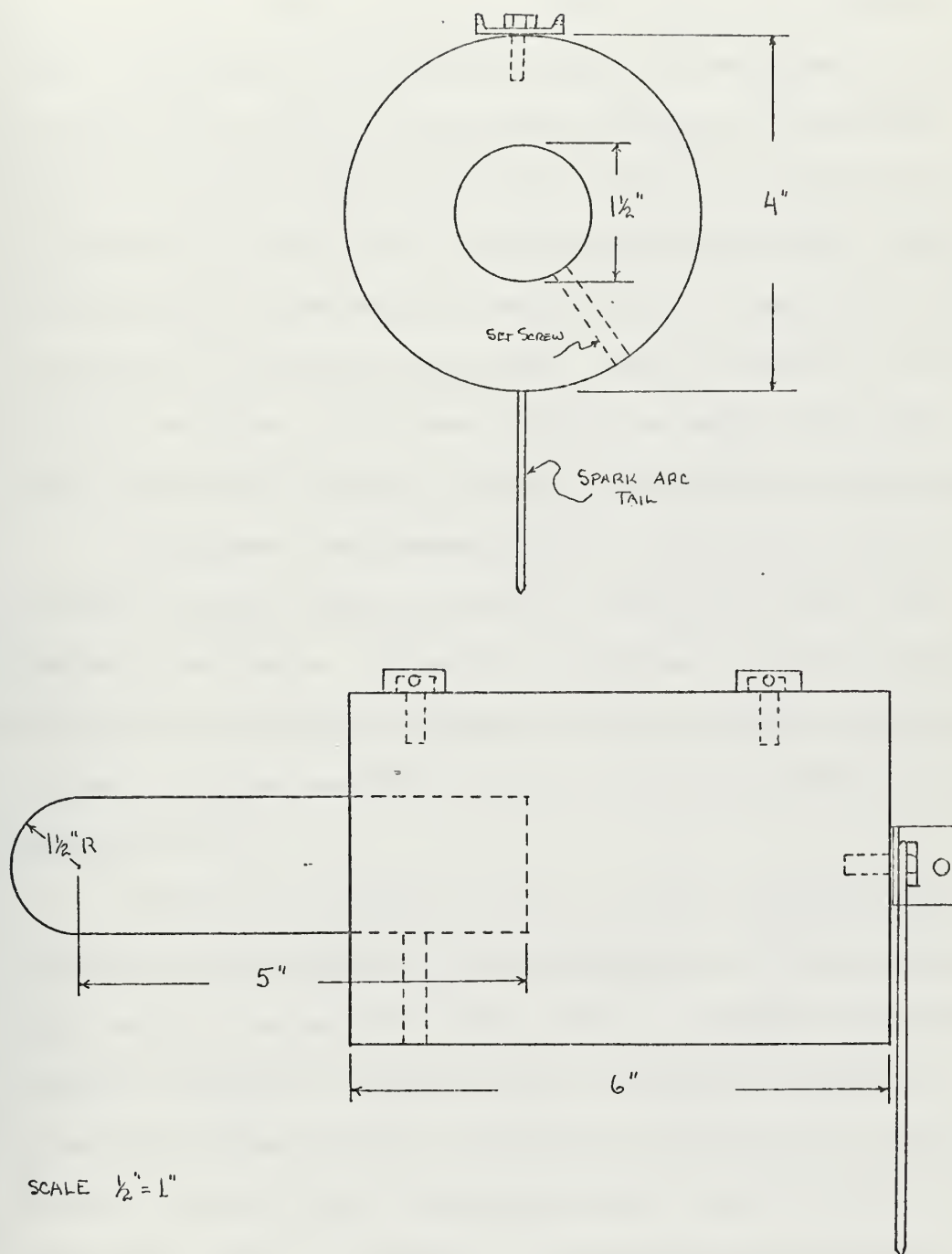


FIGURE 20





IMPACT STRIKER

FIGURE 21



to the top and bottom flanges with 9/16 inches clearance between the face and the angle to allow the sample plate to be slipped in place. The angles were drilled and tapped for set screws so that the sample plate could be held firmly in position. The sample was mounted on the sample plate which was 0.5 inch mild steel, 12 inches by 14 inches, with an 8-inch square hole in the center. The sample was clamped onto the sample plate with angle iron running the length of the sample on two sides. The other sides of the sample were not restrained. All faces touching the sample were lined with 1/8-inch thick rubber to prevent local crushing of the sample.

The receiver was suspended by four piano wires attached to the webs of 1-inch channel pieces which were bolted to the upper flanges of the I-beam. The points of attachment for the channels were such that the point of suspension was equidistant from the center of mass of the receiver with the sample plate and sample in place. See Figure 22.

In order to accurately measure the swing and the rebound of the striker and the receiver, it was necessary to utilize a system which would not mechanically induce losses. The spark trace method provides a simple and accurate method of obtaining a permanent record of pendulum movement without coupling the pendulum to the ground. The spark was arced from a copper face plate which was laid on the curved ramps under the pendulum to a sharpened wire attached at the rear of both striker and receiver.





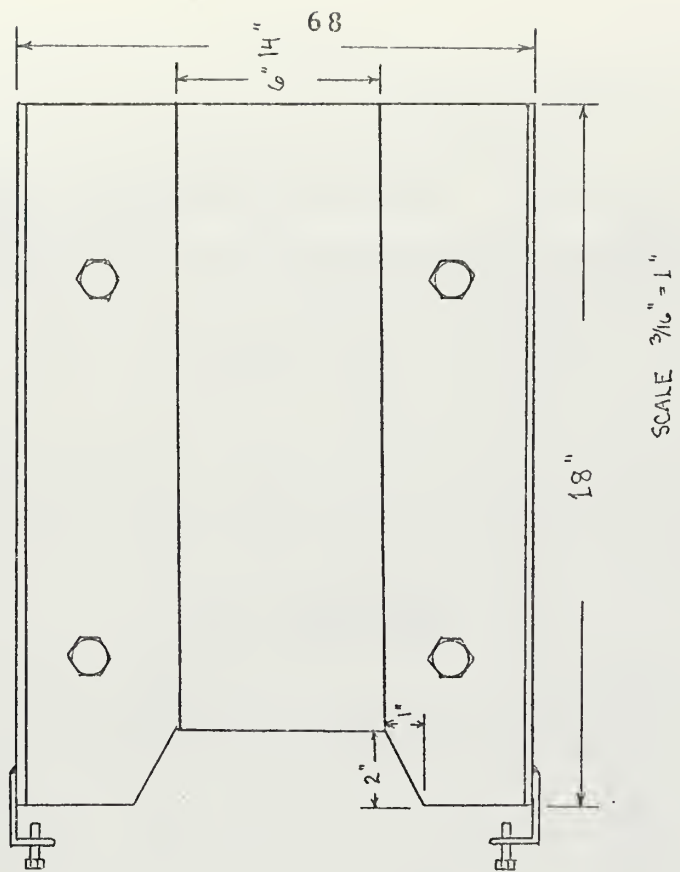
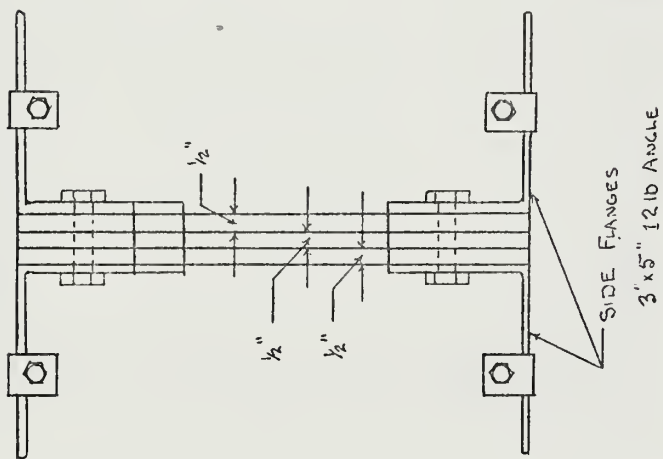


FIGURE 22 IMPACT RECEIVER



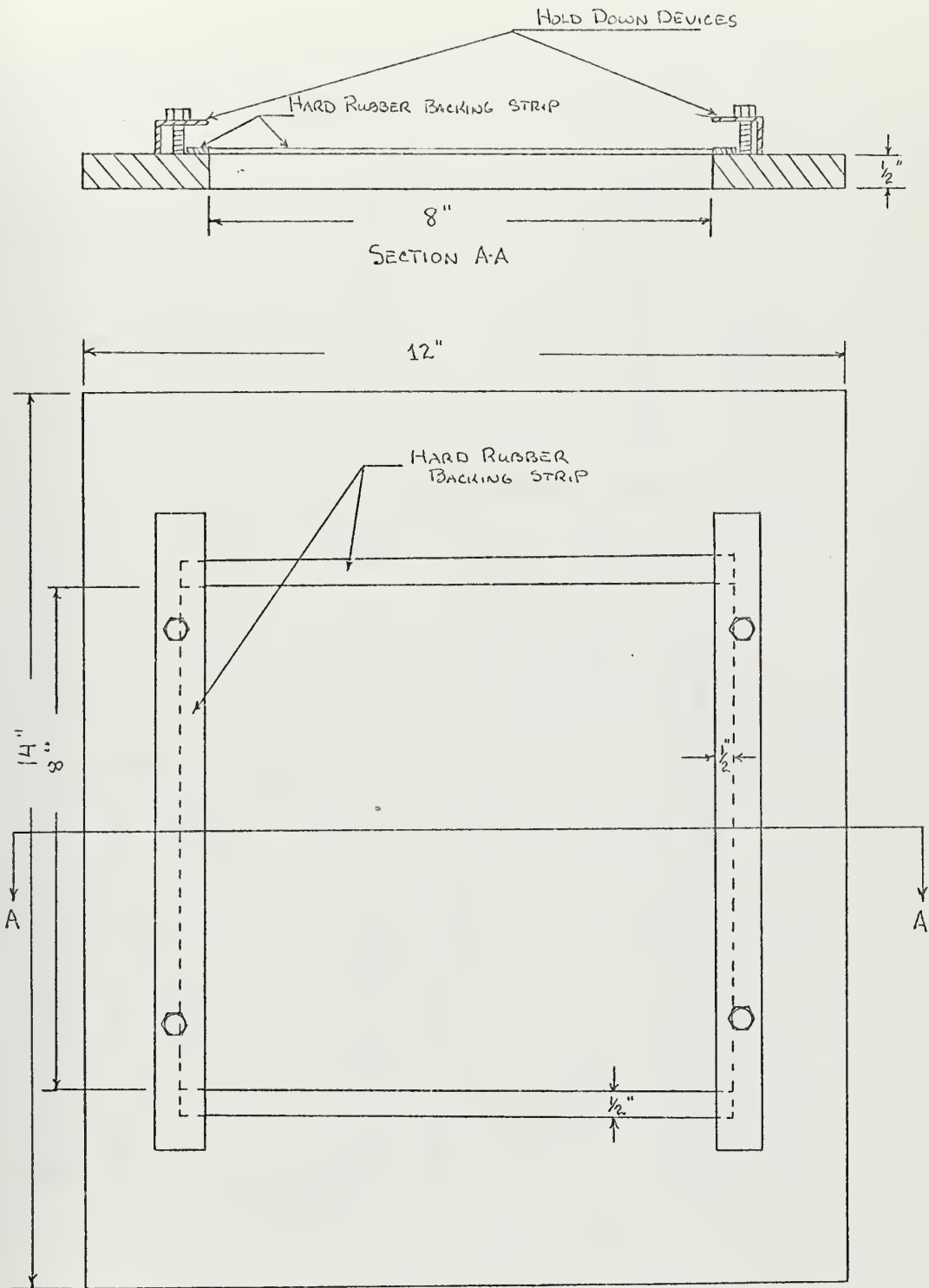


FIGURE 22.5 SAMPLE HOLDER



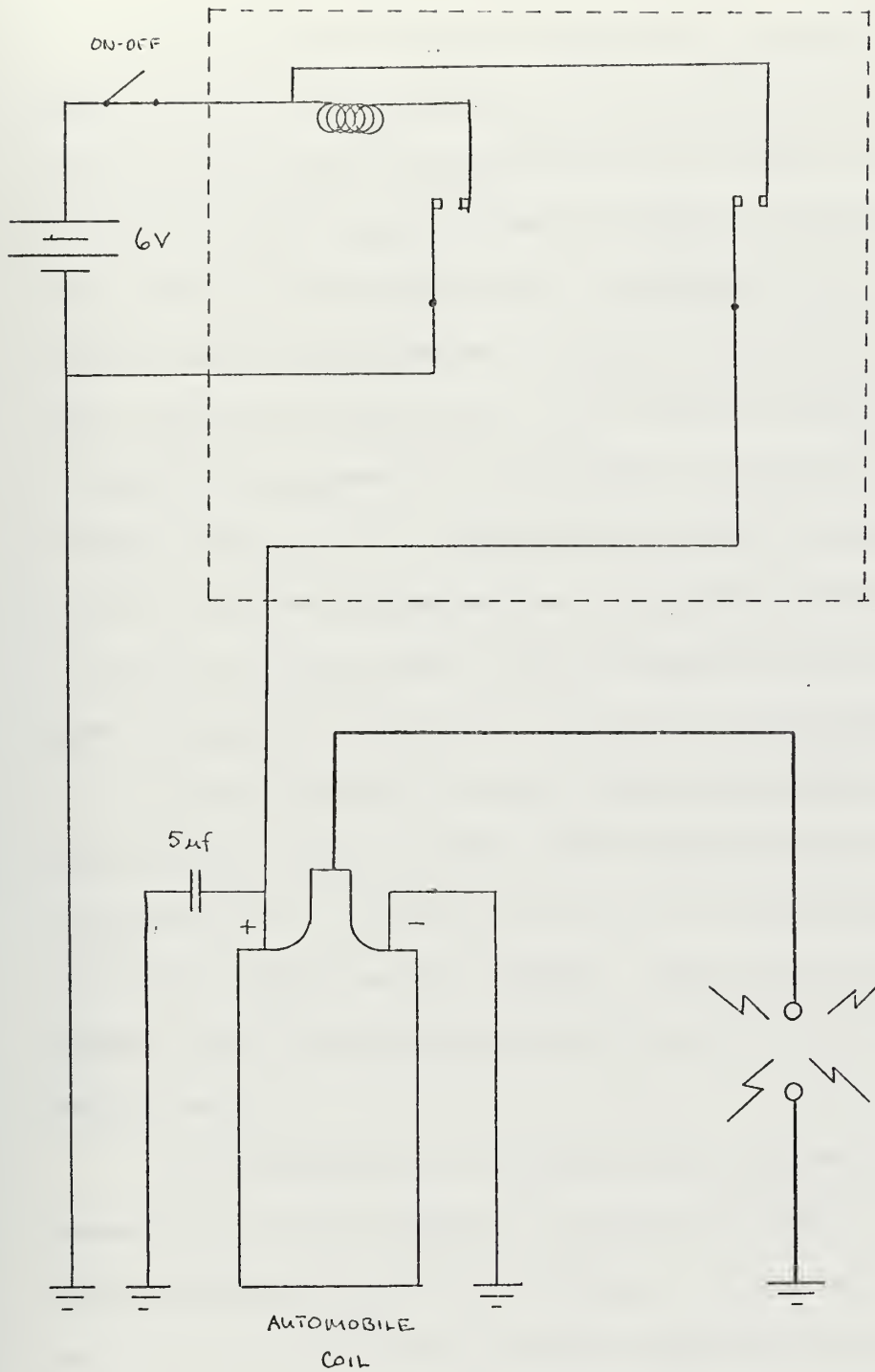


FIGURE 23 SPARK ARC SCHEMATIC



The secondary coil of a transformer is connected to the face plate while the primary coil of the transformer is connected in series with a 6-volt power source and two sets of breaker points. The breaker points open and close alternately interrupting the current flow to the primary coil. The collapse of the electro-magnetic field induces a voltage of approximately  $30 \times 10^3$  volts across the secondary coil. The voltage produced is sufficient to jump the gap between the wire pointer and the face plates. Figure 23 shows the diagrammatic layout of this device. Recorder paper is laid on the face plates so that the pointer is over the paper at all points of the swing. The arc generated marks the paper and gives a permanent record of the movement of the pendulum.

Both the striker and the receiver were calibrated prior to the investigations so that losses inherent in the machine could be accounted for. Figures 24 and 25 are the calibration curves of both the striker and the receiver. Figure 26 is included as a reference aid in determining energy levels directly from observed pendulum swing.

In consideration of the difficulty experienced by other investigators in establishing a criterion of damage, special consideration was given to the problem. A criterion was selected which would prove to be the most interesting for the purpose intended for the ferro-cement. It was felt that the flow of a liquid through





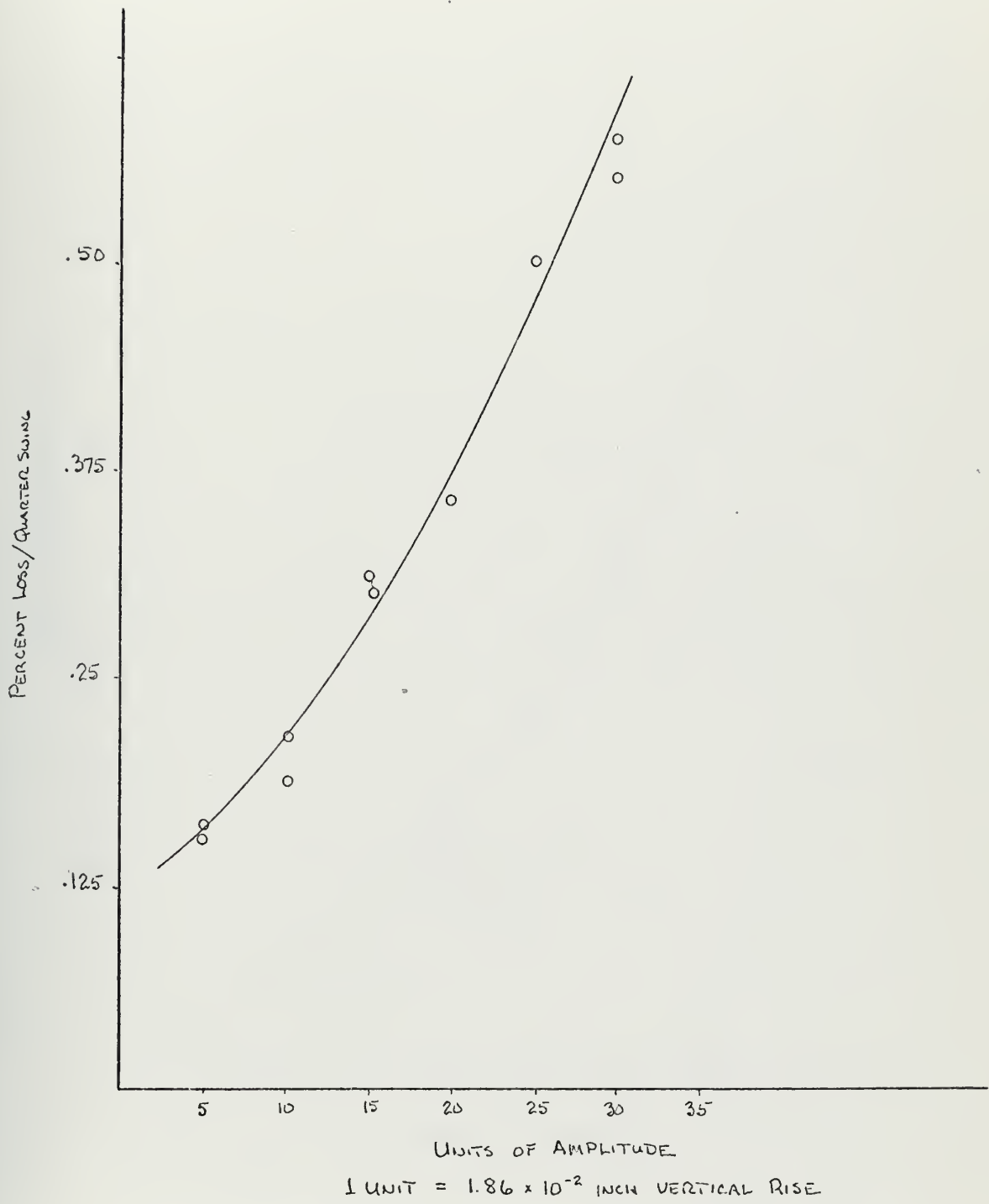


FIGURE 24 STRIKER CALIBRATION CURVE



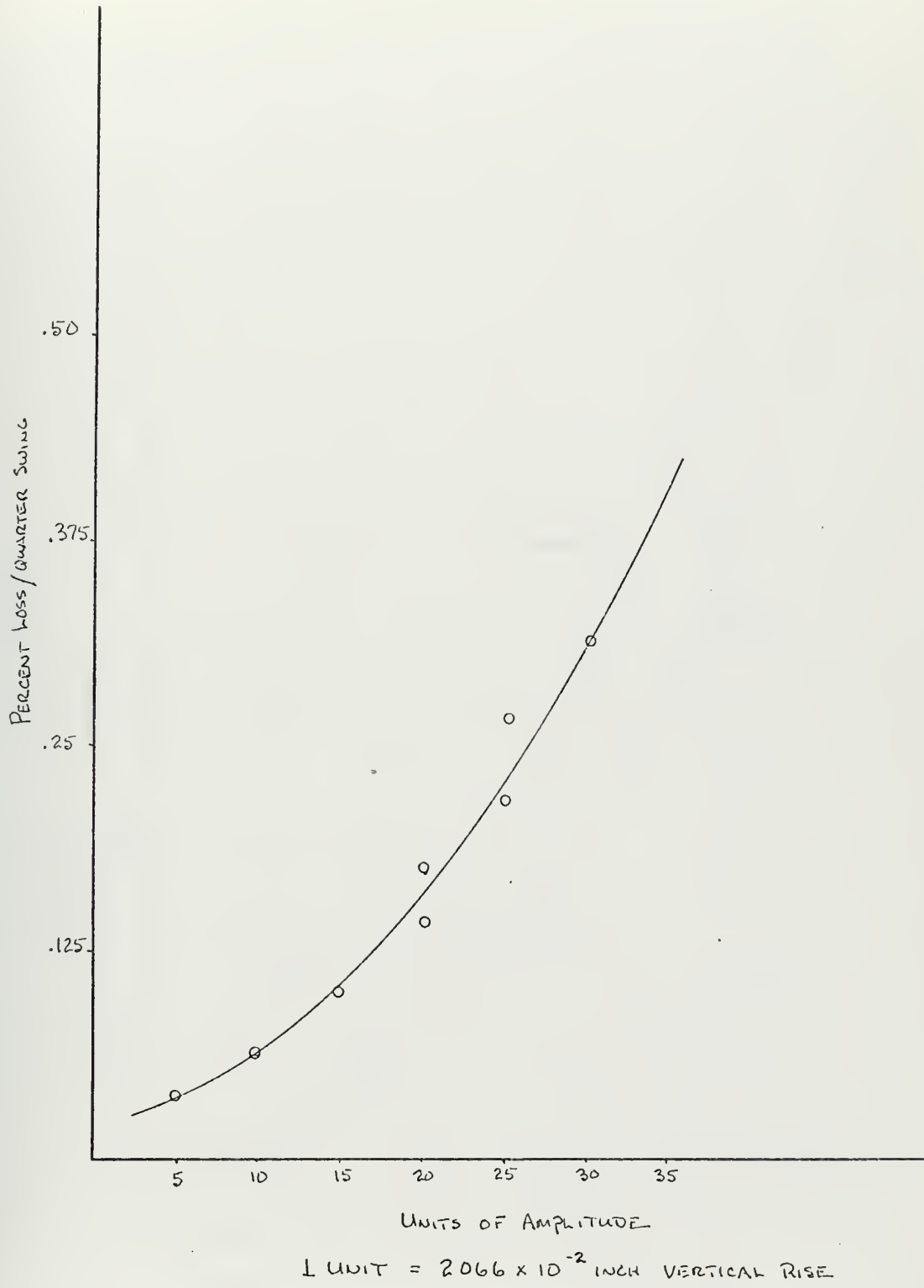
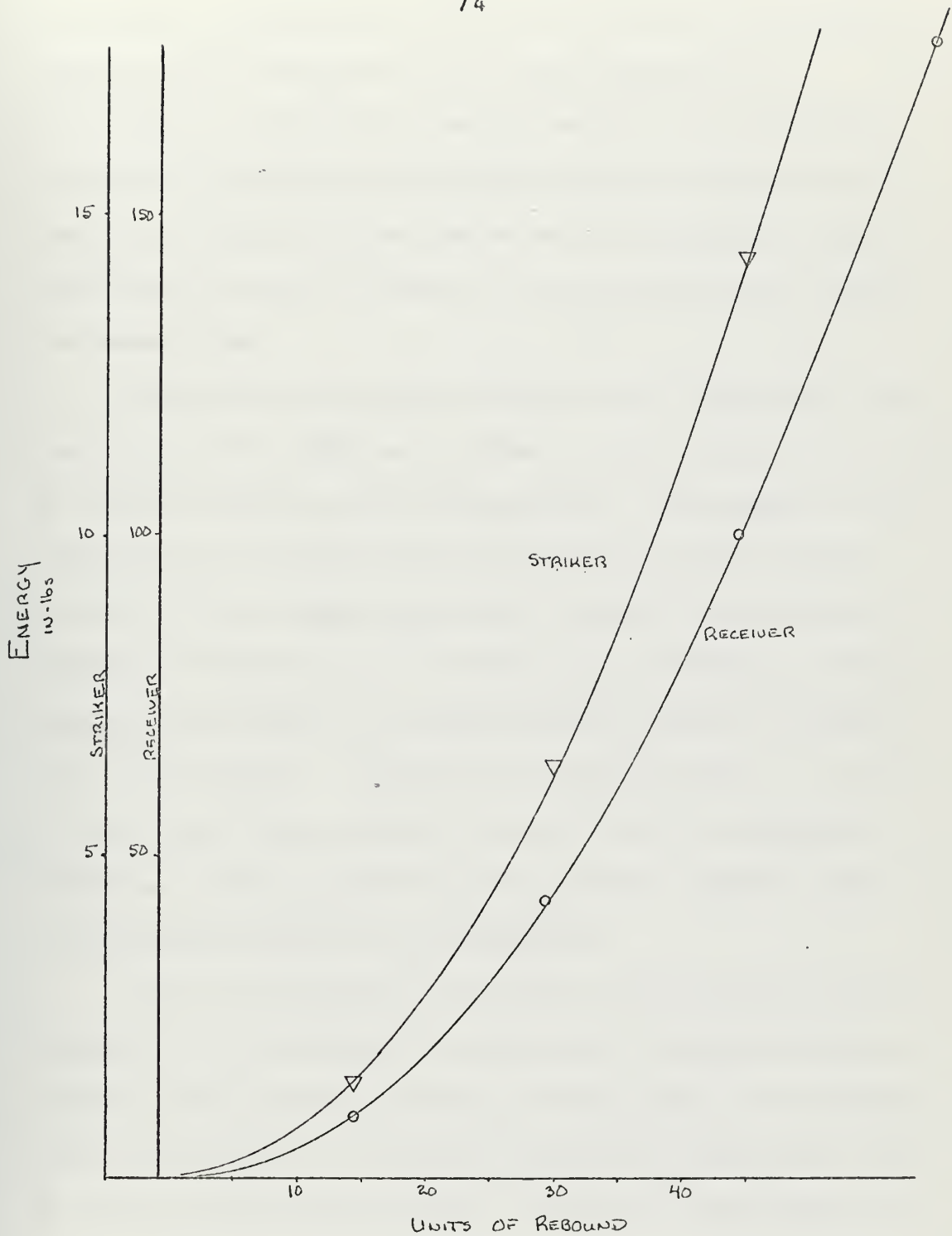


FIGURE 25 RECEIVER CALIBRATION CURVE





STRIKER 1 UNIT =  $1.86 \times 10^{-2}$  INCH VERTICAL RISE

RECEIVER 1 UNIT =  $2.066 \times 10^{-2}$  INCH VERTICAL RISE

FIGURE 26 AID TO DETERMINATION OF ENERGY



the damaged area would give an accurate indication of the total damage suffered regardless of the outward appearance of the specimen. This method of testing would give an indication of the total continuity of the material and also validate the assertion of Bezukladov that the action of the mesh in holding the crushed particles of concrete in place retarded flow through the damaged areas.

The water-testing device consisted of a pressure box which was fitted to the sample and a storage container which was maintained at a constant height above the pressure box. The pressure box was constructed of an 8-inch square mild steel plate with a 2-inch section of 6-inch diameter steel pipe, 1/4 inch wall thickness, welded to the bottom face. The outer lip of the pipe was fitted with a 0.5-inch thick soft neoprene gasket to insure an adequate seal on all surfaces. The plate was tapped to receive a standard 3/8 inch pipe fitting to which, through the use of appropriate adapters, a standard garden hose was attached. Figure 27 shows the construction details of the apparatus.

The hose connected a five gallon storage reservoir and the pressure box. The reservoir was fitted with a glass sight-gauge, enabling one to maintain a constant starting head on all samples. The reservoir was also fitted with appropriate connections so that it could be filled between tests. A standard 0.5-inch globe valve





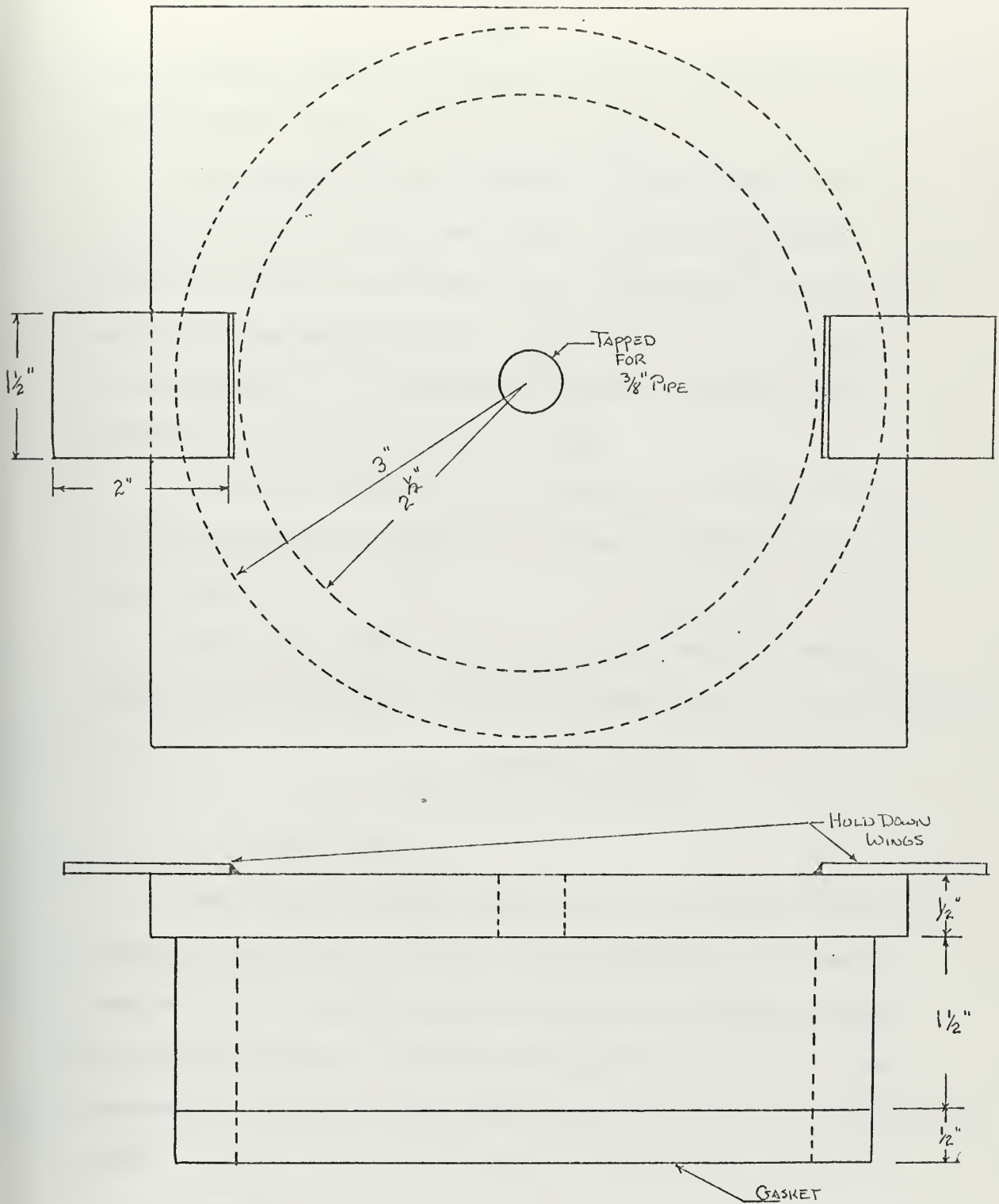


FIGURE 27 WATER TEST DEVICE



was utilized to control the flow of water to the pressure box.

Figure 28 shows the reservoir and the pressure box.

The pressure box was clamped on to the sample by two C-clamps while the sample was attached to the sample plate. Sufficient pressure was applied with the C-clamps to compress the neoprene on the sample and give a water-tight fit. The pressure box was applied to the rear face of the sample and the entire combination was placed over a catch pan.

The water collected in the catch pan in a fixed amount of time was measured in a graduated container to obtain the flow rate after damage.

The maximum investigated flow rate through the existing connections was determined through experimentation to be 4900 ml/min.

## IX. TESTING PROCEDURES

### A. TENSILE TESTS

The tensile specimens were tested in an INSTRON Universal testing machine in pure tension. The load-deflection curve was recorded on the machine's graph recorder for a permanent record. The loading rate in all tests was 0.05 inches per minute. Upon completion of the test, the desired data was taken from the recorded chart.

Naaman<sup>52</sup> noted that the method of utilizing the load-deflection



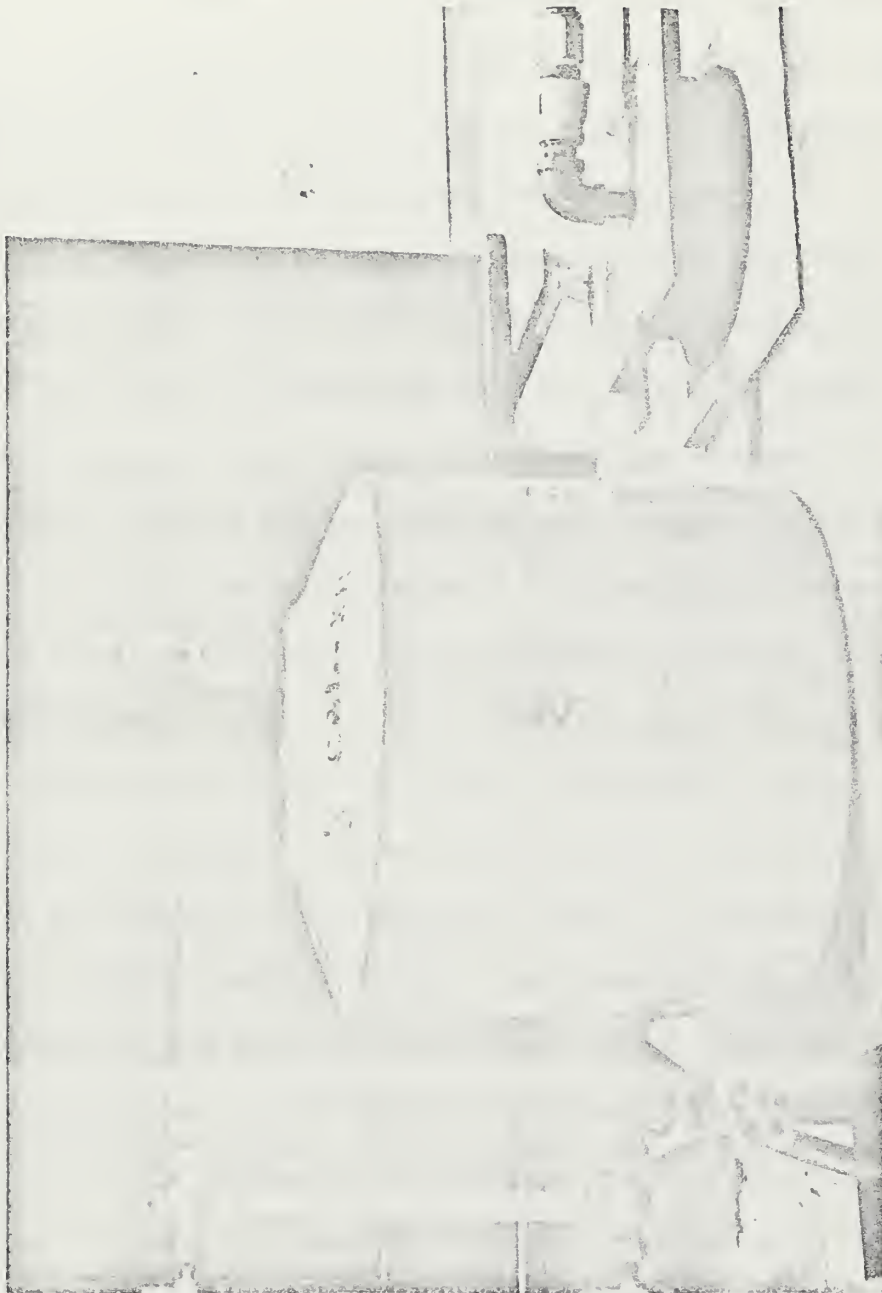


FIGURE 28



curve of the INSTRON was affected by the strain of the machine. He stressed the machine alone and measured the load-deflection curve. A significant strain was measured for the machine alone as seen in Figure 29 . On all samples, a machine correction factor was applied before any calculations were attempted.

Upon completion of testing, however, there was noted a discrepancy between the values of the modulus for welded mesh and for steel alone. Welded mesh does not have to straighten out, and therefore should have the same modulus as steel. This discrepancy could not be rectified and would indicate that the INSTRON correction was not adequate. It would appear, however, that the data obtained still indicates trends, although off by constant factor.

The load-deflection curve was, in all cases, linear to some point where it changed slope and was again linear until the yield point of the material became obvious. Naaman and Muhlert noticed that this initial change in slope of the load-deflection curve denotes the cracking of the specimen and also noted that once past this point, generally no further cracks are formed. In consideration of the above and the difficulty of ascertaining visually the first crack, the point of change of slope of the load-deflection curve was utilized to denote the stress of the first crack in the composite. The tangent modulus was used to determine the modulus of the composite, both before and after cracking.





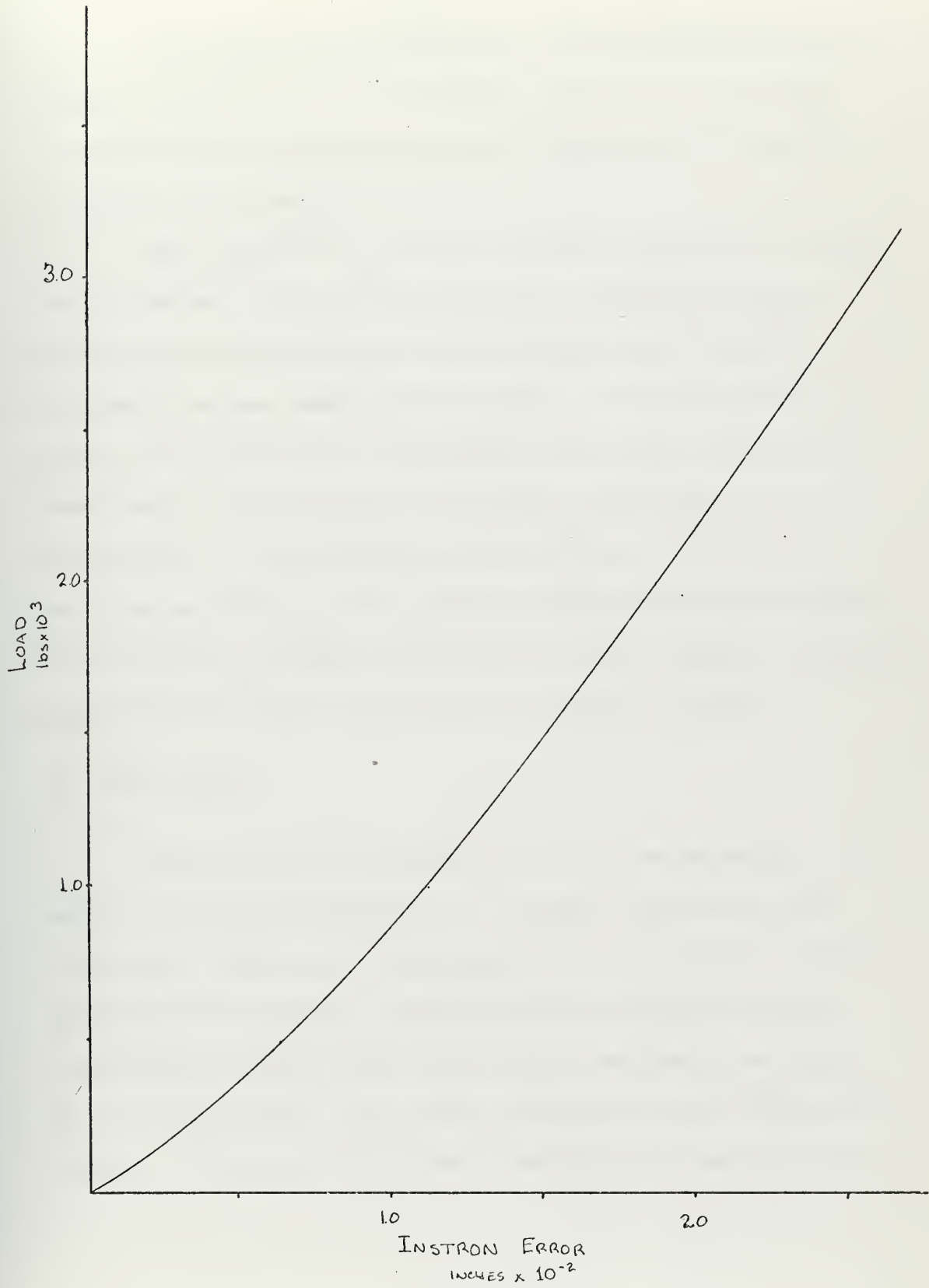


FIGURE 29



The specimen was observed with a 5x magnifying glass while being stressed and immediately before failure, the total number of cracks was noted and the position of each crack was marked on the sample with a pencil.

Upon completion of the test, selected samples were examined and the average crack width was determined visually, by taking the average of five widths on each sample and then averaging this value for each sample and obtaining an average value for the series. The five points of measurement were spaced evenly on the sample and a representative crack located in the region of a point was measured. It was necessary to be arbitrary in the selection of the crack as a result of the generally destructive mode of failure of the sample. The sample was coated with lime and water (whitewash) on the observed face to facilitate the location of cracks.

#### B. IMPACT TESTS

Impact tests were conducted in the following manner. The sample was tested successively at a constant loading level and after each loading cycle was subjected to the water test for the determination of damage. The water head was applied for thirty seconds and the water which flowed through the sample was measured in a graduated beaker. Also, upon completion of each loading cycle, the rear deflection and the front indentation were measured with an



Ames .001 inch dial indicator and visual observations were made and recorded.

A test was halted at the sixth loading cycle or at complete failure of the matrix (complete fallout), whichever came first.

The rear face of the sample was, as in the tensile specimens, coated with lime and a circular grid was inscribed in the lime to facilitate identity of damage.

The energy absorbed by the sample was the difference between the potential energy of the striker before impact and the potential energy of both the striker and the receiver at their point of maximum travel. Total energy absorbed by the sample is a sum of the energy absorbed in each loading cycle up to the maximum number.

The weight of the striker pendulum was determined to be 22.938 pounds representing a potential energy of 243.716 inch pounds when raised to a release height of 10.625 inches. The release height of 10.625 inches was maintained constant throughout the experiment. The weight of the receiver pendulum, with the sample in place, was determined to be 143.686 pounds.

The starting head of water used in the water tests was maintained constant at 3.37 feet throughout the investigation. No allowance was made to maintain a constant head while the experiment was in progress.



## X. EXPERIMENTAL RESULTS

### A. TENSILE TESTS

Tabular results of all tensile test series H, M and L, and X are presented in Appendix A. Also found in Appendix A are photographs of the tensile samples taken after the specimens had been tested.

### B. IMPACT TESTS

Tabular and graphical display of impact tests series H, M, and L are presented in Appendix B. Also found in Appendix B are photographs taken at completion of testing.

### C. WIRE MESH

Tabular results of observed performance of wire meshes can be found in Appendix C.





## XI. DISCUSSION OF RESULTS

## A. TENSILE TESTS

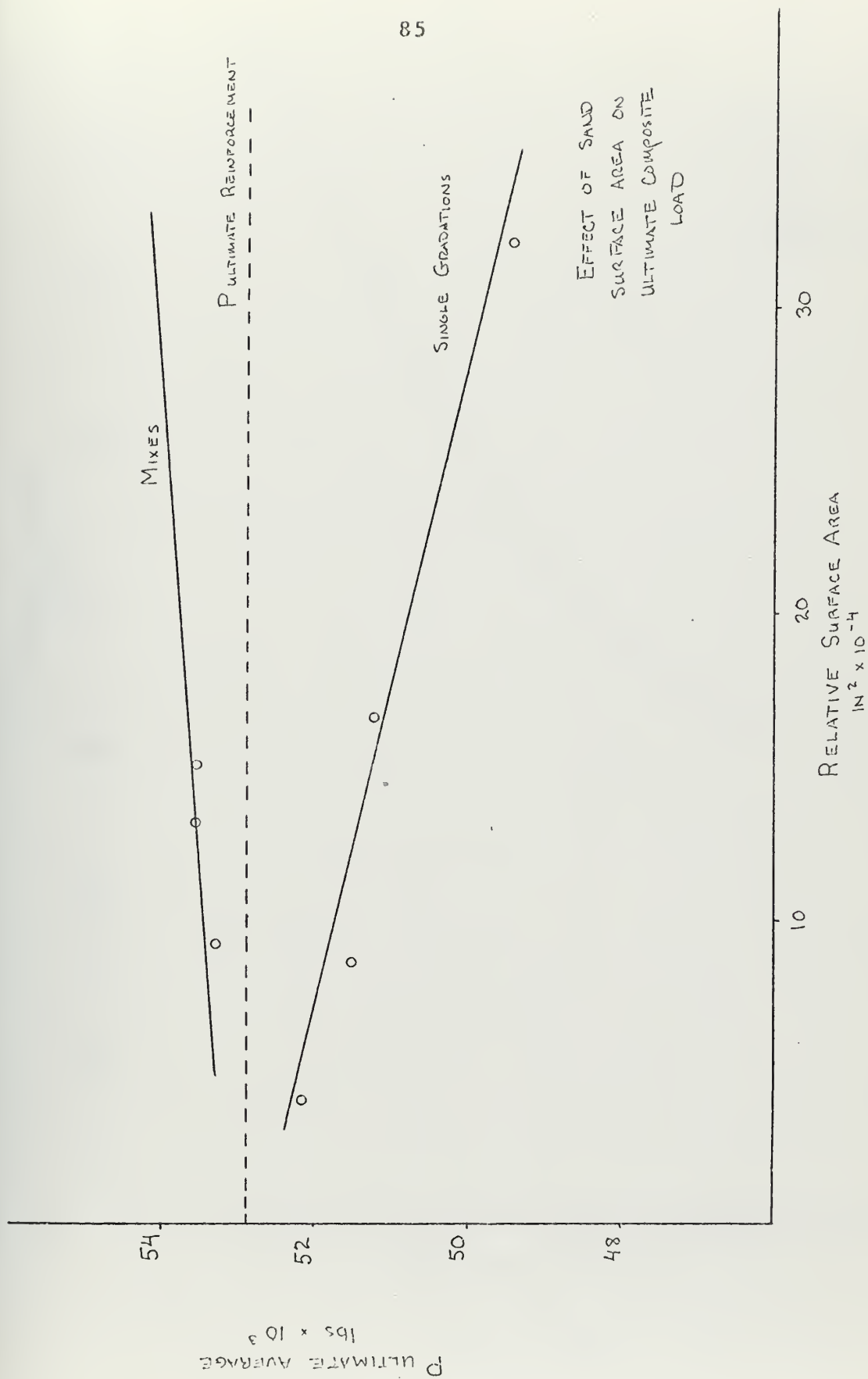
Series X data indicated that the composition of the matrix had little effect on the performance of ferro-cement. Figure 30 shows the ultimate composite load as a function of relative surface area of the sand and the total variation of ultimate load was less than 10%. There is, however, a noticeable trend of increasing ultimate load with decreasing surface area of sand with single gradations and increasing ultimate load with increasing surface area of sand for mixes.

Values for ultimate loads obtained experimentally exceeded slightly the calculated ultimate load for the reinforcement alone, indicating a slight contribution from the matrix.

Experimental results obtained from the investigation of the effect of sand/cement ratio do not correlate with those of Collen as he indicated an optimum sand/cement ratio of 1.51 and this investigation showed an increasing trend of ultimate load with decreasing sand/cement ratio. Figure 31 shows the plotted values.

Figure 32 gives the performance of ferro-cement made with lightweight aggregates. It can be seen that while expanded shale did not reach the ultimate load of the wire, vermiculite did. The weight savings for expanded shale was less than 10% while vermiculite gave better than 30%.





EFFECT OF SAND  
SURFACE AREA ON  
ULTIMATE COMPOSITE  
LOAD

FIGURE 30



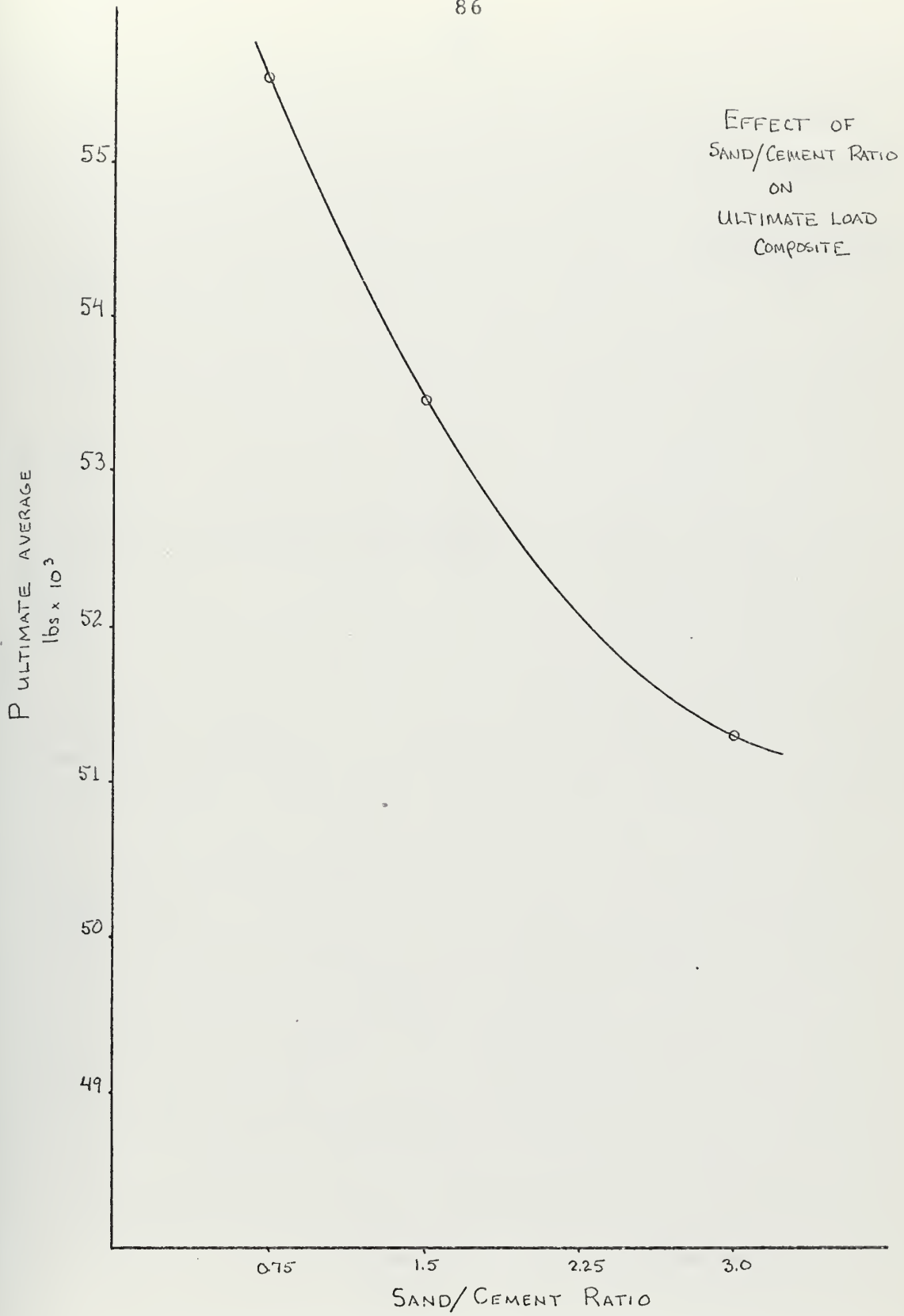


FIGURE 31



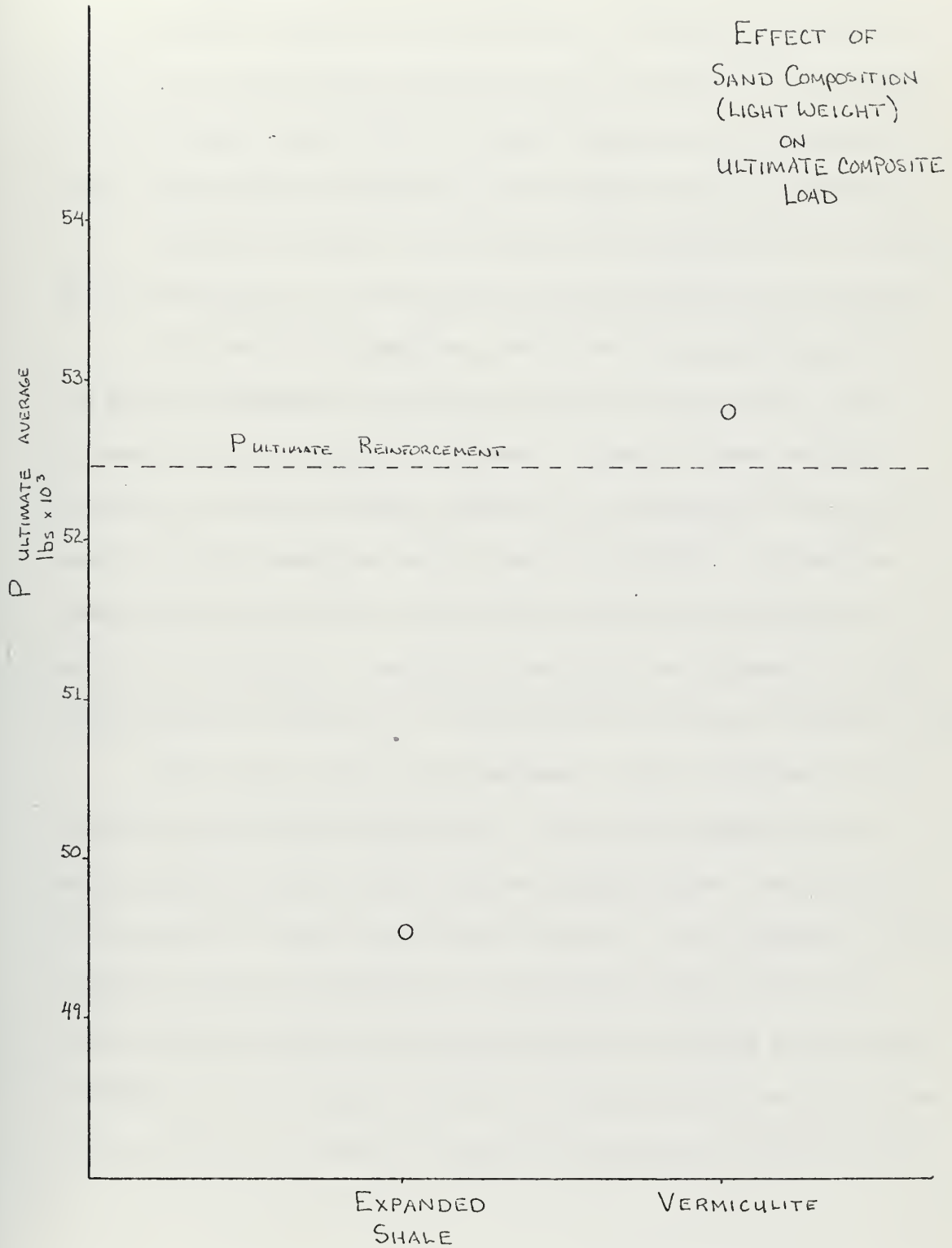


FIGURE 32





The failure of the samples in the above investigations to continuously exceed by a large amount the calculated ultimate load of the reinforcement indicates that the effect of the matrix on the ultimate capabilities of ferro-cement is very little and would indicate that the effect of the reinforcement is dominant.

Series H, M, and L, as a result of the above, were continued as an investigation of the effect of reinforcement on ferro-cement.

In these investigations, the volume of reinforcing steel was held approximately constant so that the stress in the reinforcement was approximately constant. Stress is transferred to the matrix through the shear bond and is a function of the surface area of reinforcement per unit volume of material. The surface area of reinforcement per unit volume of material is defined as specific surface,  $S_s$ . The specific surface was increased in these investigations by going to a greater number of smaller diameter wires.

The matrix, being non-homogenous, can be expected to have variations in strength capability. The stress induced in the matrix combined with areas of stress concentrations cause failure of the matrix at these preferential points. As the specific surface increases, stress transferred to the matrix becomes more evenly distributed and cracks will occur initially at points of low matrix strength until all areas in which the induced stress and the stress concentration can combine to exceed the capability of the matrix,



at which time there will be no further cracking.

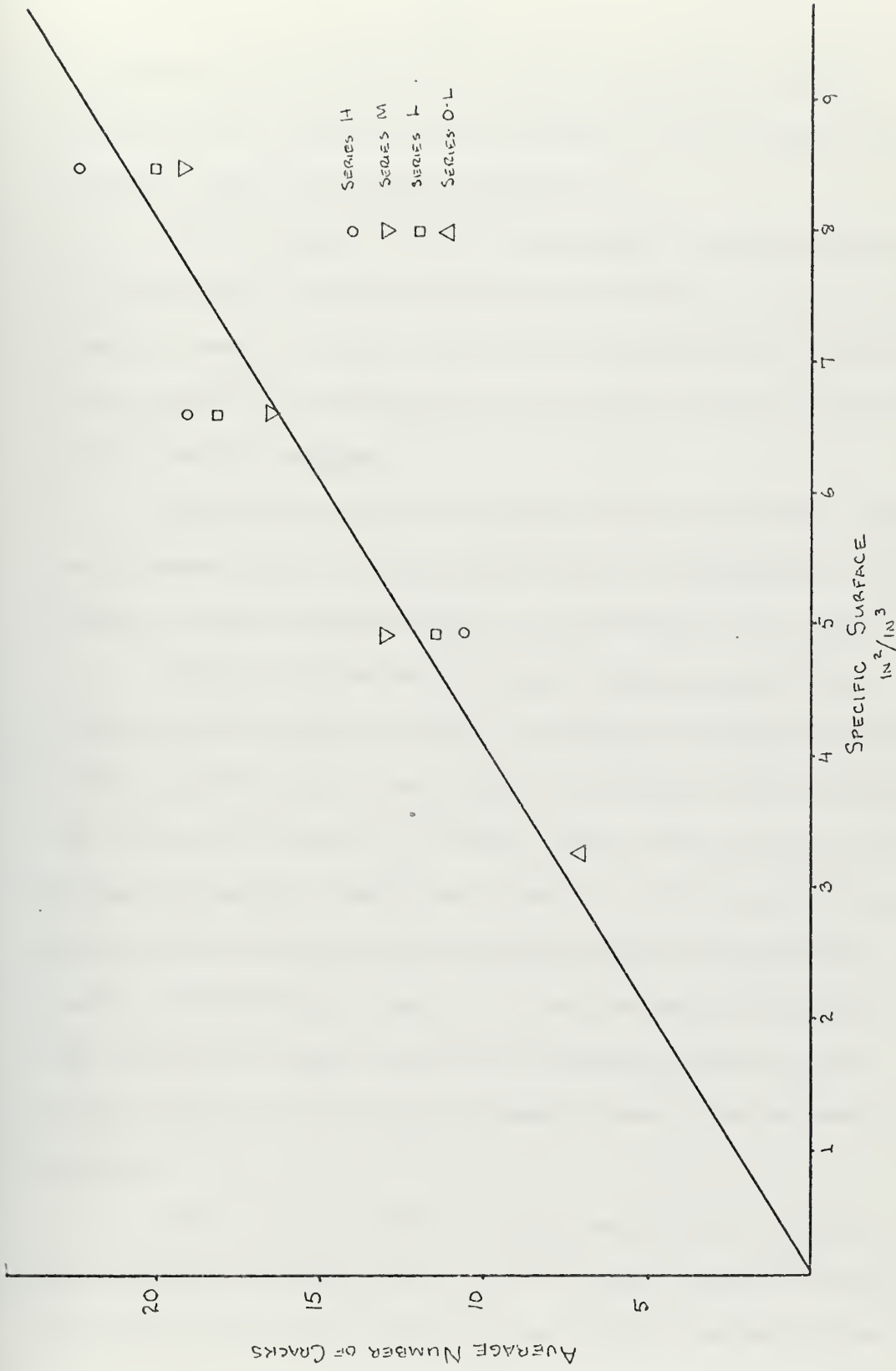
As the specific surface increases, stress transferred to the matrix becomes more evenly distributed with fewer areas of high induced stress. Since the stress is more evenly distributed, a stress which exceeds the tensile strength of the mortar at first crack should be reached at a higher composite stress.

As a result of the woven wire mesh reinforcement, there exists in tension a point of stress concentration where each wire crosses over another. As the stressed wires attempt to straighten out, they attempt to force the transverse wires outward, causing highly stressed areas in the matrix in these regions.



It may be drawn from this that with increasing specific surface, an increasing number of cracks can be expected until a maximum number is reached, as in Figure 33. This maximum number should correspond to the number of transverse wires in the section and the cracks should occur preferentially over the cross-over or nodal points. It also can be expected that there will be no further cracking due to the lack of additional areas of stress concentration to raise the total stress in the composite remaining to  $\sigma_c$ .





EFFECT OF SPECIFIC SURFACE ON NUMBER OF CRACKS  
FIGURE 33



It further can be expected that increasing specific surface will raise the composite stress necessary for the formation of the first crack as is shown in Figure 34 .

Now if Figure 33, where the number of cracks is plotted as a function of specific surface is considered, it can be seen that the number of cracks appears to be insensitive to changes in the strength of the reinforcement and only performs as a function of the specific surface.

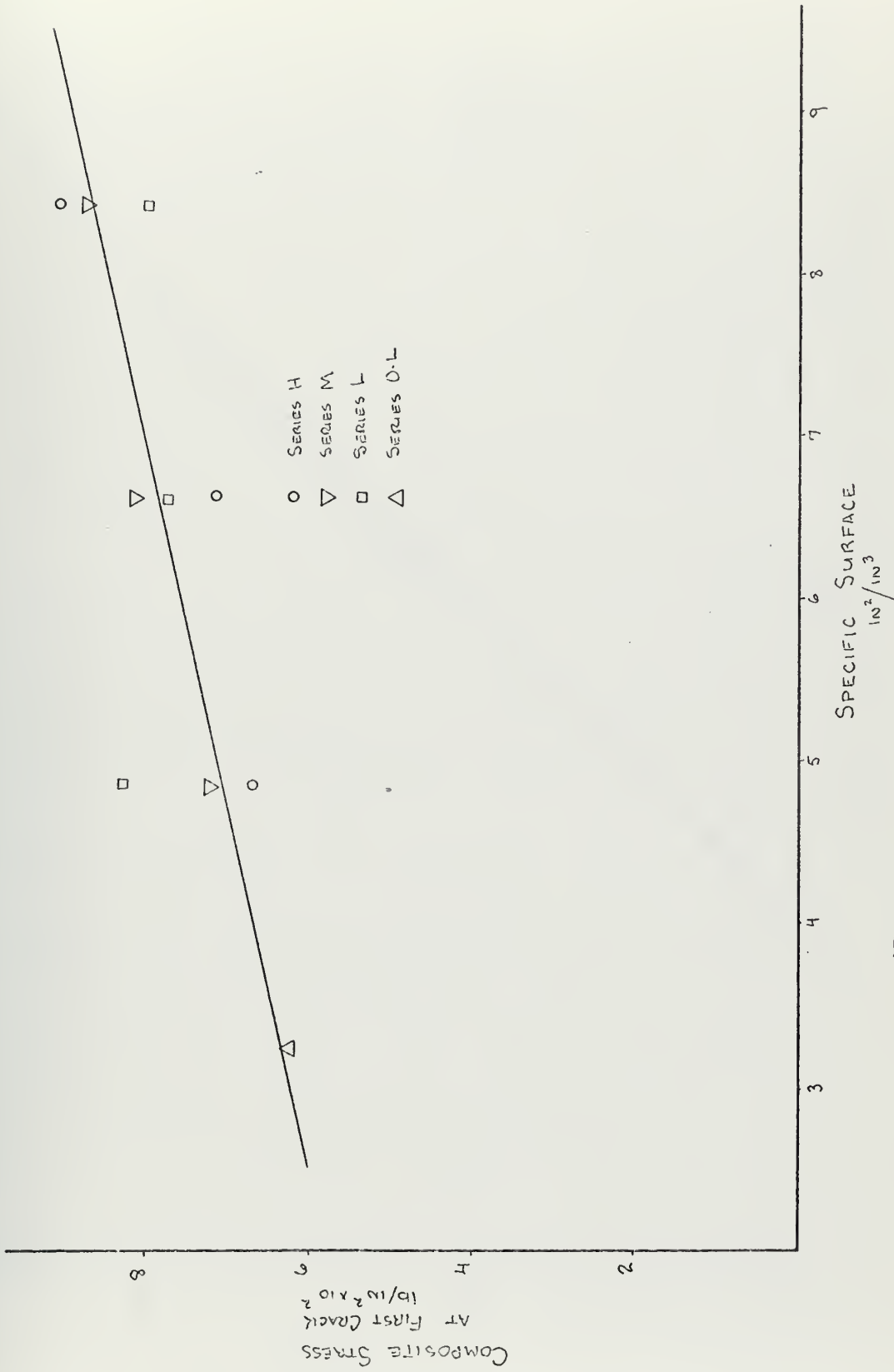
Once the number of cracks has reached the maximum number as discussed above, it would appear that the performance of the material becomes dependent upon the performance of the steel.

Figure 35 shows the calculated ultimate load of the reinforcement as plotted against the observed ultimate strength of the composite and it can be seen that only one point exceeded the calculated ultimate. The other points fell below the calculated ultimate strength, probably as a result of the selective failure of one or two strands with the resultant complete failure due to excess load on the remaining strands. It does not appear that there exists any synergistic action and that the ultimate strength of the reinforcement is the limit of ultimate strength ferro-cement in tension.

Once the full number of cracks has formed, the modulus of the composites should appear to be the same because the modulus of steel is  $30.0 \times 10^6$  lb/in<sup>2</sup> and the steel is exposed between the







EFFECT OF SPECIFIC SURFACE ON COMPOSITE STRESS AT 1<sup>ST</sup> CRACK  
FIGURE 34



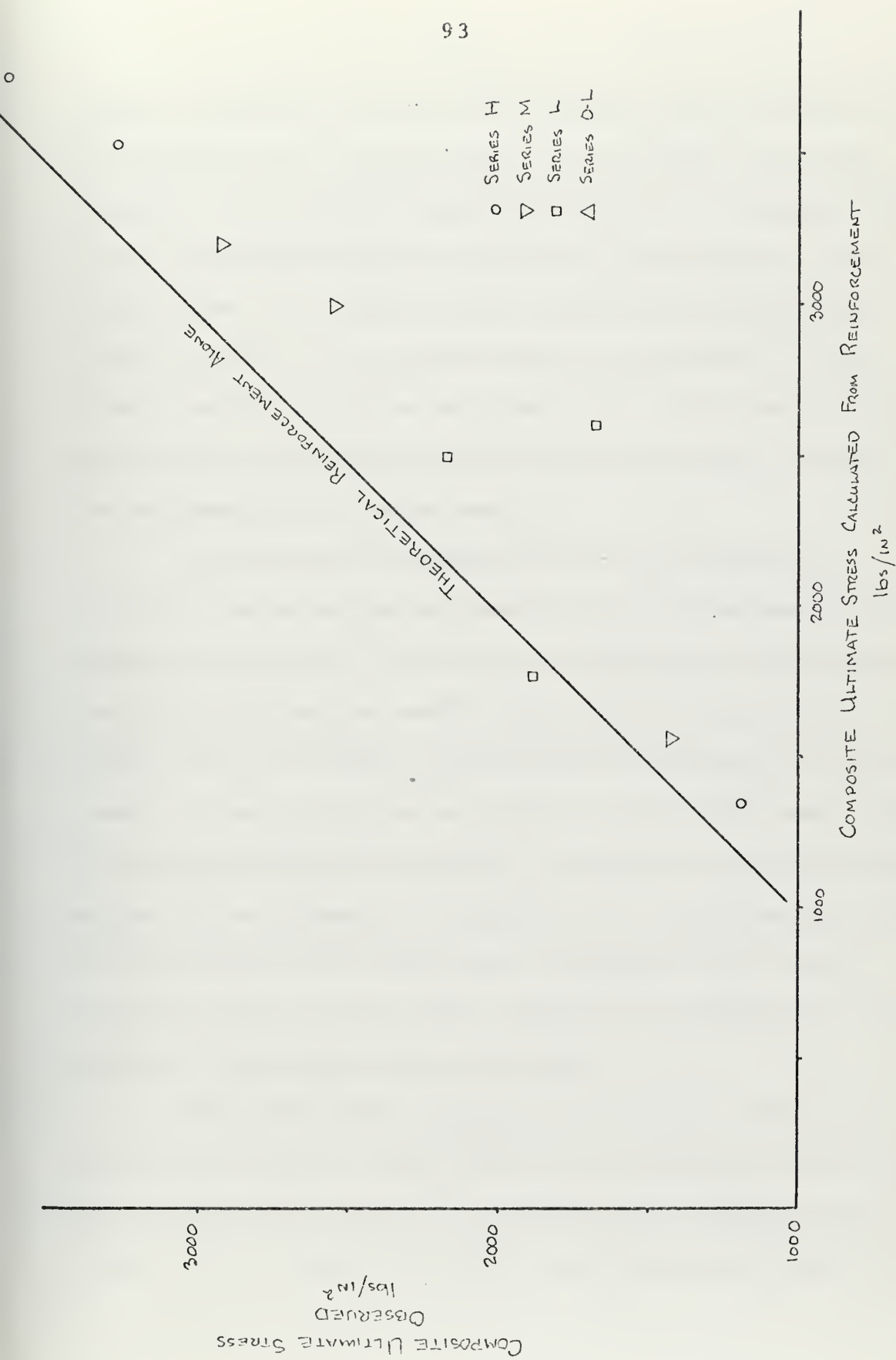


FIGURE 35



cracks. In Table 10 it can be seen, however, that the modulus of the composite after cracking varies as the strength of the reinforcement. Examination of Appendix C shows that the apparent modulus of wire alone also varies as a function of the strength of the reinforcement. As a result of the strength of the reinforcement having an effect on the apparent modulus of elasticity, it would appear then that as long as the stress on the reinforcement remained in the elastic region, the strength of the reinforcement affects the performance of the ferro-cement.

If the modulus of elasticity of the reinforcement is calculated, using the observed results of the reinforcement tensile tests and is compared to the modulus calculated from the observed results of the composite tensile tests, then it can be seen in Figure 36 that the modulus calculated from the composite, in most cases, is greater than that calculated from the reinforcement alone. It would appear that in some cases, the presence of the matrix does enhance the performance of the composite to a certain degree; however, it would appear that a lower bound, as indicated by the line of calculated modulus of wire alone, exists for the prediction of the modulus of the composite after cracking.

Once yield stress is exceeded for the mesh, cracks will widen until failure occurs. Crack width will be a function of the ductility of the reinforcement, which is a function of the strength of the steel. Figure 37 shows crack width after failure as a function of



Sample	Average Composite Modulus Before Cracking	Average Composite Modulus After Cracking
6-0-H	$2.59 \times 10^6$	$0.559 \times 10^6$
6-0-M	$1.94 \times 10^6$	$0.509 \times 10^6$
6-0-L	$1.43 \times 10^6$	$0.472 \times 10^6$
4-1-H	$1.11 \times 10^6$	$0.52 \times 10^6$
4-1-M	$1.56 \times 10^6$	$0.547 \times 10^6$
4-1-L	$0.978 \times 10^6$	$0.481 \times 10^6$
2-2-H	$2.37 \times 10^6$	$0.633 \times 10^6$
2-2-M	$1.32 \times 10^6$	$0.617 \times 10^6$
2-2-L	$0.879 \times 10^6$	$0.475 \times 10^6$

TABLE 10





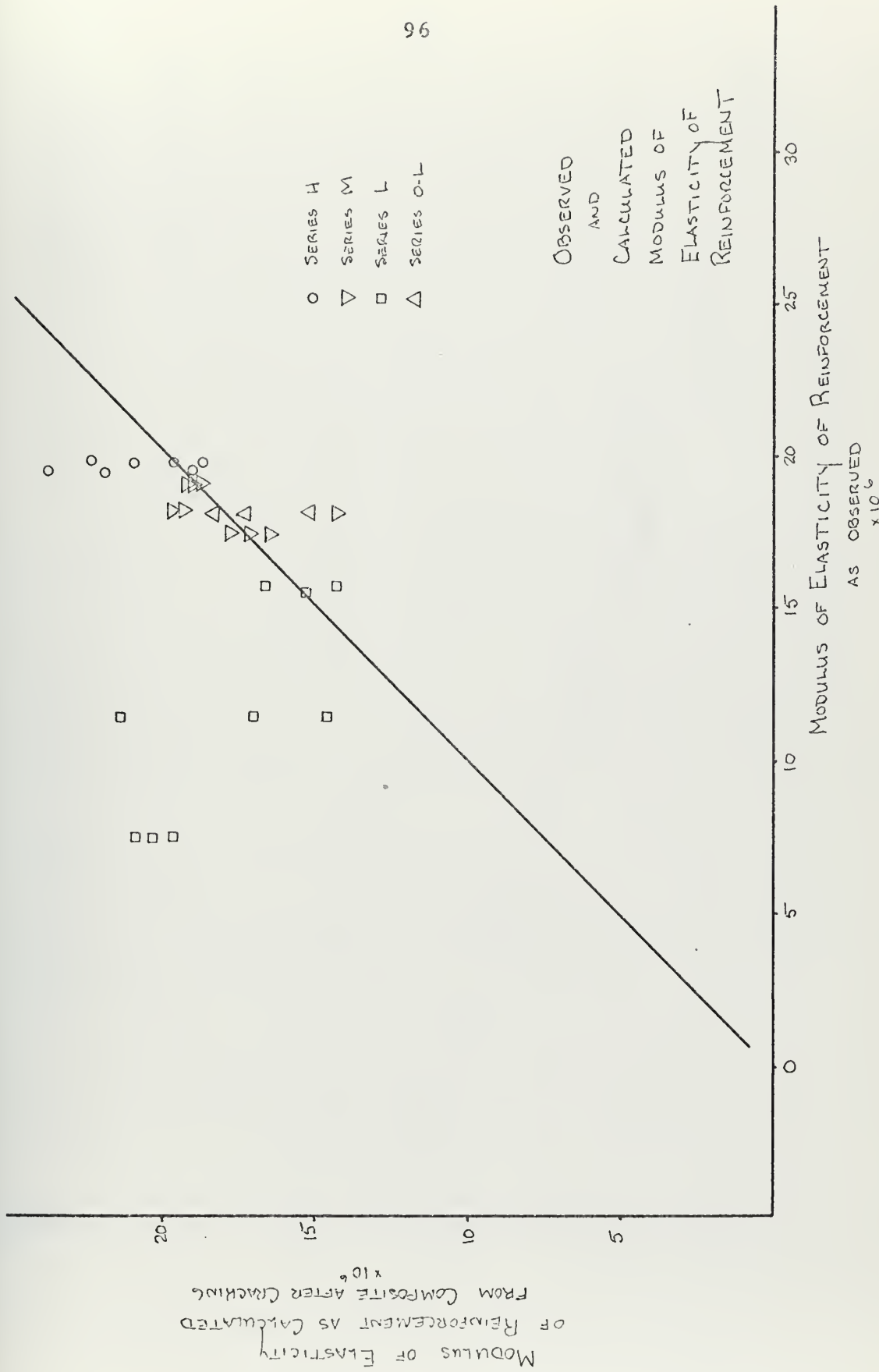


FIGURE 36



EFFECT OF  
ULTIMATE LOAD OF  
REINFORCEMENT  
ON  
CRACK WIDTH AFTER  
FAILURE

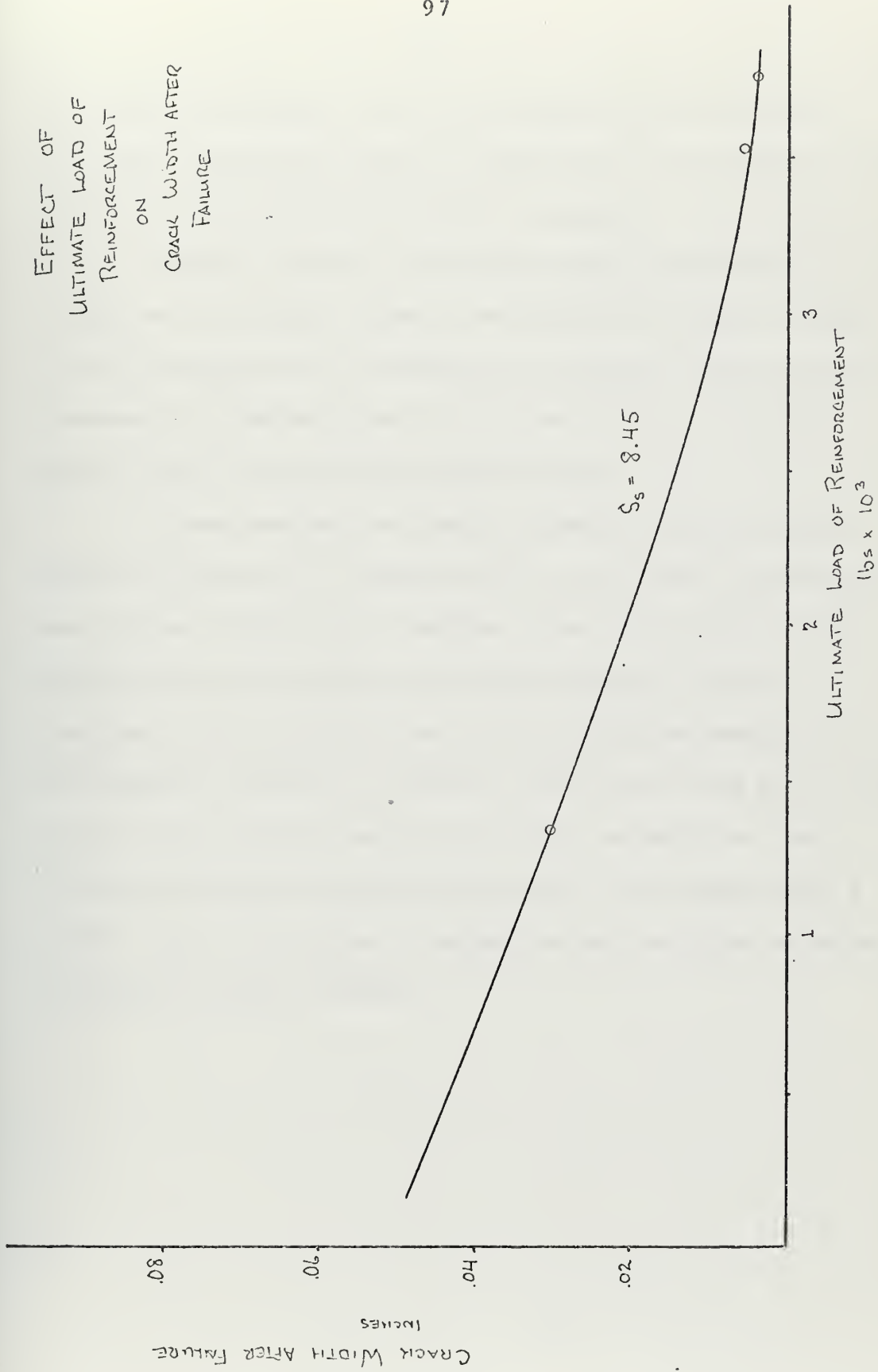


FIGURE 37



the calculated ultimate load of the sample and it can be seen that with increasing strength of reinforcement, the average crack width for constant specific surface decreases.

Ultimate strength of the woven mesh reinforcement has an effect on the cracking stress of the composite as seen in Figure 38. It was anticipated that increasing the strength of the mesh would increase the cracking stress and this was observed in the 6-0 series where there was observed 15% increase.

It was observed, as shown in Appendix C, that although steel has a modulus of elasticity of  $30 \times 10^6$  lb/in<sup>2</sup>, the woven wire mesh did not display such a modulus. Since the variance of the modulus of steel is small and the mesh is steel, it must be concluded that the observed modulus is an apparent modulus,  $E_a$ . The apparent modulus is a function of the weave of the mesh, the gauge of the wire, and the strength of the wire composing the mesh. Interaction between the woof and the warp of the weave causes a normal force to be created to deform the mesh to allow the wires to straighten out under tension.



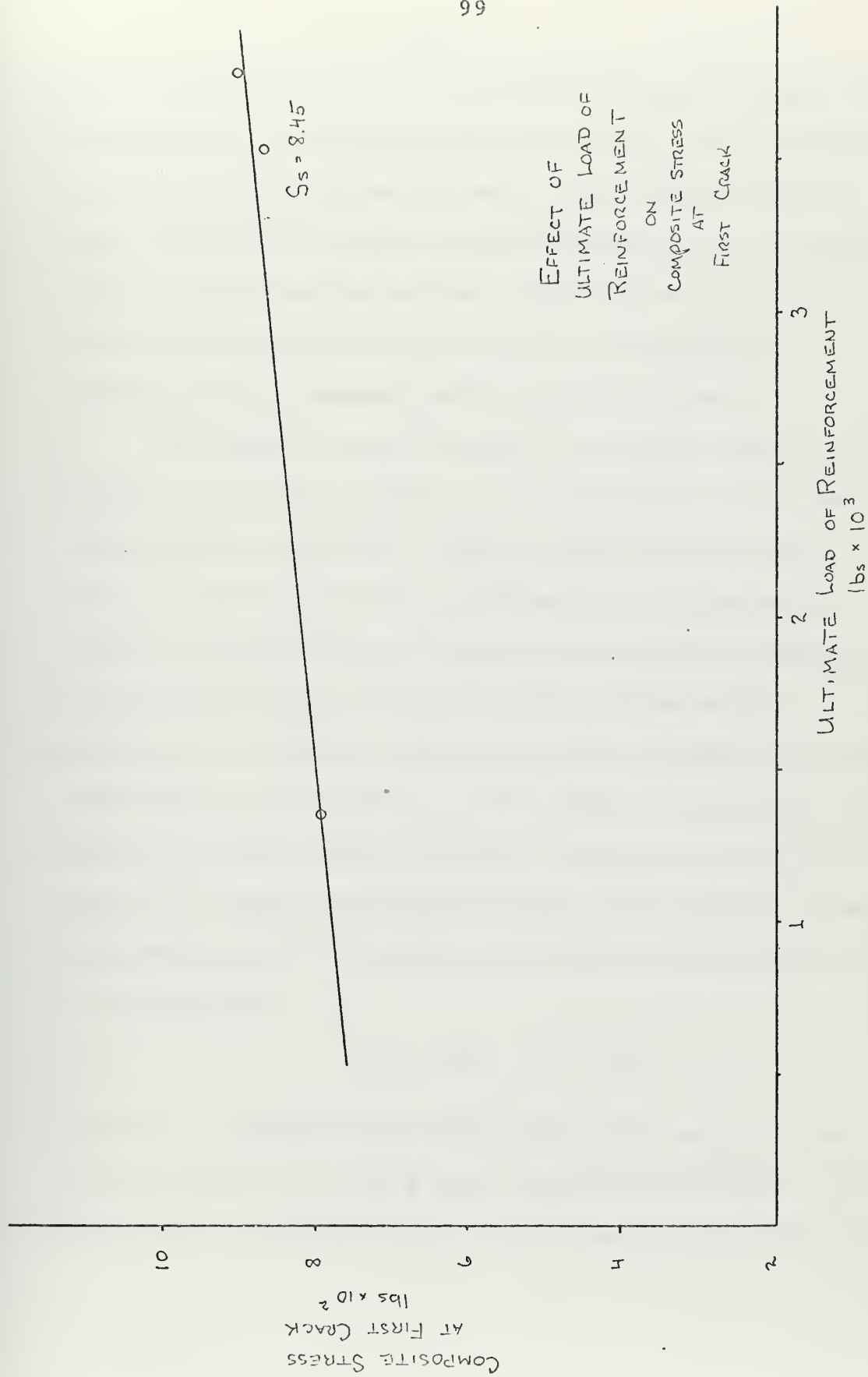


FIGURE 38





The perpendicular wires oppose the deformation and this opposition is a function of the yield strength of the mesh and any mechanical bond that exists in galvanized mesh. With a higher strength mesh, deformation is opposed, apparent elongation of the stressed wires is reduced and the apparent modulus increases, or if a mechanical bond exists at the nodal point, restraint will be introduced and the apparent modulus will be increased.

Following the same reasoning, if the gauge of the wire is decreased (increasing diameter), the angle formed by the wires crossing will be increased. Since the normal force is equal to  $T \sin X$ , increasing the angle  $X$  decreases the tensile force  $T$  required to deform the mesh, increasing the apparent elongation of the stressed wire, and decreasing the apparent modulus. If the gauge of the wires is held constant, and the mesh size decreased, there will be the same effect as decreasing the gauge of the wire. Therefore it would seem that mesh with a large angle  $X$  or low yield stress will exhibit low apparent modulus. The modulus of a composite is a combination of the modulus of the matrix and the modulus of the reinforcement.

$$E_c = E_r V_r + E_m (1 - V_r)$$

Therefore, a composite with reinforcement which exhibits a low apparent modulus will have a lower composite modulus than a composite modulus than a composite with a high apparent modulus reinforcement.



The composite with the lowest modulus will, for equal stress, be strained more than a composite with a larger modulus. It would appear then, that a composite with a reinforcement which exhibits a high apparent modulus will crack at a higher stress than one with a lower modulus reinforcement.

When the 6-0 series, which consisted of one strength reinforcement, is considered, it can be seen that the composite with the reinforcement which has a higher yield stress than the others, cracks at higher stress.

Figure 39 shows the performance of the composite as a function of the ultimate strength of the outer reinforcement. It can be seen that each series that used increased ultimate strength of the outer reinforcement caused an increase in the ultimate capacity of the composite. Series 6-0 and 4-1 showed a continuing increase with the increasing strength of reinforcement while 2-2 appeared to reach a maximum strength and then decreased with increasing reinforcement strength. An explanation for this performance could be as explained above.

It appears, however, that the incompatibility of the ultimate strength and the difference in volumes of the two types of reinforcement causes a premature failure of the single layer of outer reinforcement, with a resultant drop in the ultimate capability of the composite.



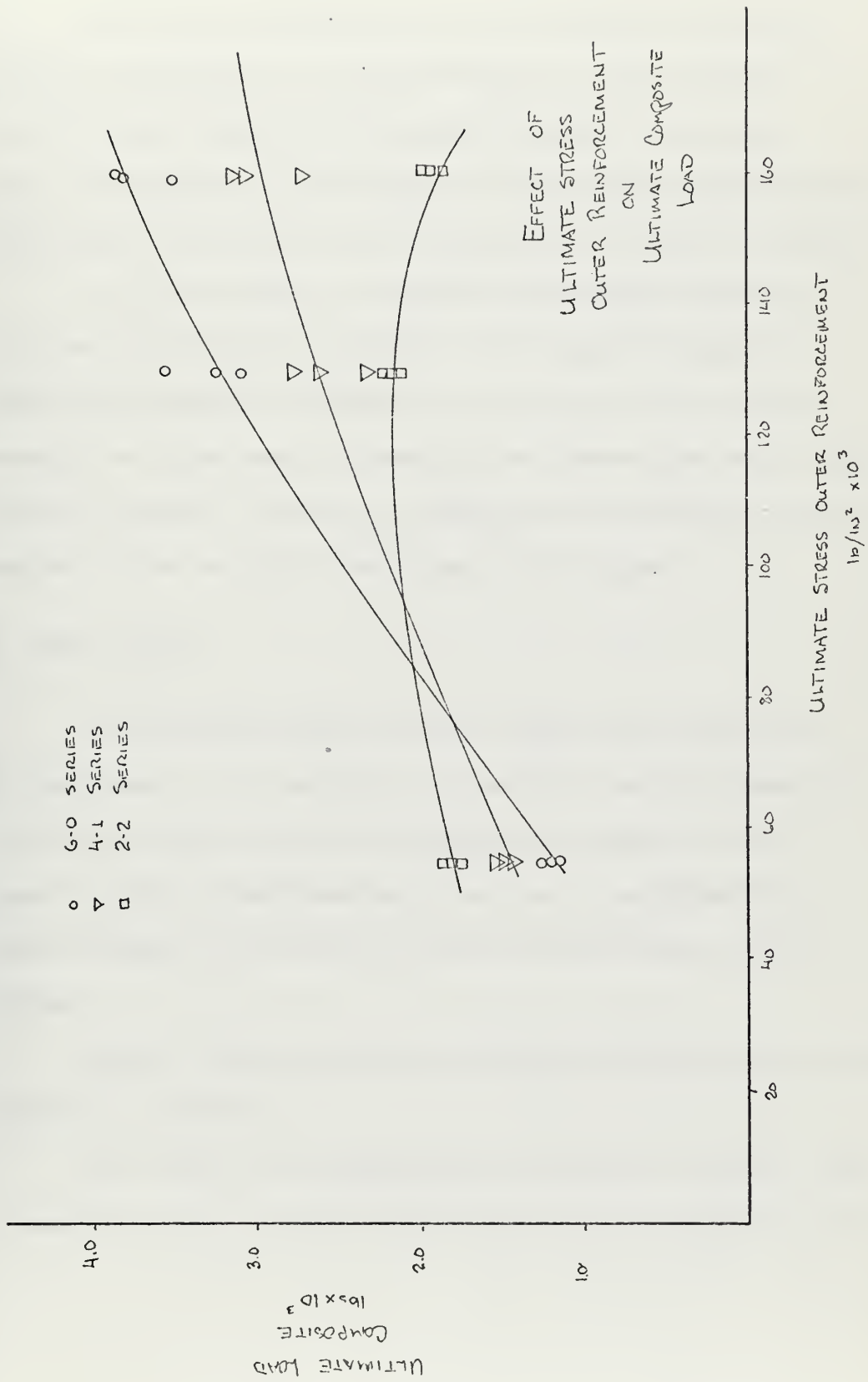


FIGURE 39



The increased performance of the composite when higher strength reinforcement is used would seem to follow from the fact that once a crack has formed and no further cracks are formed, the property of the composite is dependent upon the material properties of the steel, which is exposed in the crack or cracks.

It is not possible to consider the results obtained as being any indication of the effect of the number of layers of outer reinforcement. The effect of the difference in ultimate strength was large enough to override any observations which could have been possible. The use of compatible reinforcements would be required before any valid conclusion could be drawn.

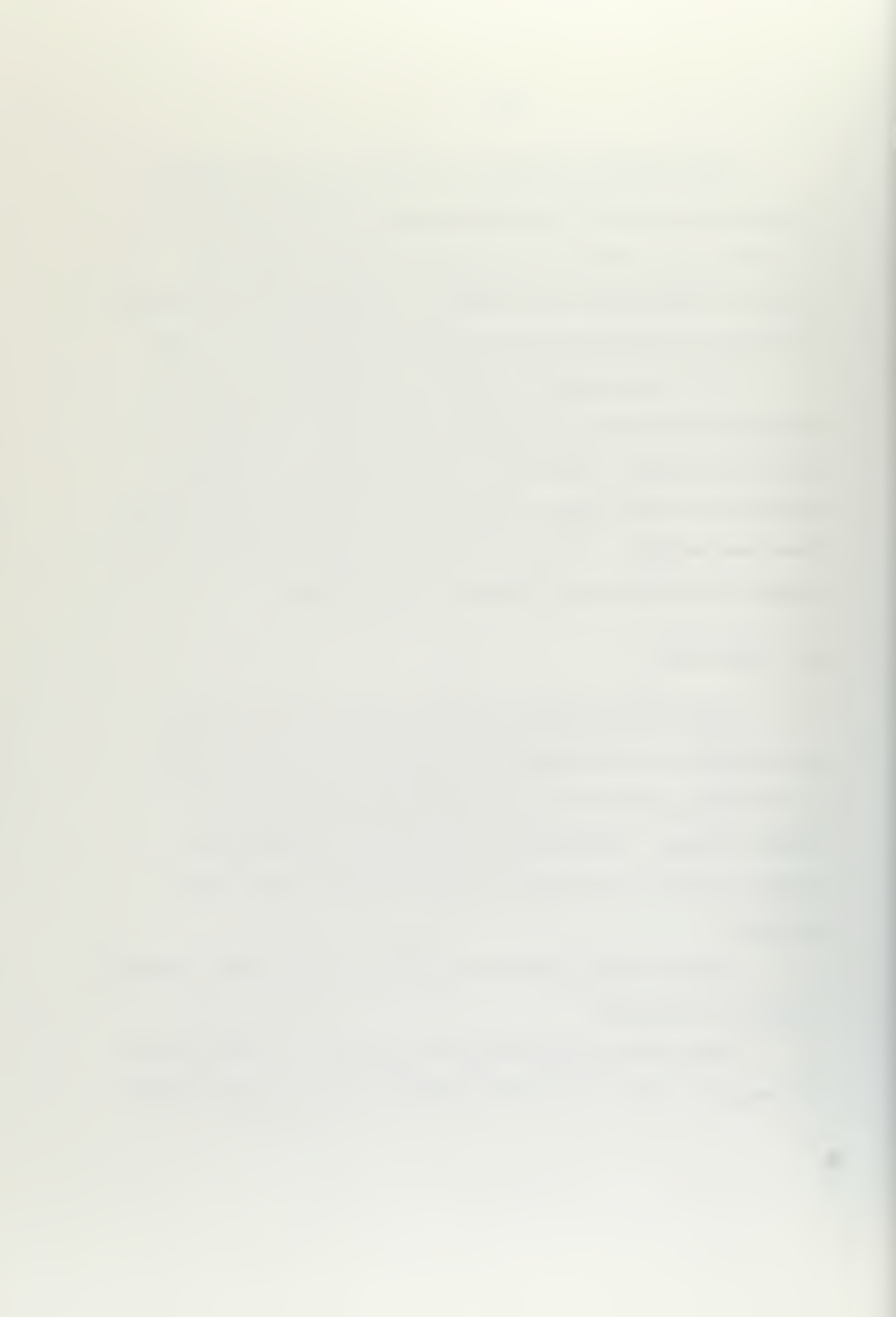
#### B. IMPACT TESTS

If the above is true that once cracks have formed then the performance of the material is dependent upon the properties of the steel, then it should be possible to extend this into dynamic loading. Two-dimensional loads can be explained by a similar argument as the above, so that the above theory can be applied.

Dynamic loading cannot be considered as equivalent to tensile loading in complexity.

Many people have investigated the effects of dynamic loads on concrete as well as many other metallic and non-metallic solids.





However, due to the complexity of the problem there exist only solutions for elastic and semi-plastic solids which would not be applicable in a situation with a composite material.

If an homogenous solid is subject to impact loading, an initial stress wave propagates from the point of impact spherically outward. The stress wave caused in the material can be approximated by the following equation, where its particle velocity can be calculated from the impact.

$$\sigma_x = \rho c_x V$$

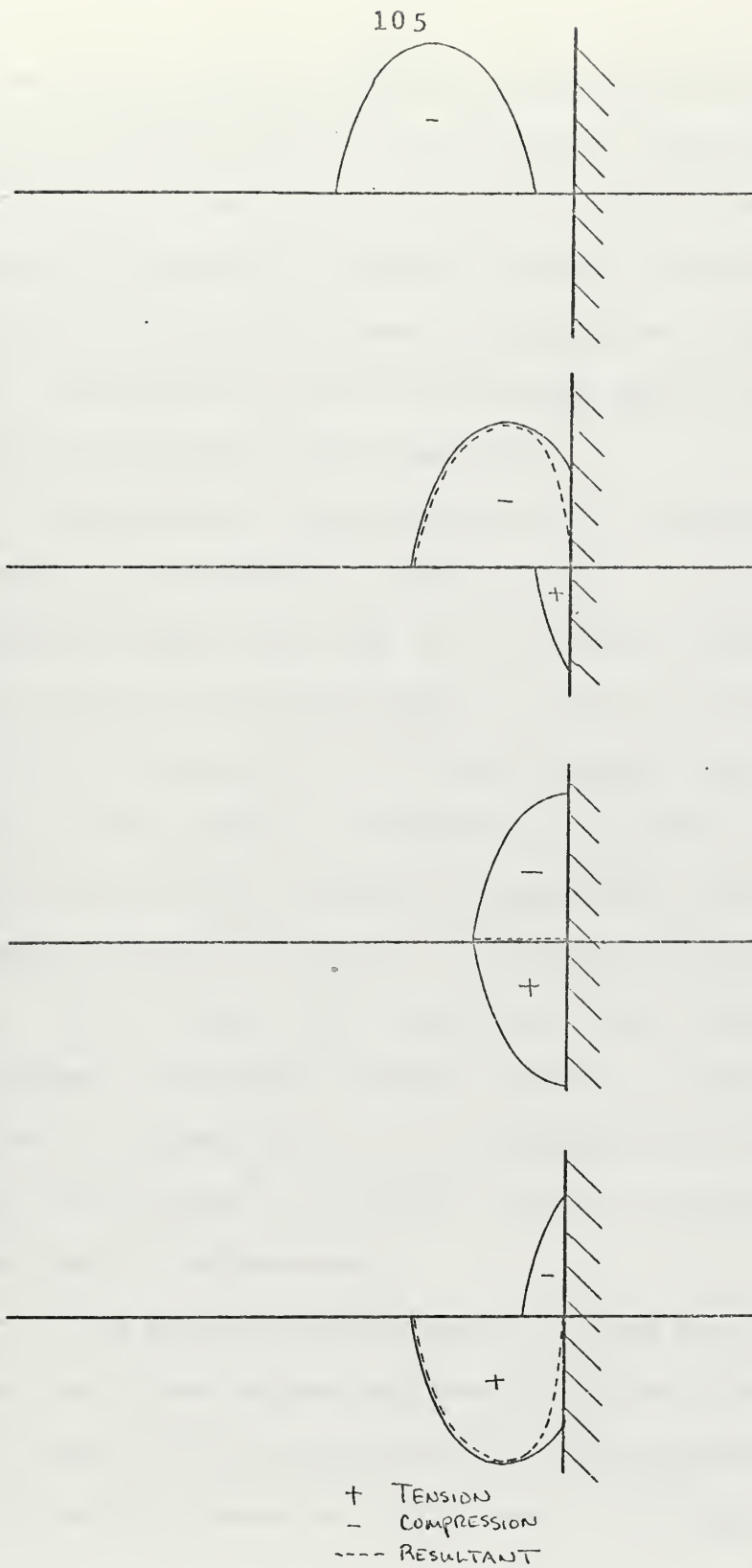
$\rho$  = density

$c_x$  = seismic velocity

$V$  = particle velocity

The wave created by the impact propagates as a compressive wave until it is reflected from a free surface. The reflected wave is of the opposite sign of the incident wave. The incident wave and the reflected wave combine and cancel until the reflected wave is fully developed. Figure 40 illustrates the process of reflection and combination of the two waves. When the reflected or tensile wave is sufficiently developed so that the stress developed exceeds the tensile capability of the material, a fracture will occur. Also, as the tensile wave combines and cancels with the compressive wave until a finite distance from the free surface is reached, the fracture generally occurs beneath the free surface. This procedure can





STRESS WAVE REFLECTION  
 FIGURE 40



continue until the wave is dissipated and multiple fractures may occur from a single blow. As the stress wave radiates spherically from the point of impact, it is reflected from all free surfaces. The principle wave will be reflected from the rear face of the plate and there will be secondary waves reflected from the edges of the plate. The secondary waves are sufficiently small so as to produce no damage and therefore may be neglected.

The material in this investigation is a composite and will not perform as an isotropic, elastic material. Since steel is considerably denser than mortar it should appear invisible to the stress wave and cause little damping. There will be minor reflections from the free surface of the wire and the matrix, but if a bond exists, it is not felt that the reflected waves will be sufficient. If this is so, then the composite in compression, unless the compressive strength of the mortar is exceeded, should perform as mortar. Upon build-up of the tension wave after reflection from the free surface, the composite could be expected to perform as mortar with hard inclusions. Since the reinforcement is not continuous through the thickness of the plate, there are no beneficial effects derived from the reinforcement.

If the reflected tensile wave is a plane wave, then the fracture could occur without any beneficial effect from the reinforcement. However, in this case the wave is three-dimensional and the fracture surface crosses the reinforcement at an angle, so that



some useful contribution of the reinforcement could be expected. Literature has indicated that mortar reinforced with steel fibers exhibits the same dynamic cracking strength as mortar without fibrous reinforcing.

There appears to be no contribution other than the mechanical effect of holding the fracture surfaces together after fracture has occurred. The fact that fibers are randomly orientated implies that there could possibly be more benefit through their use than the use of layered reinforcement. Fibrous reinforcement, being randomly orientated, should have more steel orientated in a more beneficial direction to resist the tensile fracture. It would seem that since investigation has shown that fibrous reinforcement has no effect on dynamic strength of the mortar, and fibrous reinforcement appears to be more beneficial than layered reinforcement, it may be concluded that layered steel reinforcement should have little effect on dynamic strength of the mortar. However, it can be expected that energy absorption and deformation characteristics of ferro-cement in the post cracking phase will reflect the type and amount of steel used.

Figures 1 through 6, Appendix B, show the effect of the strength of reinforcement on both front and rear deflection. It follows from the tensile tests where samples with high strength reinforcement performed better than those with lower strength reinforcement, that the same performance should be observed here. In all cases, the sample with the lower strength reinforcement had

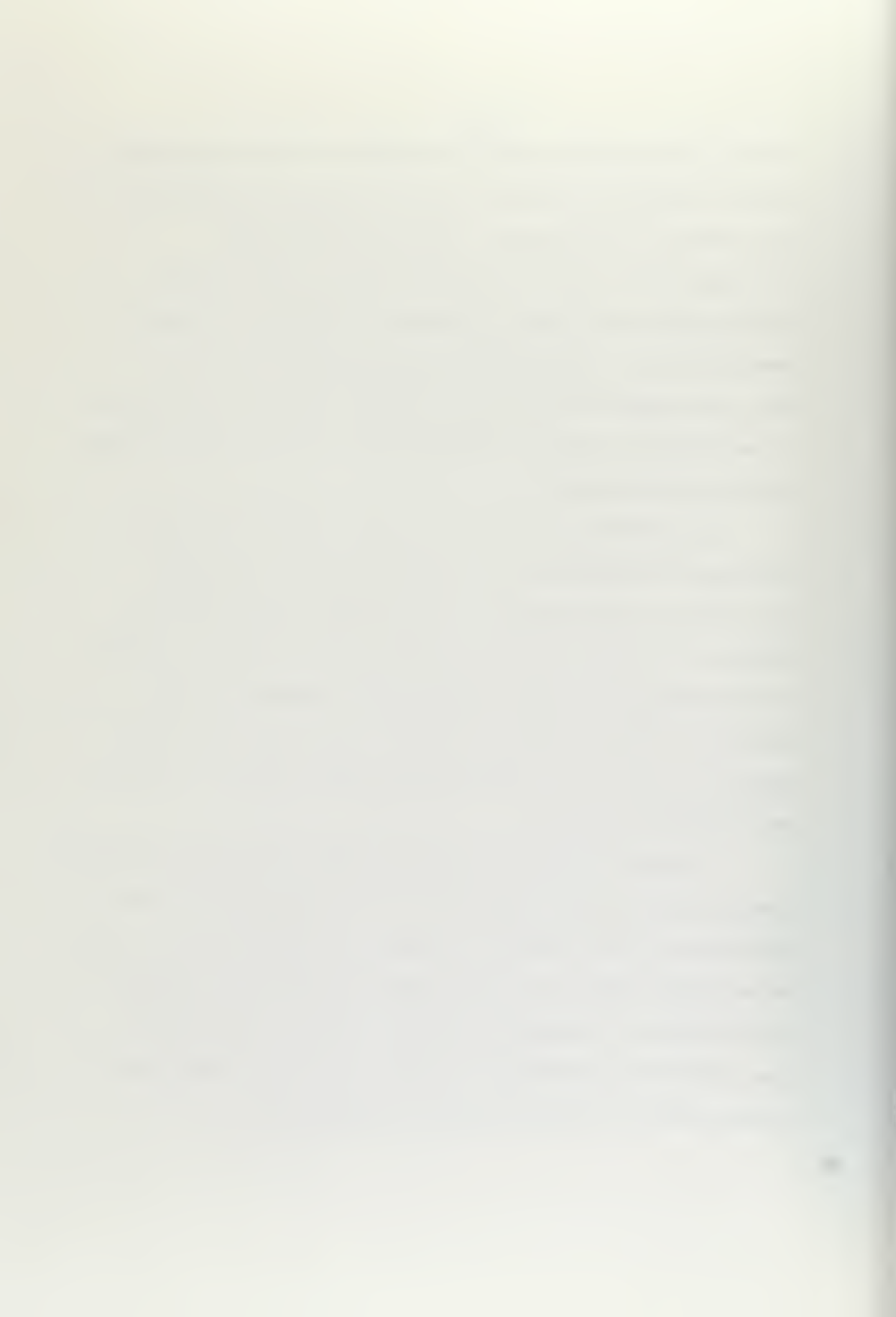




a greater deflection than those with higher strength reinforcement. Figures 7 through 12, Appendix B, show the effect of varying the outer layers of reinforcement. The curves do not follow the thought that decreasing the outer layers of high strength reinforcement should cause an increase in deflection. In several cases, 4-1 and 2-2 appeared in reversed positions. It is felt that in the explanation given in the tensile tests for the variance of the 2-2 series, that the incompatibility of the two reinforcements caused the inconsistency.

The performance of fibrous-reinforced concrete is plotted in Figures 1-12, Appendix B, so that performance can be judged in relation to a reinforcement with approximately the same yield strength. It can be seen that the overall performance of the fibers is less than for continuous reinforcement. Appearance of the sample after loading indicated pull-out of the fibers rather than fracture, so possibly an increase in the aspect ratios of the fiber would improve performance.

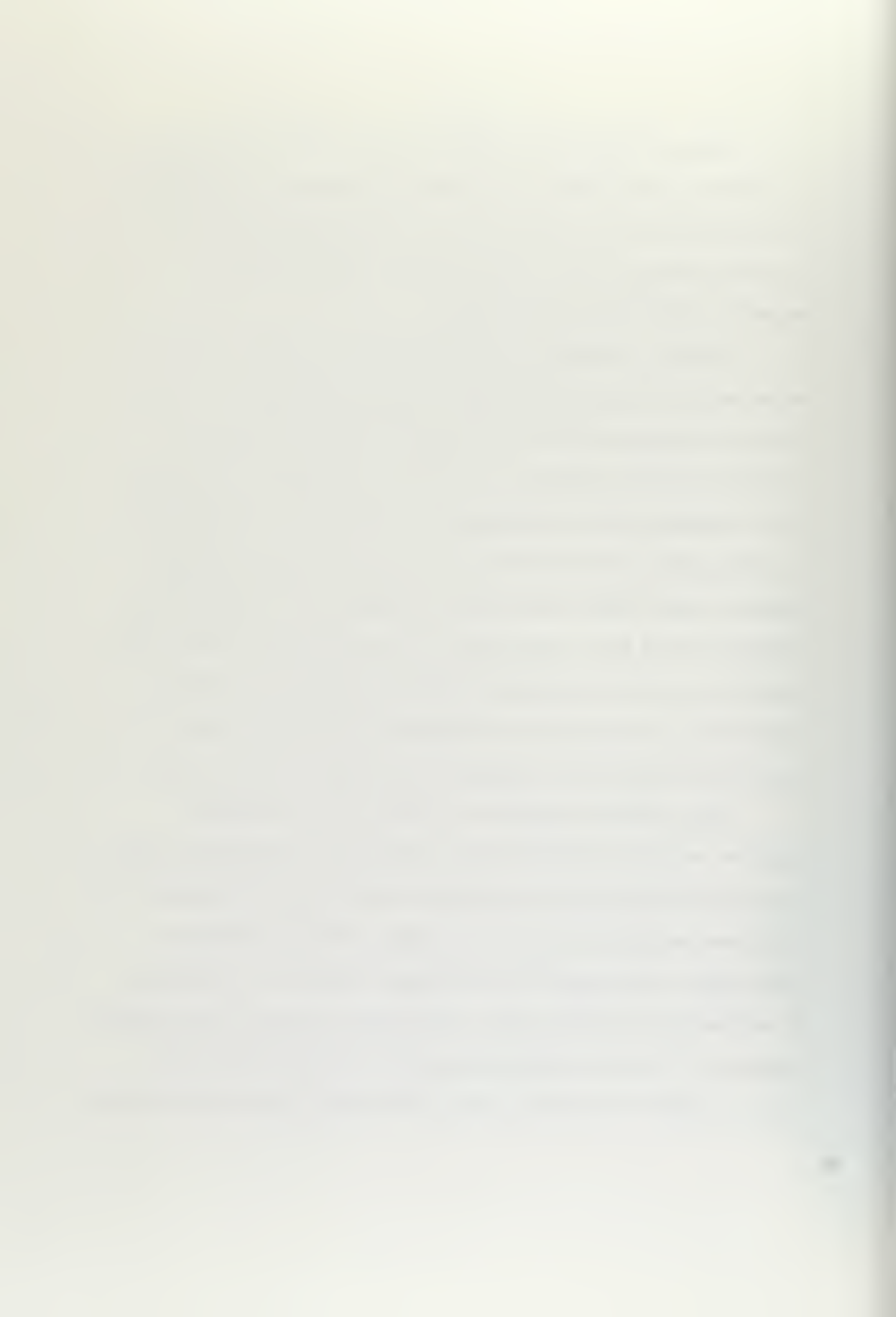
Once the initial fracture has occurred in the matrix, further loadings cause permanent deformation of the reinforcement. There would appear to be a mechanical interaction resulting from the matrix which remains bonded to the reinforcement and either the adjoining reinforcement or an adjacent fragment of matrix. If this is so, then additional energy would be required to deform a sample with a mortar matrix than one with only wire reinforcement.



Again, although this appears to be a valid argument, for the purposes of this paper and because all phases of the material of interest will have a mortar matrix, the mechanical effect of the matrix material will be neglected when considering the mechanical properties of the samples.

However, continuity of the matrix is of extreme importance in any use which imposes requirements of water-tightness. If the fact that reinforcement does not effect the dynamic strength of the mortar and the previously postulated explanation of the effect of the strength of the reinforcement on crack size are considered, it would appear that although the matrix is fractured, a higher strength reinforcement would prevent excessive crack width growth. Bezukladov noted that a crack width of less than 0.001 mm will not seep water, so it may be implied that as crack widths increase from 0.001 mm, water flow will increase as a function of the area of the opening, the viscosity of the liquid, and the head.

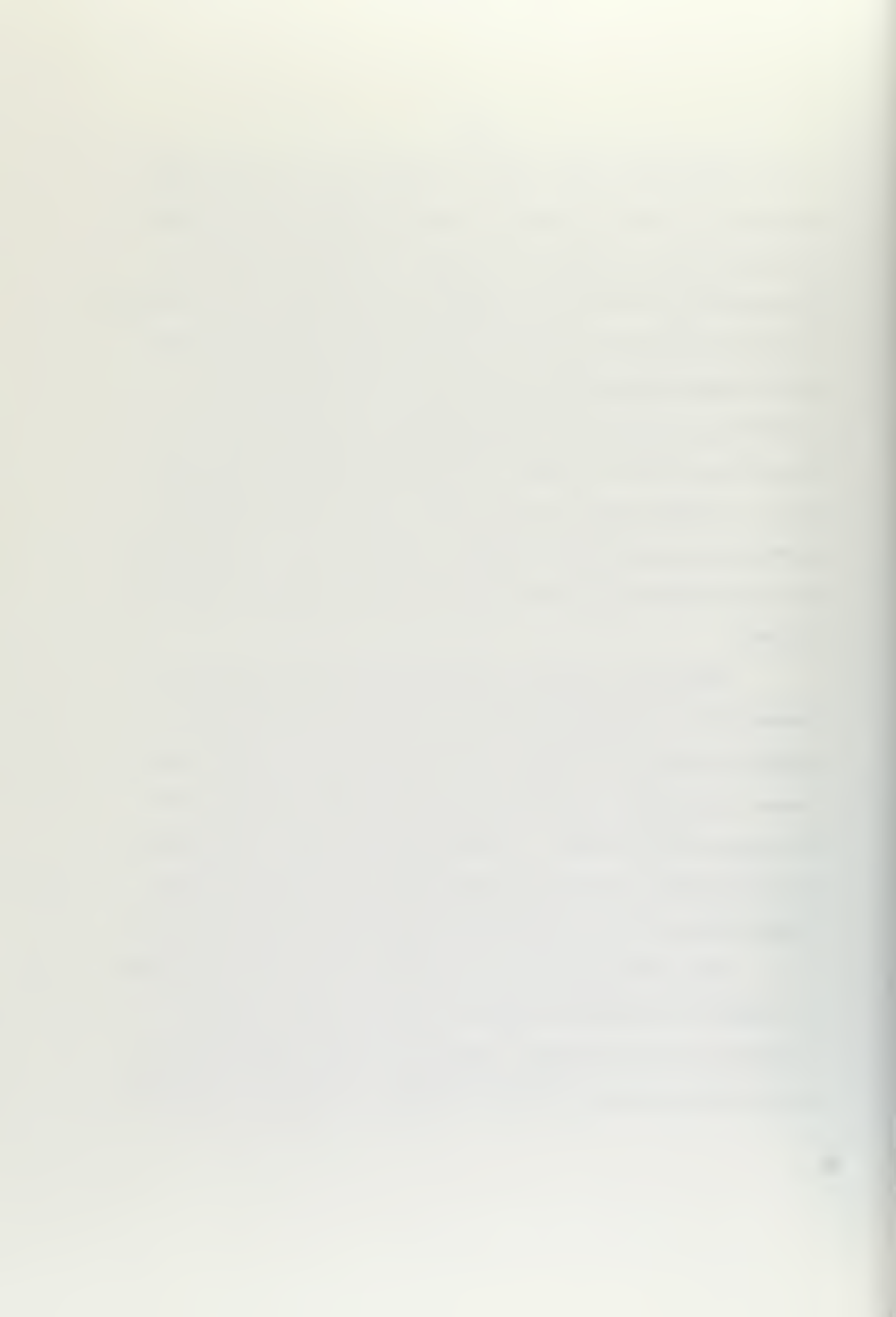
With wire mesh netting, the matrix may be completely fractured and the particles will be restrained mechanically so that true crack width cannot be considered a parameter. The retention of the broken particles in place by the mesh provides an apparent crack width, the average distance between fragments. As the mesh is deformed by successive blows, the average spacing of the fragments increases. It may be expected that with succeeding blows past a limit of complete disruption, water flow should increase until failure



of the reinforcement occurs where a maximum flow rate will occur. Figures 13, 14 and 15, Appendix B show the effect of the strength of reinforcement on damaged flow rate. In each case, there was wide separation between low strength and high strength reinforcement, as would be expected. In Series 6-0 and 4-1, the medium-strength reinforcement performed nearly as well as the high-strength, indicating the validity of the suggestion that small mesh on the surface would hold the crushed concrete in place, reducing water flow. It appears that the low strength sample has insufficient strength in the other reinforcement to prevent gross disruption of the crushed mortar and therefore would allow a greater flow, which it does.

Figures 16, 17 and 18, Appendix B show the relationship between flow and energy absorbed as a function of the number of layers of small outside mesh. As the number of small mesh outer layers is decreased, the flow rate increases, in accordance with the crushed mortar theory. A larger number of small outer layers of reinforcement will better hold in place the broken matrix and thereby limit the flow of water until failure of the reinforcement.

The performance of the fibrous-reinforced sample is plotted in Figures 13 through 18, Appendix B so as to give a relative comparison of the performance compared to a mesh reinforcement of approximately the same ultimate strength. The poor performance of



the fibers can be attributed to the lack of continuity, indicating again possible increases in performance with increased bond strengths.

If Figure 37, which shows the relationship between calculated ultimate load of the composite and observed crack width can be compared to Figure 41, which relates flow rate and calculated ultimate load of the composite, it can be seen that with decreasing ultimate load the crack width increased in one case and the flow rate increased in the other. A comparison of the results would imply that the tensile and the impact tests are related and valid conclusions may be drawn from the comparison.

The effect of specific surface on the tensile stress at first crack can be seen in Figure 34 where with decreasing specific surface, the stress at first crack decreased. A comparison with Figure 41 shows that decreasing specific surface also caused an increase in the flow rate. If cracks form sooner for a given energy level, then flow rate will be higher for that energy level. It is felt that the relationship between the tensile and impact tests is valid for a variation of specific surface and valid conclusions may be drawn from a comparison of the two.

If the two above comparisons can be accepted, then a method of relating tensile performance and impact performance exists. Figures 42 and 43 show the relationships, as observed, between tensile and impact performance as a function of specific surface and calculated ultimate load. It can be seen that either flow









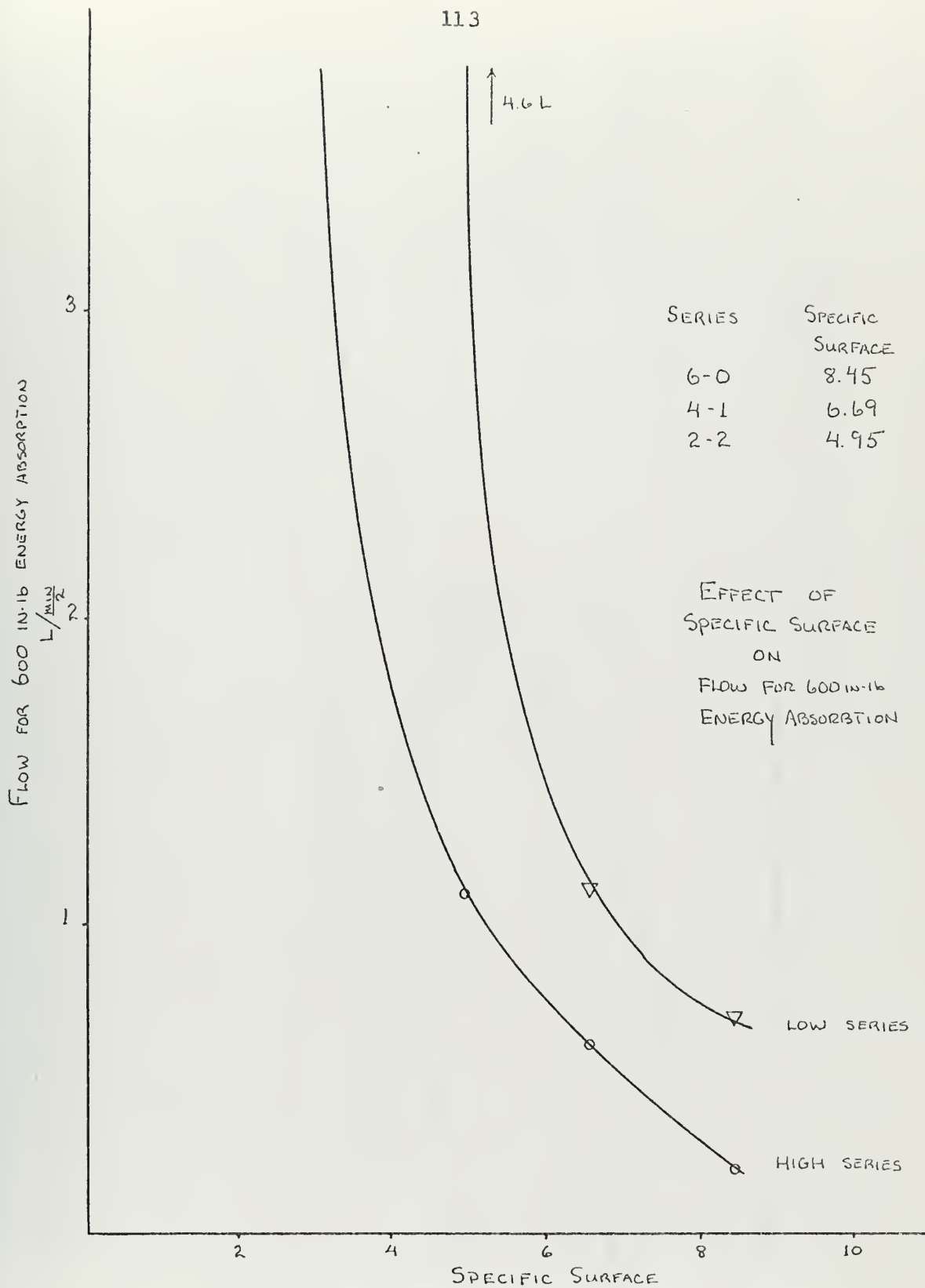


FIGURE 42



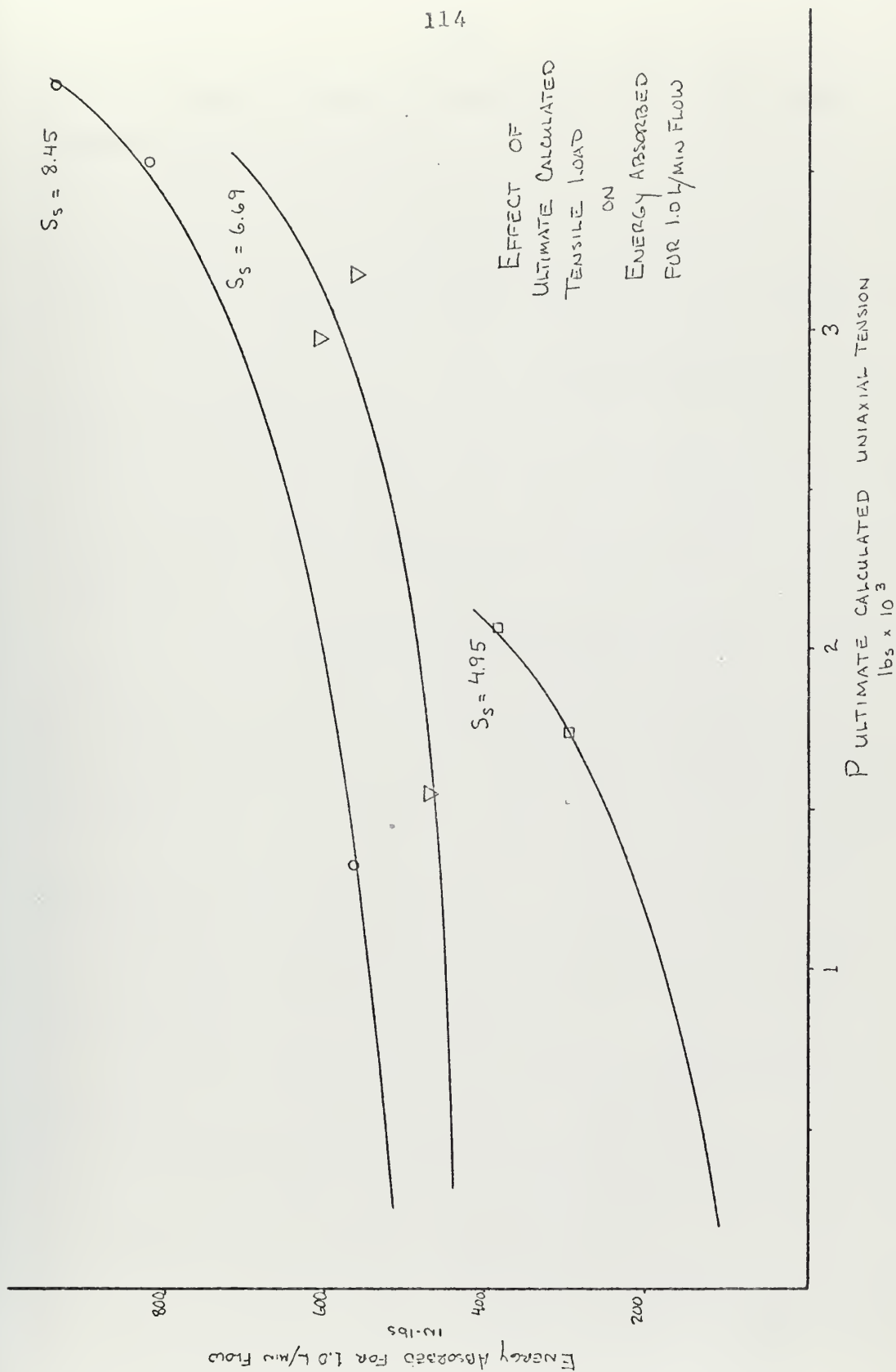


FIGURE 43



rate or energy absorbed at a constant specific surface can be determined from the figures.





## XII. CONCLUSIONS

The following conclusions are drawn from this investigation although it must be realized that these conclusions will only be valid for results obtained using woven wire mesh reinforcement.

1. Composition of the matrix had a small effect on the ultimate performance of the composite.
2. The total number of cracks in a tensile specimen will be a function of the mesh dimensions and the specific surface of the reinforcement.
3. The total number of cracks does not appear to be a function of the ultimate stress of the reinforcement.
4. Initial cracking is delayed by increasing specific surface and by the use of reinforcement with a high ultimate stress.
5. The modulus of elasticity of the composite can be predicted from the observed modulus of the reinforcement.
6. The ultimate load of the composite can be predicted from the ultimate load of the reinforcement.
7. The apparent damage, as measured with the flow device, decreases with increasing strength of reinforcement.
8. Decreasing the number of small mesh layers in the outer reinforcement increases the damaged flow rate.
9. There appears to be a relationship between tensile and impact performance and impact performance can be predicted from observed tensile performance.

3925

INT ROBLES, R.

TERMINAL BALLISTICS CONCRETE

PAGE 1

0 REPORTS RETRIEVED

3923

INT ROBLES, R.

TERMINAL BALLISTICS FERROCEMENT

PAGE 1

0 REPORTS RETRIEVED

3922

INT ROBLES, R.

IMPACT FERROCEMENT

PAGE 1

T133726

MASSACHUSETTS INSTITUTE OF TECHNOLOGY. KEY, WILLIAM H. IMPACT RESISTANCE BY FERRO-CEMENT PLATES, M.S. THESIS. MAY 1970. 192P. SHELVED IN THE UNCLASSIFIED THESIS COLLECTION AT-K396.

1 REPORTS RETRIEVED

3924

INT ROBLES, R.

IMPACT CONCRETE

PAGE 1

T133726

MASSACHUSETTS INSTITUTE OF TECHNOLOGY. KEY, WILLIAM H. IMPACT RESISTANCE BY FERRO-CEMENT PLATES, M.S. THESIS. MAY 1970. 192P. SHELVED IN THE UNCLASSIFIED THESIS COLLECTION AT-K396.

C REPORTS RETRIEVED

0 REPORTS RETRIEVED

3924

ARC ROBLES, R.

IMPACT CONCRETE

PAGE 1

U077750

LEHIGH UNIVERSITY. BOMB DAMAGE ANALYSIS, FINAL REPORT. VOLUME II. PART I. PHASE L-B. TERMINAL BALLISTICS. SECTIONS I-III. CONDITIONS PRIOR TO FUNCTIONING. SECTION IV. BOMB FUZES. SECTION V. INCENDIARY BOMBS. L949. V.P.

1 RECORDS RETRIEVED

L077798

LEHIGH UNIVERSITY. BOMB DAMAGE ANALYSIS, FINAL REPORT. VOLUME II. PART I. PHASE L-B. TERMINAL BALLISTICS. SECTIONS I-III. CONDITIONS PRIOR TO FUNCTIONING. SECTION IV. BOMB FUZES. SECTION V. INCENDIARY BOMBS. L949. V.P.

1 REPORTS RETRIEVED

10. Fibrous reinforcement, as investigated in this experiment, did not perform as well as continuous mesh reinforcement.

### XIII. RECOMMENDATIONS

Future crack work in the area of impact resistance should be pursued to further knowledge in this area. It is suggested that future work be closely coordinated with the mesh manufacturers so that reinforcement with more optimum properties can be utilized. It is believed that with matching reinforcement, more definite indications could be obtained than was possible in this paper.

It is also recommended that further work be done on the use of a continuous wire mesh with fibrous reinforcement interspersed in the matrix. It is felt that this will add to the continuity of the crushed particles of the matrix, giving better damage flow resistance.





## SELECTED BIBLIOGRAPHY

1. Atchley, B.L., Purr, H.L., "Strength and Energy Absorption Capabilities of Plain Concrete Under Dynamic and Static Loadings." Journal of the American Concrete Institute: 64, No. 11 (November 1967), p. 744.
2. Bezukladov, V.F., Amel'yanovich, K.K., Verbitskiy, C.D., Bogoyavelnskiy, L.P., "Ship Hulls Made of Reinforced Concrete." Naval Ship Systems Command Translation No. 1148, 1968.
3. Byrne, J.G., Wright, W., "Reinforced Cement Mortar Construction- An Investigation of Ferro-cement Using Expanded Metal." Concrete and Constructional Engineering, December 1961, p. 429.
4. Cassie, Fisher, "Lambot's Boats - A Personal Rediscovery." Concrete, November 1967. p. 380.
5. Chang, W.F., "Test Report of Sandwich Ferro-cement Plates." For E.V. Associates, Department of Civil Engineering, University of Miami, 17 March 1969.
6. Claman, John S., "Bending of Ferro-cement Plates." Naval Engineering Thesis, Department of Naval Architecture, Massachusetts Institute of Technology, June 1969.
7. Collen, L.D.G., "Some Experiments in Design and Construction of Ferro-cement." Civil Engineering and Public Works Review: 55, No. 643 (February 1960), p. 225.
8. Collen, L.D.G., "The Mechanical Properties of Ferro-cement." Civil Engineering and Public Works Review, December 1958, p. 217.
9. Collen, L.D.G., Kirwan, R.W., "Some Notes on the Characteristics of Ferro-cement." Civil Engineering and Public Works Review, February 1959, p. 195.
10. Collier, B.A., Symonds, P.S., "Plastic Deformations of a Beam Under Impulsive Loadings." Proceedings of the American Society of Civil Engineers: 81, (1955).
11. Collins, J.F., "Tensile Strength of Mesh Reinforced Mortar." Unpublished Term Report, Department of Civil Engineering, Massachusetts Institute of Technology, May 1968.



12. Collins, J.F., "An Investigation of Bond Strength in Ferro-cement." Master's Thesis, Department of Naval Architecture, Massachusetts Institute of Technology, June 1969.
13. Collins, J.F., Claman, J.S., "Ferro-cement for Marine Application, An Engineering Evaluation." Paper, New England Section, Society of Naval Architects and Marine Engineers, March 1969.
14. Collins, J.F., Claman, J.S., "The Design and Construction of Barge: Auxiliary Reinforced Ferro-cement (BARF -1)." Unpublished Term Report, Department of Naval Architecture, Massachusetts Institute of Technology, January 1969.
15. Crow, H.E., "Crack Formation Arrest and Propagation in Concrete Slabs Reinforced with Closely Spaced Steel Wires." Master's Thesis, Department of Naval Architecture, Massachusetts Institute of Technology, June 1969.
16. Eringer, A.C., "Transverse Impact on Beams and Plates." Journal of Applied Mechanics: 20 (1953), p. 461.
17. Evans, R.H., "Effect of Rate of Loading on Mechanical Properties of Some Materials." Institute of Civil Engineering (London): 18, No. 7-8 (June 1942), p. 296.
18. Fehr, R.O., Parker, E.R., "Measurement of Dynamic Stress and Strain in Tensile Test Specimens." Journal of Applied Mechanics, Series E:27 (1960), p. 717.
19. Fraser, D.J., "Estimated Hull Work and Material Content for 100-ft. Combination Fishing Vessel in Different Materials." Paper, Conference on Fishing Vessel Construction Materials, Montreal, Canada, October 1968.
20. Goldsmith, W., Impact: The Theory and Physical Behavior of Colliding Solids. London: E. Arnold, 1960



21. Goldsmith, W., "Dynamic Behavior of Concrete." Experimental Mechanics: 6, No. 2 (1966), p. 65
22. Goldsmith, W., Austin, C.F., "Some Dynamic Characteristics of Rocks." Stress Waves in Inelastic Solids, Berlin: Springer, 1964, p. 277.
23. Goldsmith, W., Kennes, V.F., "Dynamic Loading of Several Concrete-like Mixtures." Proceedings of the Structural Division, American Society of Civil Engineers: 94, No. ST7 (July 1968), p. 1803.
24. Goldsmith, W., Lyman, P.T., Jr., "The Penetration of Hard Steel Spheres Into Plane Metal Surfaces." Journal of Applied Mechanics, Series E:27 (1960), p. 717.
25. Graves, M.J., Mavis, F.T., "Inelastic Behavior of Impulsively Loaded Beams." Proceedings of the American Society of Civil Engineers: 83, No. ST3 (May 1957), p. 1232
26. Green, H., "Impact Strength of Concrete." Proceedings of the Institute of Civil Engineering (London): 28 (July 1964), p. 383.
27. Griner, F.J., Ali, M.A., "The Strengths of Cements Reinforced with Glass Fibers." Magazine of Concrete Research: 21, No. 66 (March 1969).
28. Haviland, Jean, "American Concrete Steamers of the First and Second World Wars." The American Neptune: 22 (1962), p. 157.
29. Hurd, M.K., "Ferro-cement Boats." Journal of the American Concrete Institute, March 1969, p. 202.
30. Jackson, G.W., Sutherland, W. Morley, Concrete in Boat Building. Tuckahoe, New York: John De Graff, Inc., 1969.
31. Jergowich, N., Unpublished report, Department of Naval Architecture and School of Marine Engineering, University of Michigan, 1968.





32. Jones, N., Griffin, R.N., Van Duzer, R.F., "An Experimental Study Into the Dynamic Plastic Behavior of Wide Beams and Rectangular Plates." Department of Naval Architecture, Massachusetts Institute of Technology, Report No. 69-12, 1969.
33. Jones, N., Uran, T.O., Tekin, S.A., "The Dynamic Plastic Behavior of Fully Clamped Rectangular Plates." Department of Naval Architecture, Massachusetts Institute of Technology, Report No. 69-13, December 1969.
34. Jones, P.L., Richart, F.E., "The Effect of Testing Speed on Strength and Elastic Properties of Concrete." Proceedings of the American Society for Testing Materials: 36, part II, (1936, p. 380.
35. Kelly, A.M., Mouat, T.W., "Ferro-cement as a Fishing Vessel Construction Material." Paper, Conference on Fishing Vessel Construction Materials, Montreal, October 1968.
36. Key, W.H., "Investigation into Various Properties of Ferro-cement." Unpublished Term Report, Department of Civil Engineering, Massachusetts Institute of Technology, January 1970.
37. Kluge, F.W., "Impact Resistance of Reinforced Concrete Slabs." Proceedings of the American Concrete Institute: 14 (1942-43), pp. 397-412.
38. Lachance, L., "Ferro-Concrete for Thin Shell Structures." Department of Civil Engineering, Laval University, Quebec, February 1969.
39. Littman, H.Z., "Mesh Reinforcement for Doubly-curved Slabs." Concrete and Constructional Engineering: 55, No. 2 (February 1960), p. 103.
40. Malvern, L.E., "The Propagation of Long Waves of Plastic Deformation in a Bar of Material Exhibiting a Strain Rate Effect." Journal of Applied Mechanics: 18, No. 2 (1951), p. 203.





41. Mann, H.C., "The Relation Between the Tension Statics and Dynamic Tests." Proceedings of the American Society for Testing Materials: 35, part II (1935), p. 323.
42. Mann, H.C., "High Velocity Tension Impact Tests." Proceedings of the American Society for Testing Materials: 36, part II (1936), pp. 85-97.
43. Mavis, F.T., Richards, F.A., "Impulse Testing of Concrete Beams." Journal of the American Concrete Institute: 52, No. 1 (September 1955), p. 93.
44. Mavis, F.T., Greaves, M.J., "Destructive Impulse Loading of Reinforced Concrete Beams." Journal of the American Concrete Institute: 54, No. 3 (September 1957), p. 233.
45. Mavis, F.T., Stewart, J.J., "Further Tests of Dynamically Loaded Beams." Journal of the American Concrete Institute: 55, No. 11 (May 1959), p. 1215.
46. Mellinger, F.N., Birkimer, D.L., "Measurement of Stress and Strain on Cylindrical Test Specimens of Rock and Concrete Under Impact Loading." Ohio River Laboratories, Corps of Engineers, Technical Report No. 4-46, April 1966.
47. Merchant Marine Technical Note 4-69, Guide for Ferro-cement and Its Use in Boat Construction, Commandant U.S. Coast Guard, November 1969.
48. Moavenzadeh, F., Kuguel, R., "Fracture of Concrete." Journal of Materials: 4, No. 3 (September 1969), pp. 497-519.
49. Morgan, R.G., Reed, S.C., Personal Correspondence, 29 May 1969.
50. Morgan, R.G., Letter to Editor, Concrete, March 1968, p. 128.



51. Muhlert, J.F., "Analysis of Ferro-cement in Bending."  
Paper, Eastern Canadian Section, Society of  
Naval Architects and Marine Engineers,  
Montreal, December 1969.
52. Naaman, Antoine, "Effects of Steel Reinforcement on the  
Failure Mechanism of Ferro-cement in Tension."  
Unpublished Term Report, Department of Civil  
Engineering, Massachusetts Institute of  
Technology, January 1970.
53. Naval Facilities Engineering Command, "Dynamic Properties  
of Plain Portland Cement Concrete." Technical  
Report R447, June 1966.
54. Nawy, E.G., "Fluxual Cracking in Two Way Concrete Slabs  
Reinforced with High Strength Welded Wire Mesh."  
Proceedings of the American Concrete Institute:  
61 (August 1964), pp. 997-1008.
55. Nawy, E.G., "Crack Control in Reinforced Concrete Structures."  
Proceedings of the American Concrete Institute:  
October 1968, p. 825.
56. Nelson, B., "Performance of Hexagonal Mesh in Ferro-cement."  
Unpublished Term Report, Department of Civil  
Engineering, Massachusetts Institute of Technology,  
February 1970.
57. Perry, D.A., Pinto, J.E., Ferro-cement: Its Potential for  
Naval Craft (A State of the Art Study). Naval  
Ship Engineering Center, SEC6101, Hyattsville,  
Maryland, 1969.
58. Romualdi, J.P., Batson, G.P., "Behavior of Reinforced  
Concrete Beams With Closely Spaced Reinforcement."  
Journal of the American Concrete Institute: 69,  
No. 6 (June 1963), pp. 775-790.
59. Romualdi, J.P., Mandel, J.A., "Tensile Strength of Concrete  
Affected by Uniformly Distributed and Closely  
Spaced Short Lengths of Wire Reinforcements."  
Journal of the American Concrete Institute,  
Proceedings: 61 (June 1964), pp. 657-671.



60. Romualdi, J.P., Batson, G.P., "Mechanics of Crack Arrest in Concrete." American Society of Civil Engineers: 89, EM3 (June 1963), p. 147.
61. Romualdi, J.P., Ramey, M.R., "Effect of Impulsive Loads on Fiber Reinforced Concrete Beams." Final Report, Department of Civil Engineering, Carnegie Institute of Technology, Pittsburgh, October 1965.
62. Samson, John, Wellens, Geoffrey, How to Build a Ferro-cement Boat, Vancouver, B.C. Samson Marine Division Enterprises, 1968.
63. Shah, S.P., Broms, B.B., "Mechanics of Crack Arrest in Concrete." Journal of Engineering Mechanics Division Proceedings of American Society of Civil Engineers: 90, No. EM1, (February 1964), p. 167.
64. Shah, S.P., Rangan, R.V., "Some Micromechanical Properties of Fiber Reinforced Concrete." Department of Civil Engineering, Massachusetts Institute of Technology, December 1969.
65. Spath, Wilhelm, Impact Testing of Materials. New York: Gordon and Branch, 1961.
66. Tuthill, L.H., "Concrete Operation in the Concrete Ship Program." Proceedings of the American Concrete Institute: 41 (1945), p. 137.
67. Vasta, J., "Concrete Ship Program of World War II." Paper, Chesapeake Section of the Society of Naval Architects and Marine Engineers, 8 May 1952.
68. Vishwanath, T., "Test of a Ferro-cement Precast Folded Plate." Proceedings of the American Society of Civil Engineers, Journal of the Structural Division: 91, No. ST6 (December 1965).
69. Wadlin, G.K., Stewart, J.S., "Comparison of Prestressed Concrete Beams and Conventionally Reinforced Concrete Beams Under Impulsive Loading." Journal of the American Concrete Institute: 58 (October 1961), p. 407.





70. Watstein, D., "Effect of Straining Rate on the Compressive Strength and Elastic Properties of Concrete." Proceedings of the American Concrete Institute: 49 (1953), p. 729.
71. Watstein, D., Parsons, D.E., "Width and Spacing of Tensile Cracks in Axially Reinforced Concrete Cylinders." National Bureau of Standards Research Paper 1545 (July 1943).
72. Wig, R.J., "Present Status of the Concrete Ship." Society of Naval Architects and Marine Engineers: 26 (1918), p. 185.
73. Wig, R.J., "Method of Construction of Concrete Ships." Society of Naval Architects and Marine Engineers: 27 (1919), p. 1.
74. Williamson, G.R., "Fibrous Reinforcements for Portland Cement Concrete." Ohio River Laboratories, Corps of Engineers, Technical Report No. 2-40 (May 1963).
75. Williamson, G.R., "Response of Fibrous-Reinforced Concrete to Explosive Loadings." Ohio River Laboratories, Corps of Engineers, Technical Report No. 2-48 (January 1966).





APPENDIX A



First Crack	Ultimate	Total no. cracks	composite modulus before	composite modulus after	calculated modulus of reinforcement
6-0-H	930	25	3.43 x 10 <sup>6</sup>	.56 x 10 <sup>6</sup>	23.8 x 10 <sup>6</sup>
	875	9	1.76	.492	20.9 x 10 <sup>6</sup>
	900	20	-	.62	26.3 x 10 <sup>6</sup>
6-0-M	860	19	2.16	.52	17.6
	900	-	2.4	.514	17.4
	835	-	1.27	.484	16.4
6-0-L	875	20	1.97	.455	19.38
	740	16	1.34	.47	20.0
	770	24	1.09	.492	20.9
4-1-H	750	18	.92	.515	19.1
	700	20	1.49	.515	19.1
	700	18	.91	.53	19.6
4-1-M	830	18	1.32	.593	19.5
	800	15	1.51	.605	19.5
	780	16	1.86	.445	14.35
4-1-L	805	16	.948	.462	17.1
	755	19	1.10	.398	14.7
	775	18	.885	.583	21.5

TABLE I



	First Crack	Ultimate	Total no. cracks	composite modulus before	composite modulus after	calculated modulus of reinforcement
2-2-H	660	1940	10	1.27	.684	22.4
	730	1950	11	3.0	.645	21.1
	625	1800	10	2.85	.57	18.7
2-2-M	690	2200	11	1.23	.61	18.75
	760	2230	12	1.23	.625	19.2
	700	2100	15	1.50	.615	18.9
2-2-L	820	1680	12	.75	.515	16.9
	805	1685	12	1.05	.47	15.4
	852	1690	9	.838	.44	14.4
0-3-L	675	1940	6	.99	.52	15.25
	600	1955	7	.94	.592	17.4
	515	1950	8	1.22	.62	18.2

TABLE I (con'd)



LOAD-DEFLECTION  
CURVES  
SERIES 6-0-XA

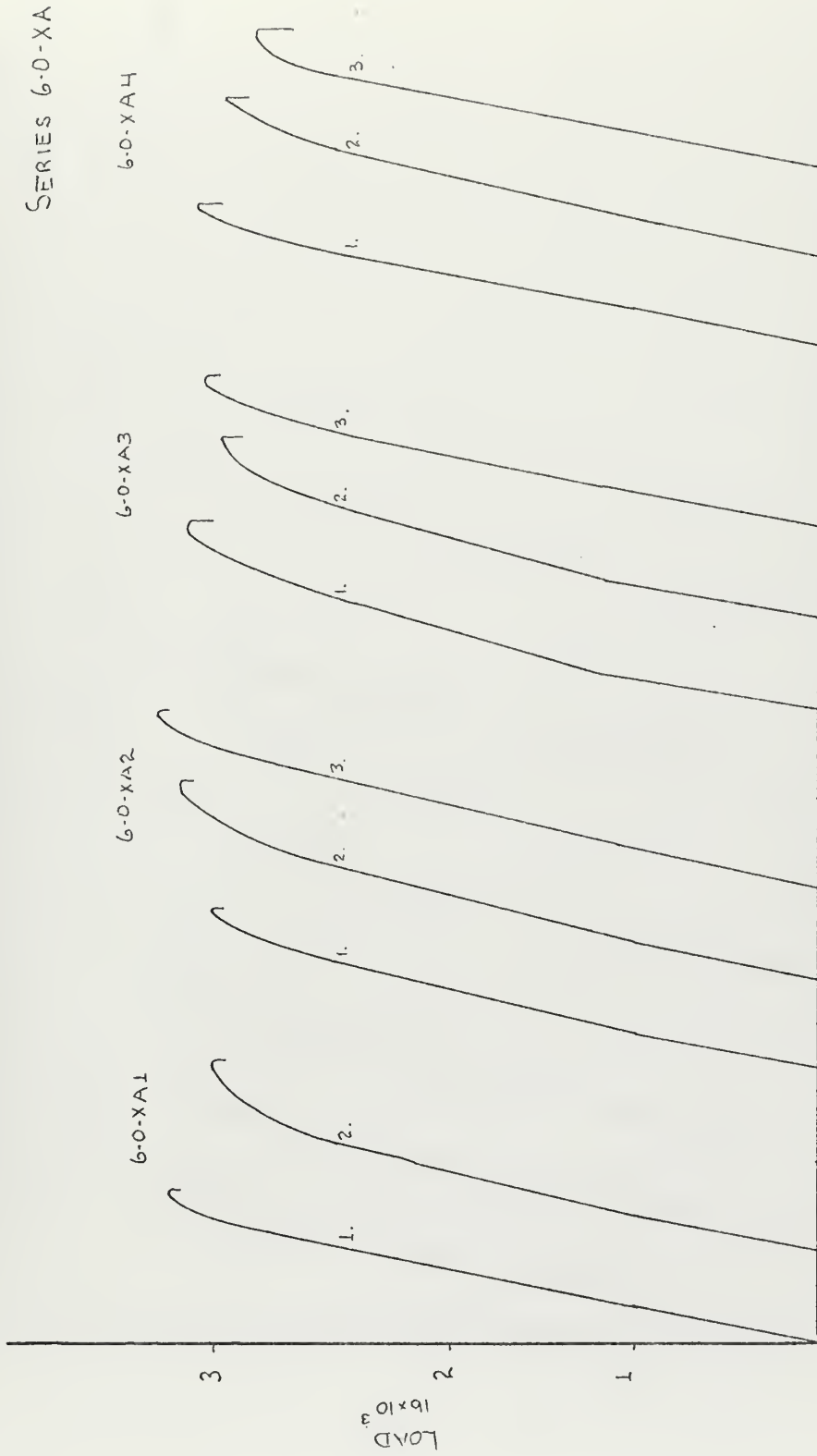


CHART DEFLECTION  
1 INCH = 1 INCH  
TO GET TRUE DEFLECTION, MULTIPLY BY  $1.25 \times 10^{-4}$   
FIGURE 1





# LOAD-DEFLECTION CURVES

SERIES 6-0-XA

LOAD RATE 0.1"/min

CHART SPEED 4.0"/min

130

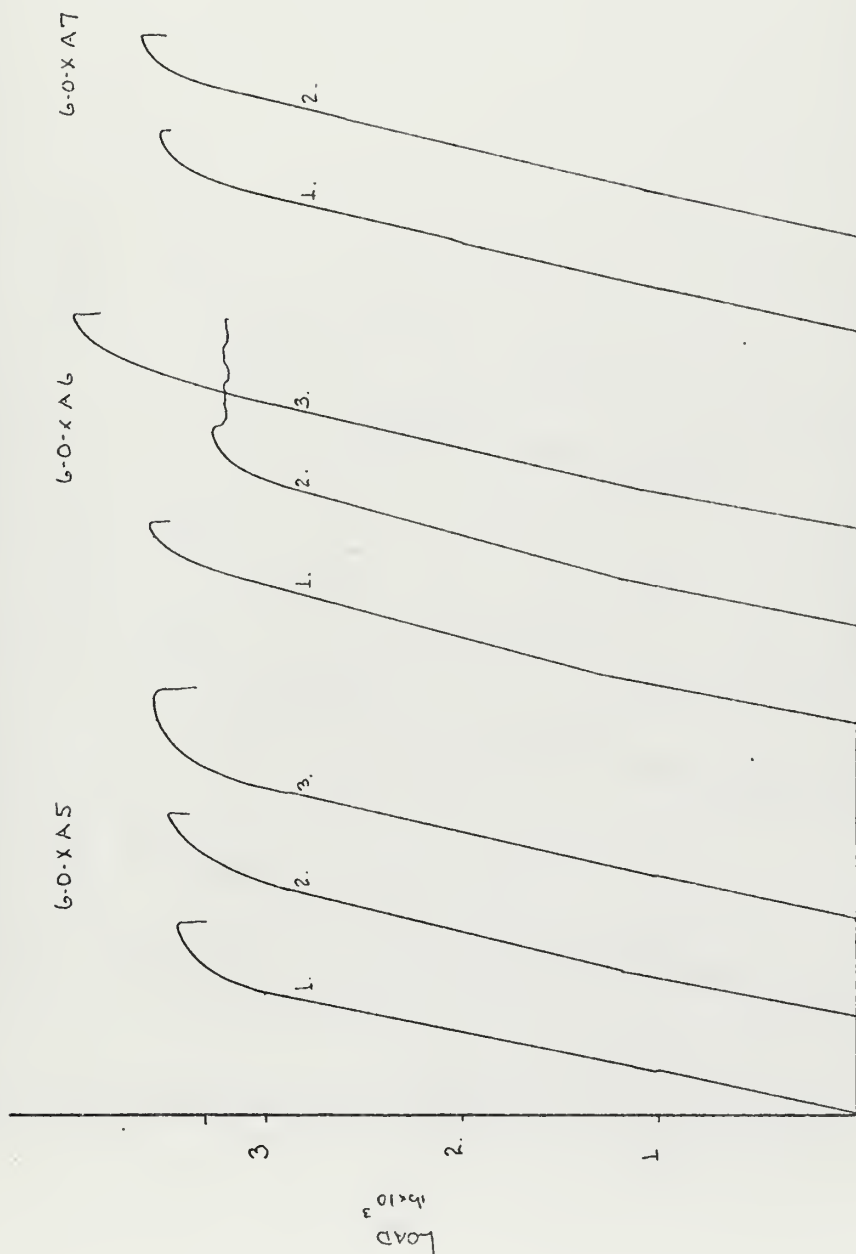


CHART DEFLECTION

1 inch = 1 inch

TO GET TRUE DEFLECTION, MULTIPLY BY  $1.25 \times 10^{-4}$

FIGURE 2



LOAD-DEFLECTION  
CURVES  
SERIES 6-0-XB

131

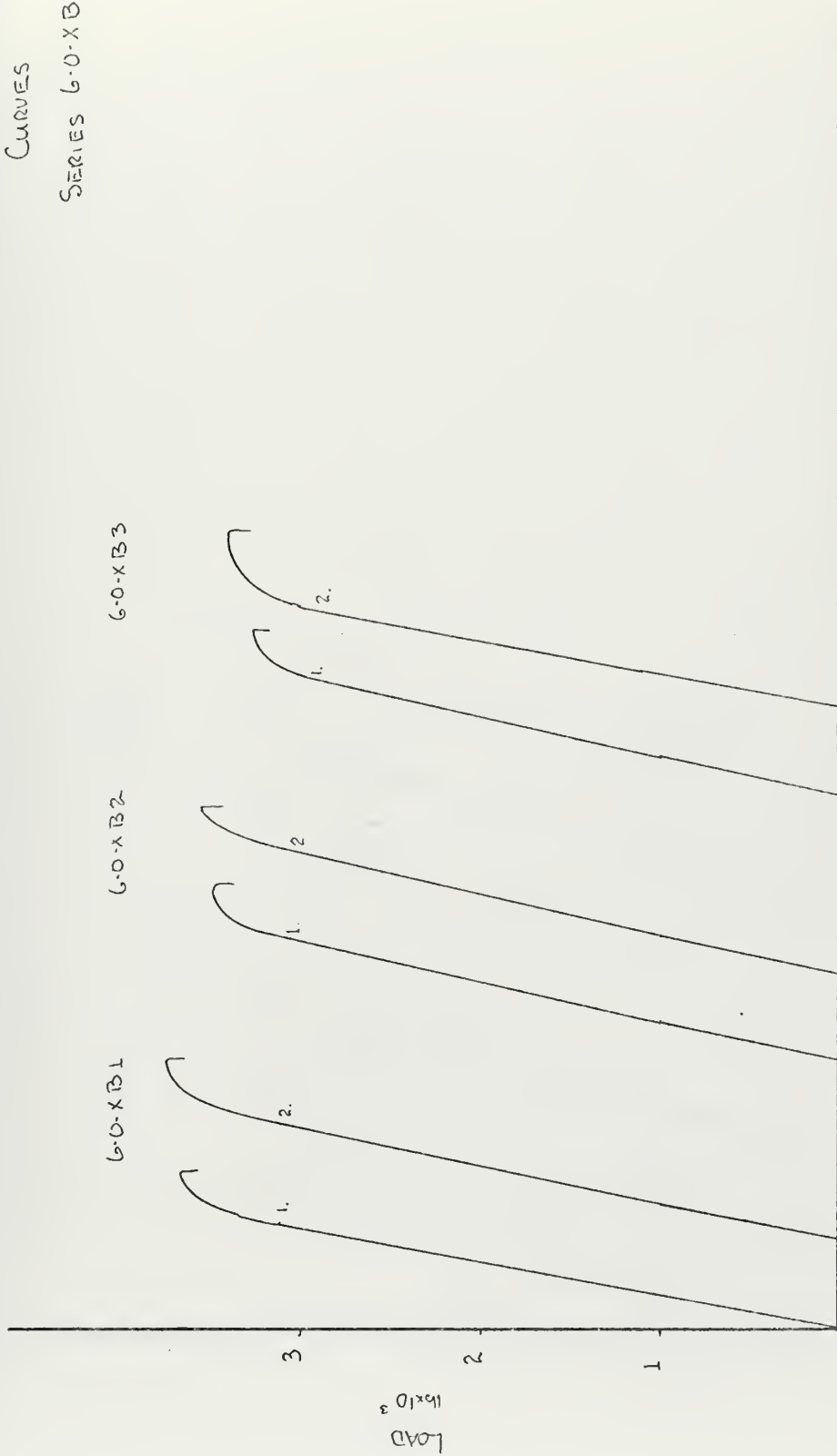


CHART DEFLECTION

1 INCH = 1 INCH

TO GET TRUE DEFLECTION, MULTIPLY BY  $1.25 \times 10^{-4}$

FIGURE 3



# LOAD-DEFLECTION CURVES SERIES 6-0-X-C

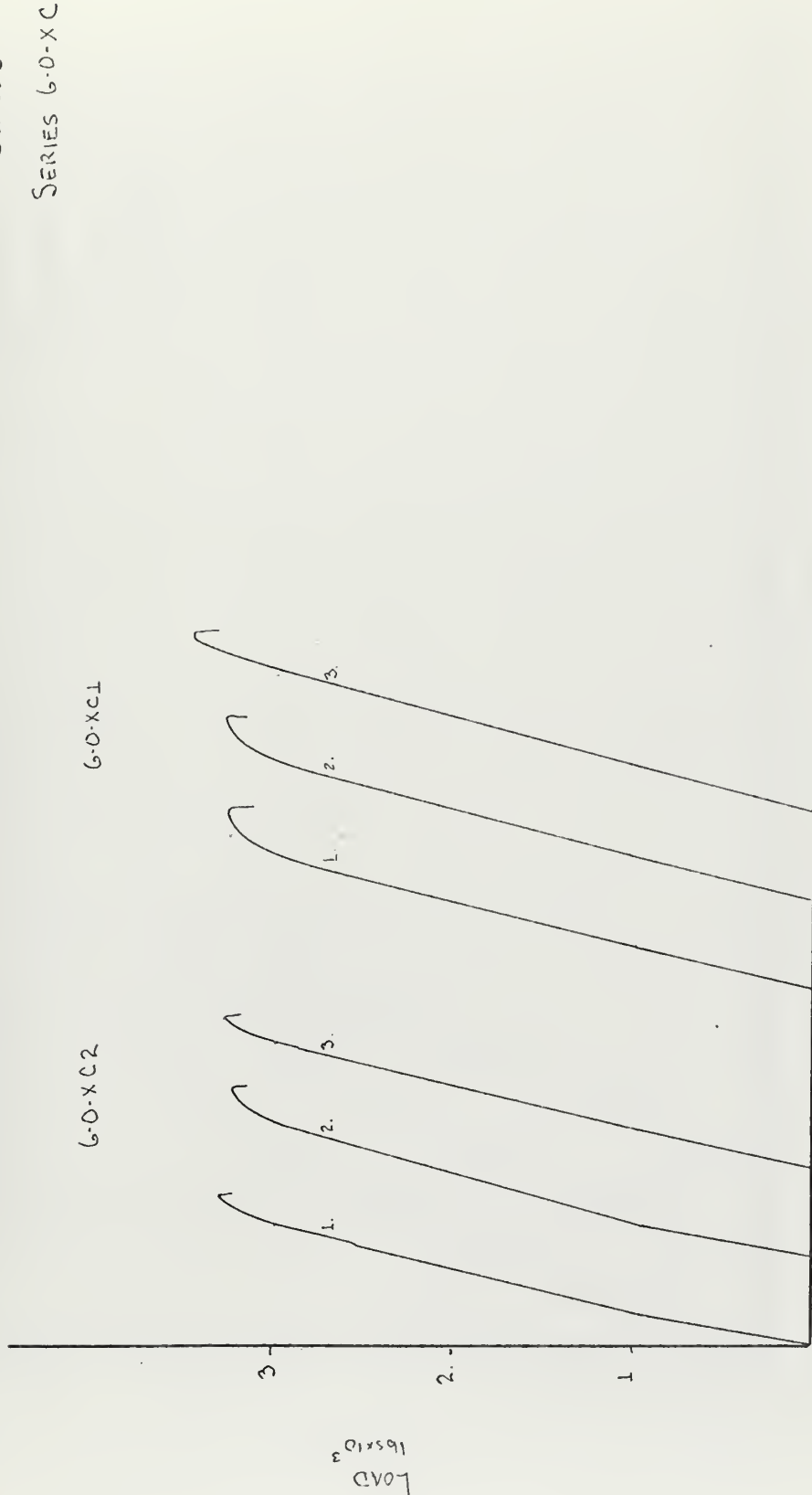


CHART DEFLECTION  
1 inch = 1 inch  
TO GET TRUE DEFLECTION, MULTIPLY BY  $1.25 \times 10^{-4}$   
FIGURE 4



SERIES 6-0-11

LOAD RATE = 0.05"/MIN

CHART SPEED = 4.0"/MIN

LOAD-DEFLECTION  
CURVES

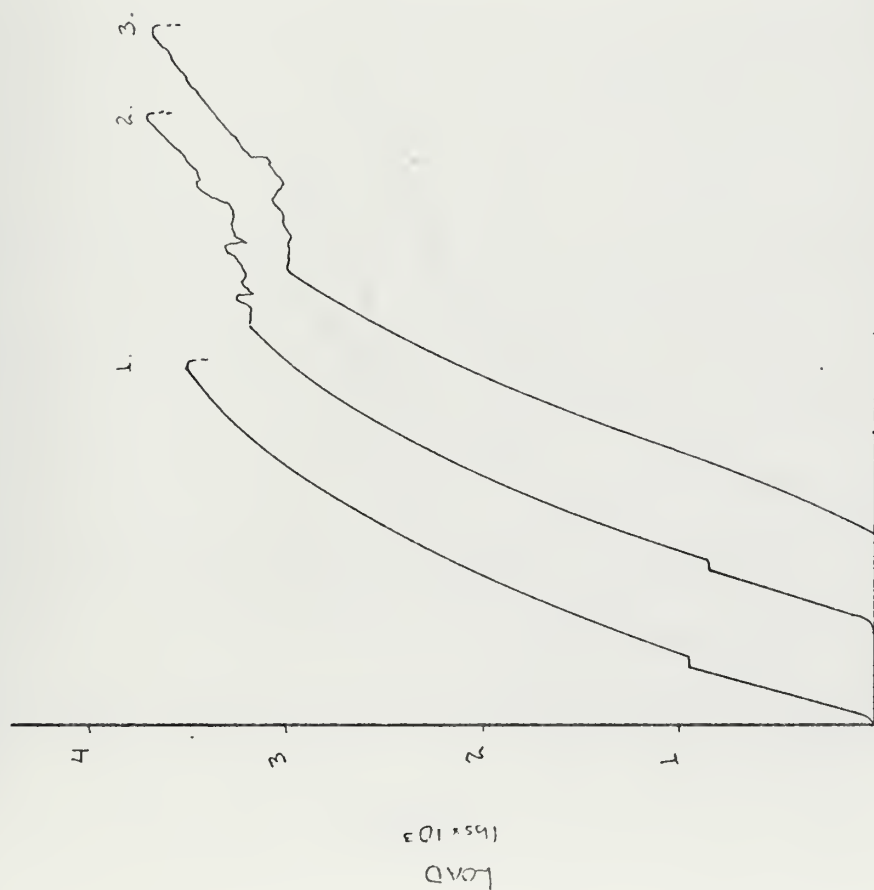


CHART DEFLECTION

1 INCH = 1 INCH

TO GET TRUE DEFLECTION, MULTIPLY BY  $1.25 \times 10^{-4}$

FIGURE 5





SAMPLE 4-1-H

LOADING RATE = 0.05"/MIN

CHART SPEED = 4.0"/MIN

TO GET TRUE DEFLECTION

MULTIPLY BY  $1.25 \times 10^{-4}$

LOAD-DEFLECTION  
CURVE

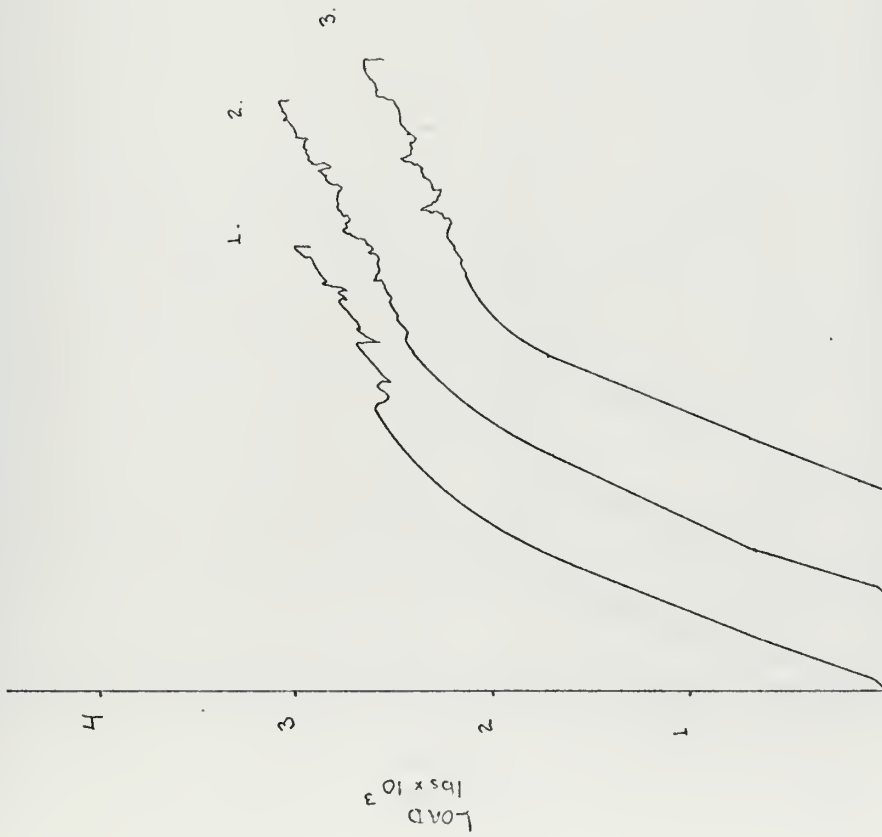


CHART DEFLECTION  
1 INCH = 1 INCH

FIGURE 6



SAMPLE 2-2-H

LOAD RATE 0.05"/MIN  
CHART SPEED 4.0"/MIN

# LOAD-DEFLECTION Curve

135

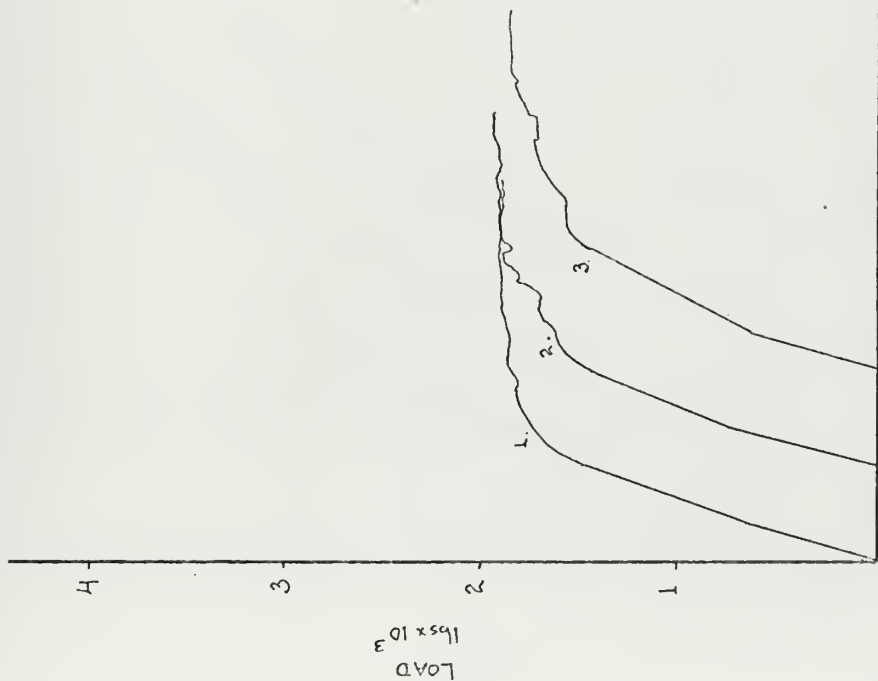


CHART DEFLECTION

1 inch =  $10^{-4}$

FOR TRUE DEFLECTION, MULTIPLY BY  $1.25 \times 10^{-4}$

FIGURE 7



SAMPLE 6-O-M

LOAD RATE = 0.05"/min  
CHART SPEED = 4.0"/min

# LOAD-DEFLECTION Curve

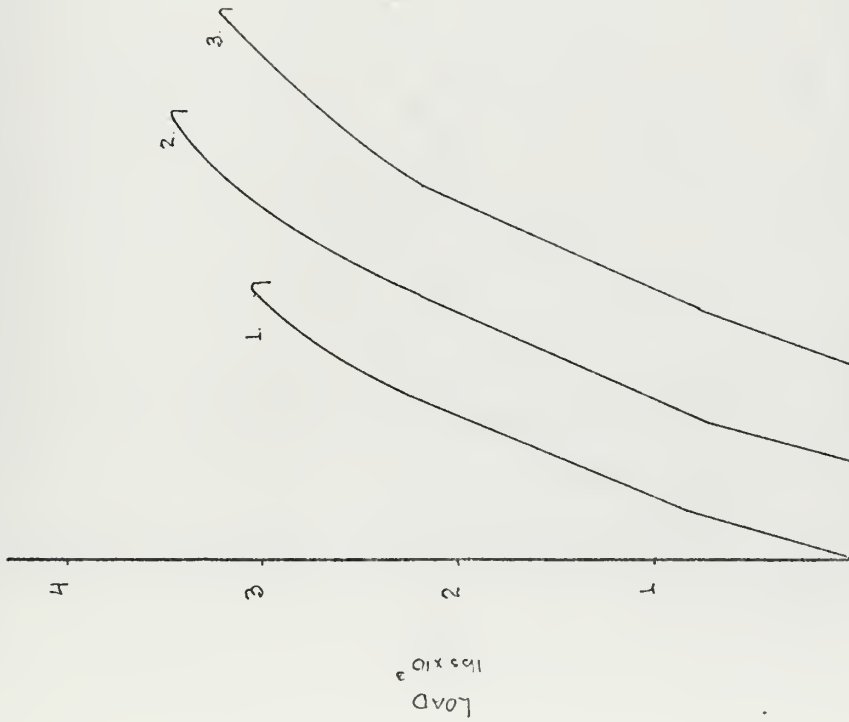


CHART DEFLECTION

1 inch = 1 inch

For DEFLECTION, Multiply By  $1.25 \times 10^{-4}$

FIGURE 8



SAMPLE 41-1-M

LOAD RATE = 0.05"/MIN

CHART SPEED = 4.0"/MIN

LOAD-DEFLECTION  
CURVE

CHART DEFLECTION

1 inch = 1 inch

FOR TRUE DEFLECTION, MULTIPLY BY  $1.25 \times 10^{-4}$ 

FIGURE 9





SAMPLE 2-2-M

LOAD RATE = 0.05"/MIN

CHART SPEED = 4.0"/MIN

# LOAD-DEFLECTION CURVE

138

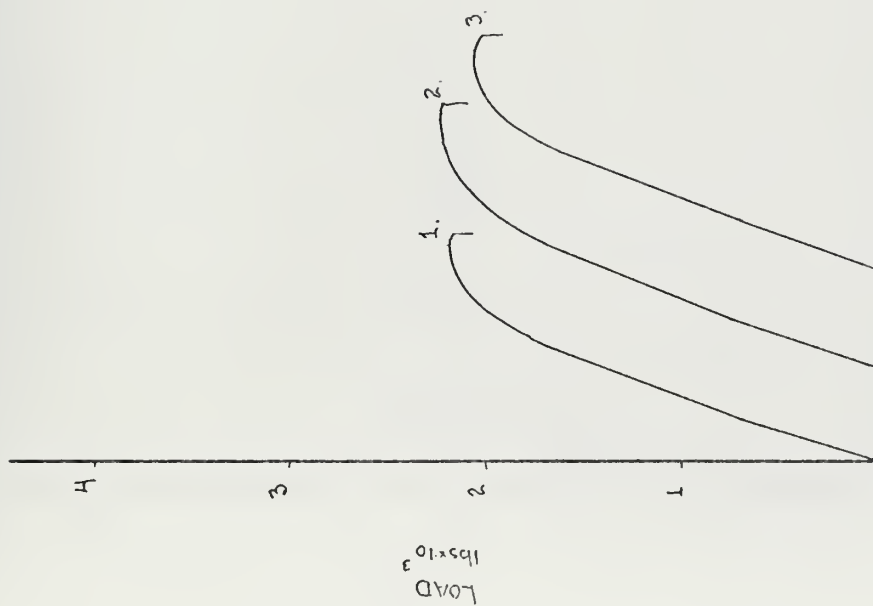


CHART DEFLECTION

1 INCH = 1 INCH

TO GET TRUE DEFLECTION, MULTIPLY BY  $1.25 \times 10^{-4}$

FIGURE 10



SAMPLE 6-O-L

LOAD RATE 0.05"/min

CHART SPEED 4.0"/min

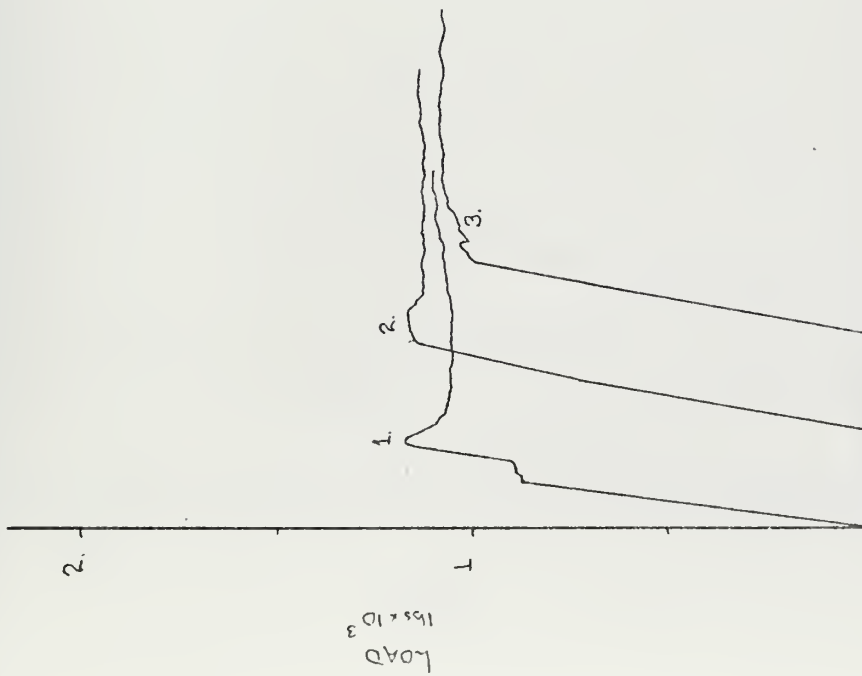
LOAD-DEFLECTION  
CURVE

CHART DEFLECTION

1 INCH = 1 INCH

TO GET TRUE DEFLECTION, MULTIPLY BY  $1.25 \times 10^{-4}$ 

FIGURE 11



SAMPLE 4.1-L  
 LOAD RATE 0.05"/MIN  
 CHART SPEED 4"/MIN

LOAD - DEFLECTION  
 CURVE

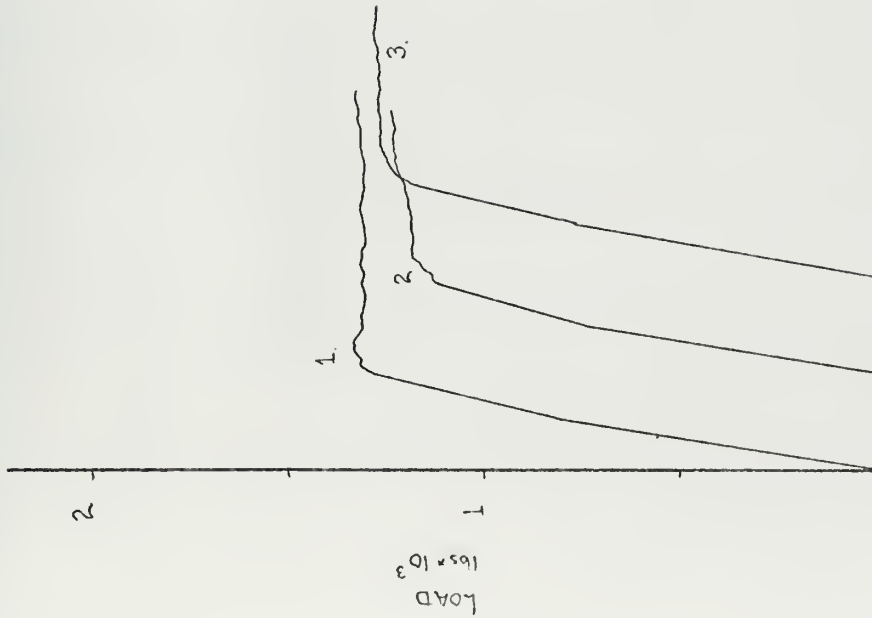


CHART DEFLECTION

1 inch = 1 inch

TO GET TRUE DEFLECTION, MULTIPLY BY  $1.25 \times 10^{-4}$

FIGURE 12



SAMPLE 2-2-L

LOAD RATE 0.05"/MIN

CHART SPEED 4"/MIN

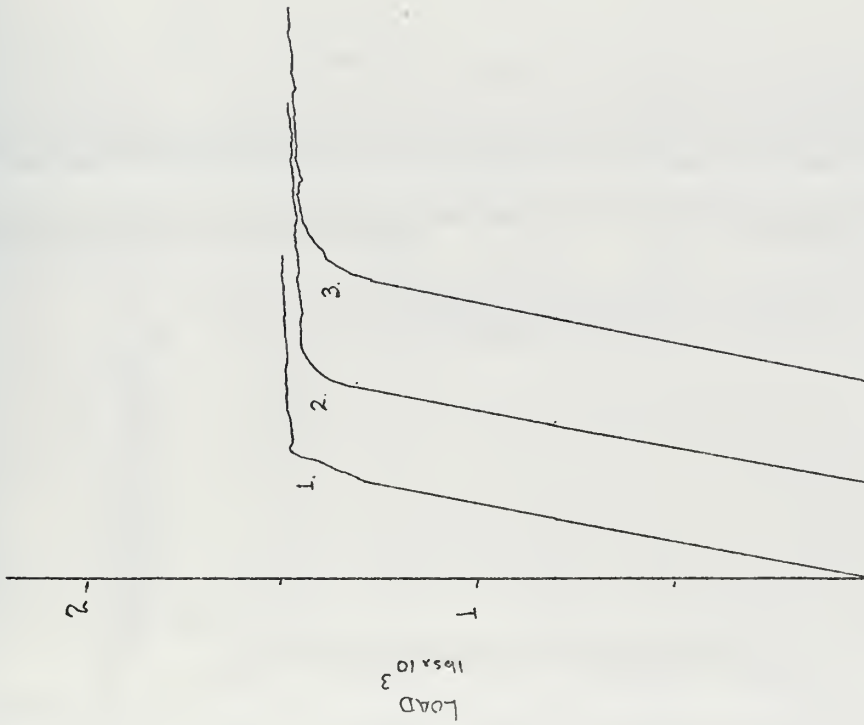
LOAD-DEFLECTION  
CURVE

CHART DEFLECTION

1 inch = 1 inch

TO GET TRUE DEFLECTION, MULTIPLY BY  $1.25 \times 10^{-4}$ 

FIGURE 13





6-0-6

4-1-H

2-2-H

11-0-0



G-9-11

2-2-M

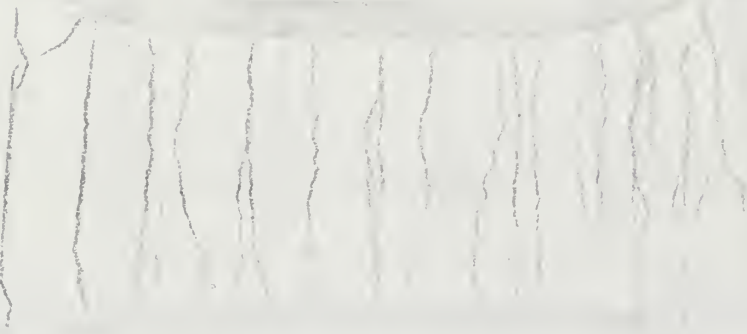
4-1-M



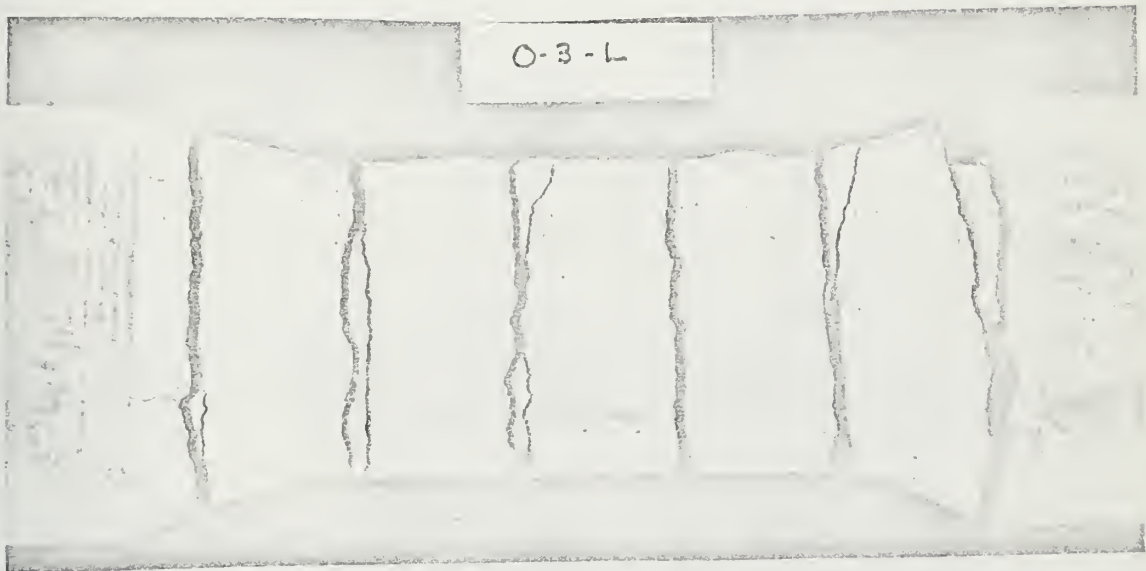
G-C-1



4-1-L











APPENDIX B



Blow Number	Deflection Rear (in x 10 <sup>3</sup> )	Indentation Front (in x 10 <sup>3</sup> )	Flow Rate (ML/0.5min)	Energy Absorbed (in-lbs)	Summation of Energy Absorbed
Sample 1					
1	6	1	0	81.26	81.26
2	81	55	0.8	176.88	258.14
3	125	100	23.5	161.84	419.98
4	174	135	138	157.88	577.86
5	228	194	410	172.03	749.89
6	325	270	480	187.98	938.87
Sample 2					
1	7	1	0	81.66	81.66
2	78	40	3.8	173.78	255.44
3	135	87	24.8	165.94	421.38
4	203	142	238	158.76	580.14
5	359	235	379	196.19	776.33
6	425	306	438	188.79	965.12
Sample 3					
1	40	25	0	179.34	179.34
2	89	75	6.8	165.57	344.91
3	161	108	125	165.33	510.24
4	237	186	409	165.33	675.57
5	395	265	495	189.30	864.87

TABLE I



## 4-1-H

Blow Number	Deflection Rear (in x 10 <sup>3</sup> )	Indentation Front (in x 10 <sup>3</sup> )	Flow Rate (ML/0.5min)	Energy Absorbed (in-lbs)	Summation of Energy absorbed
Sample 1					
1	18	8	0	88.04	88.04
2	114	90	42	180.96	269.0
3	232	141	206	174.96	443.96
4	290	225	421	182.63	626.59
5	370	312	565	177.17	803.76
6	440	386	1000	185.25	989.01
Sample 2					
1	13	9	0	87.79	87.79
2	110	95	44	181.06	268.85
3	209	156	386	175.14	449.91
4	289	217	613	167.82	625.05
5	383	312	1008	179.36	792.87
6	509	430	1780	190.06	972.23
Sample 3					
1	9	7	0	88.26	88.26
2	95	78	152	180.08	268.34
3	156	127	412	176.34	444.68
4	217	196	932	173.75	618.43
5	312	272	1600	175.61	794.04
6	430	342	2029	175.06	969.10

TABLE II



Blow Number	Deflection Rear (in x 10 <sup>3</sup> )	Indentation Front (in x 10 <sup>3</sup> )	Flow Rate (ML/0.5min)	Energy Absorbed (in-lbs)	Summation of Energy Absorbed
Sample 1					
1	63	39	198	185.46	185.46
2	173	109	956	169.28	354.74
3	281	286	1800	167.18	521.92
4	330	353	1925	162.22	684.14
5	407	-	2166	161.98	846.12
Sample 2		Machine failure			
1					
2	143	100	0	80.39	80.39
3	268	200	273	-	-
4		same	1200	-	-
5		same	-	-	-
6		same	-	-	-
Sample 3					
1	2	1	0	80.99	80.99
2	44	35	2	165.73	246.72
3	107	100	54	170.77	417.49
4	233	190	522	169.31	586.80
5	315	238	1020	164.28	751.08
6	452	306	2010	163.52	914.60

TABLE III





Sample	Blow Number	Deflection Rear (in x 10 <sup>3</sup> )	Indentation Front (in x 10 <sup>3</sup> )	Flow Rate (ML/0.5min)	Energy Absorbed (in-lbs)	Summation of energy Absorbed
Sample 1	1	49	15	0	82.47	82.47
	2	103	72	2	171.53	254.0
	3	156	121	40	155.26	409.26
	4	235	185	161	162.17	511.42
	5	330	270	349	187.88	699.30
	6	460	392	642	181.98	881.28
Sample 2	1	43	15	0	81.75	81.75
	2	98	70	1	177.88	259.13
	3	145	117	7	156.06	415.69
	4	224	175	109	160.48	576.17
	5	350	260	250	167.83	734.00
	6	500	348	334	166.29	900.29
Sample 3	1	41	12	0	82.53	82.53
	2	103	75	7	182.44	264.97
	3	160	130	43	160.81	425.78
	4	260	190	244	171.90	597.68
	5	346	262	435	189.95	787.63
	6	-	380	540	187.93	975.56

TABLE IV



4-1-M

Blow Number	Deflection Rear (in x 10 <sup>3</sup> )	Indentation Front (in x 10 <sup>3</sup> )	Flow Rate (ML/0.5min)	Energy Absorbed (in-lbs)	Summation of energy absorbed
Sample 1					
1	45	15	0	84.77	84.77
2	125	105	59	180.92	265.69
3	235	188	248	184.56	450.25
4	368	271	300	182.81	633.06
5	470	334	762	181.02	814.08
6	550	450	2336	183.09	997.17
Sample 2					
1	20	15	0	83.91	83.91
2	120	91	103	183.88	267.79
3	218	181	555	176.09	443.88
4	350	275	890	188.43	632.31
5	485	370	1561	187.15	819.46
6	560	470	2320	192.18	1011.64
Sample 3					
1	40	12	0	81.89	81.89
2	120	85	7	180.94	262.83
3	211	160	118	179.45	442.28
4	303	237	480	188.51	630.79
5	398	330	685	188.51	829.30
6	-	-	2113	184.02	1013.52

TABLE V



Blow Number	Deflection Rear (in x 10 <sup>3</sup> )	Indentation Front (in x 10 <sup>3</sup> )	Flow Rate (ML/0.5min)	Energy Absorbed (in-lbs)	Summation of energy absorbed.
Sample 1					
1	97	61	-	192.36	192.36
2	198	161	-	188.34	380.70
3	327	265	-	189.42	570.12
4	470	400	-	189.25	759.37
5	530	480	-	186.21	945.58
Sample 2					
1	82	40	-	196.30	196.30
2	181	114	-	193.55	389.85
3	275	251	-	187.84	577.69
4	391	340	-	190.77	768.46
5	480	420	-	186.73	955.19
Sample 3					
1	100	52	-	194.91	194.91
2	226	182	-	190.51	385.42
3	400	290	-	190.12	575.54
4	500	391	-	186.69	762.23
5	540	480	-	183.49	945.72

TABLE VI



6-0-0-L

Sample	Blow Number	Deflection Rear (in x 10 <sup>3</sup> )	Indentation Front (in x 10 <sup>3</sup> )	Flow Rate (ML/0.5min)	Energy Absorbed (lb-in)	Summation of energy absorbed
Sample 1	1	105	66	-	189.96	189.96
	2	187	134	-	182.65	372.61
	3	308	240	-	191.77	564.38
	4	410	314	-	180.05	744.43
	5	530	391	-	184.33	928.76
Sample 2	1	90	54	1.5	194.08	194.08
	2	189	135	2.0	185.30	379.38
	3	282	222	594	182.33	561.71
	4	362	305	1852	187.98	749.69
	5	585	504	2233	183.84	933.65
Sample 3	1	92	72	3.0	191.73	191.73
	2	213	150	8.5	188.08	379.81
	3	307	262	510	182.02	561.83
	4	388	341	2013	178.80	740.63
	5	520	446	2136	188.86	929.49

TABLE VII





Blow Number	Deflection Rear (in x 10 <sup>3</sup> )	Indentation Front (in x 10 <sup>3</sup> )	Flow Rate (ML/0.5min)	Energy Absorbed (in-lbs)	Summation of energy absorbed
Sample 1	110	32	0.5	185.85	185.85
	202	142	106	195.43	381.28
	315	235	919	187.73	569.01
	425	308	1728	182.74	751.75
	525	396	2196	186.05	937.80
Sample 2	75	55	0.5	187.15	187.15
	186	150	3.0	192.07	379.22
	272	240	702	183.20	562.42
	360	306	2020	178.16	740.58
	439	385	2280	176.74	917.32
Sample 3	62	62	2.0	193.63	193.63
	181	176	146	194.14	387.77
	265	250	904	182.20	569.97
	374	325	1957	186.90	756.87
	462	440	2073	188.96	945.83

TABLE VIII



Sample	Blow Number	Deflection Rear (in x 10 <sup>3</sup> )	Indentation Front (in x 10 <sup>3</sup> )	Flow Rate (ML/0.5min)	Energy Absorbed (in-lbs)	Summation of energy absorbed
Sample 1.	1	165	100	140	169.16	169.16
	2	317	230	958	189.0	358.16
	3	466	305	2063	177.97	536.13
	4	587	386	2273	175.26	711.39
	5	-	520	2273	176.35	877.74
Sample 2	1	98	80	187	199.24	199.24
	2	228	182	1253	183.71	382.95
	3	334	291	2133	181.76	564.71
	4	425	383	2219	177.44	742.15
	5	500	475	2219	175.11	917.26
Sample 3	1	45	13	0	180.86	180.86
	2	156	117	494	199.95	380.81
	3	292	210	1009	178.24	559.05
	4	417	381	1930	175.06	734.11
	5	498	460	2152	170.87	904.88

TABLE IX



## FIBERS

Blow Number	Deflection Rear (in x 10 <sup>3</sup> )	Indentation Front (in x 10 <sup>3</sup> )	Flow Rate (ML/0.5min)	Energy Absorbed (in-lbs)	Summation of energy Absorbed
Sample 1					
1	28	5	0	89.87	89.87
2	183	109	10	197.04	286.91
3	490	342	1731	206.96	493.87
4	--	--	2450	223.36	727.23
Sample 2					
1	70	6	0	87.90	87.90
2	218	124	20	200.56	288.46
3	520	344	1400	205.92	494.38
4	905	560	2450	205.94	700.32
5	--	--	2450	220.46	920.78
Sample 3					
1	95	5	0	90.75	90.75
2	219	115	231	201.08	291.83
3	500	335	2045	203.00	494.83
4	--	--	2450	220.66	715.49

TABLE X



0-3-L

Blow Number	Deflection Rear (in x10 <sup>3</sup> )	Indentation Front (in x 10 <sup>3</sup> )	Flow Rate (ML/0.5min)	Energy Absorbed (in-lbs)	Summation of energy absorbed
Sample 1					
1	35	20	0	86.23	86.23
2	-	-	-	-	-
3	-	-	-	-	-
4	-	-	-	-	-
Sample 2					
1	38	18	87	82.07	82.07
2	177	138	1620	190.09	272.16
3	275	244	2164	184.93	457.09
4	345	331	2245	188.83	645.92
5	-	510		186.02	831.94
Sample 3					
1	55	24	0	86.86	86.86
2	185	162	305	190.14	277.0
3	-	260	1435	183.27	460.27
4	-	360	2122	185.72	645.99
5	-	500	2425	183.82	829.81

TABLE XI





EFFECT OF  
ENERGY ABSORPTION  
ON  
FRONT INDENTATION  
H SERIES

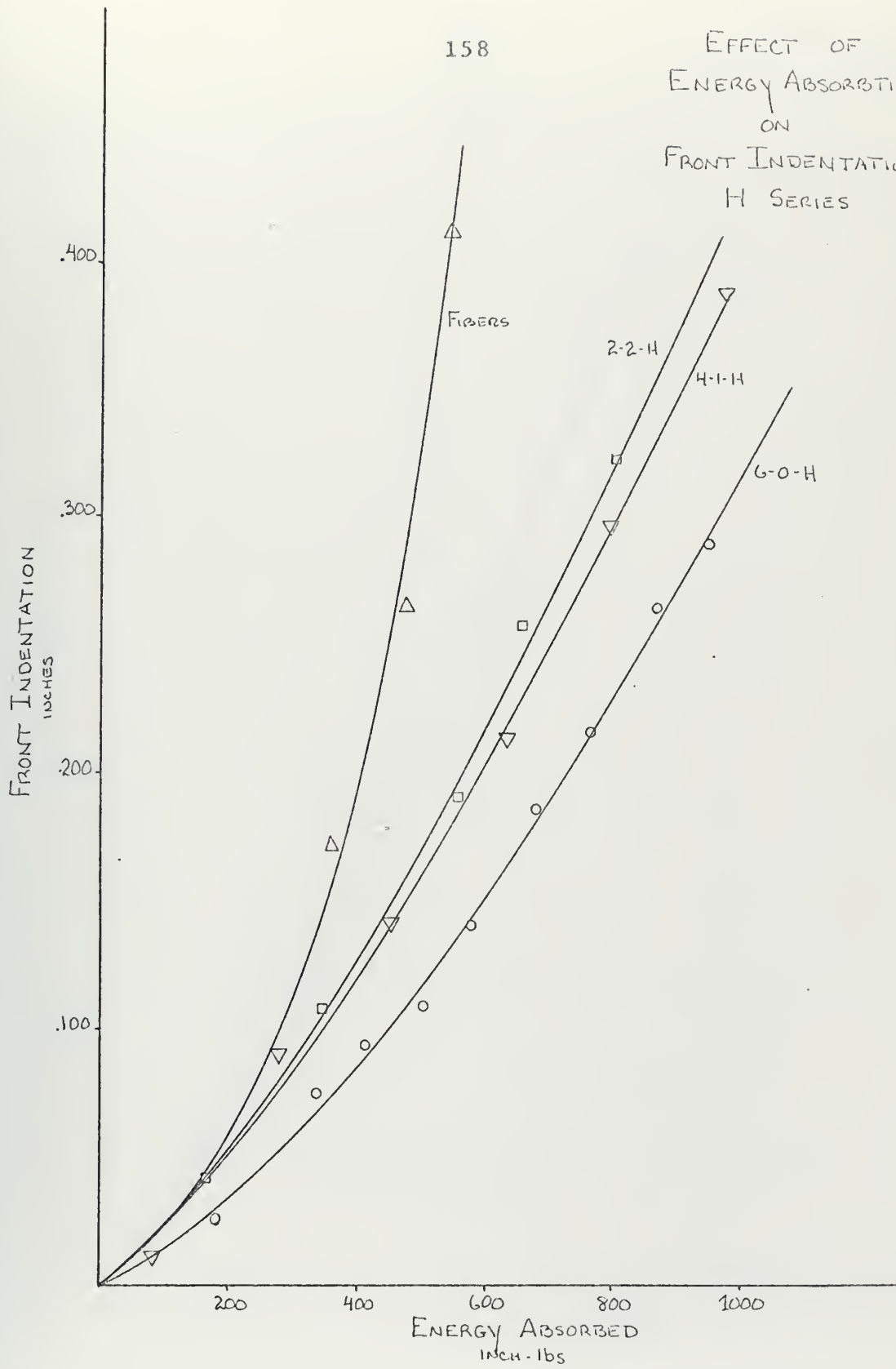


FIGURE 1



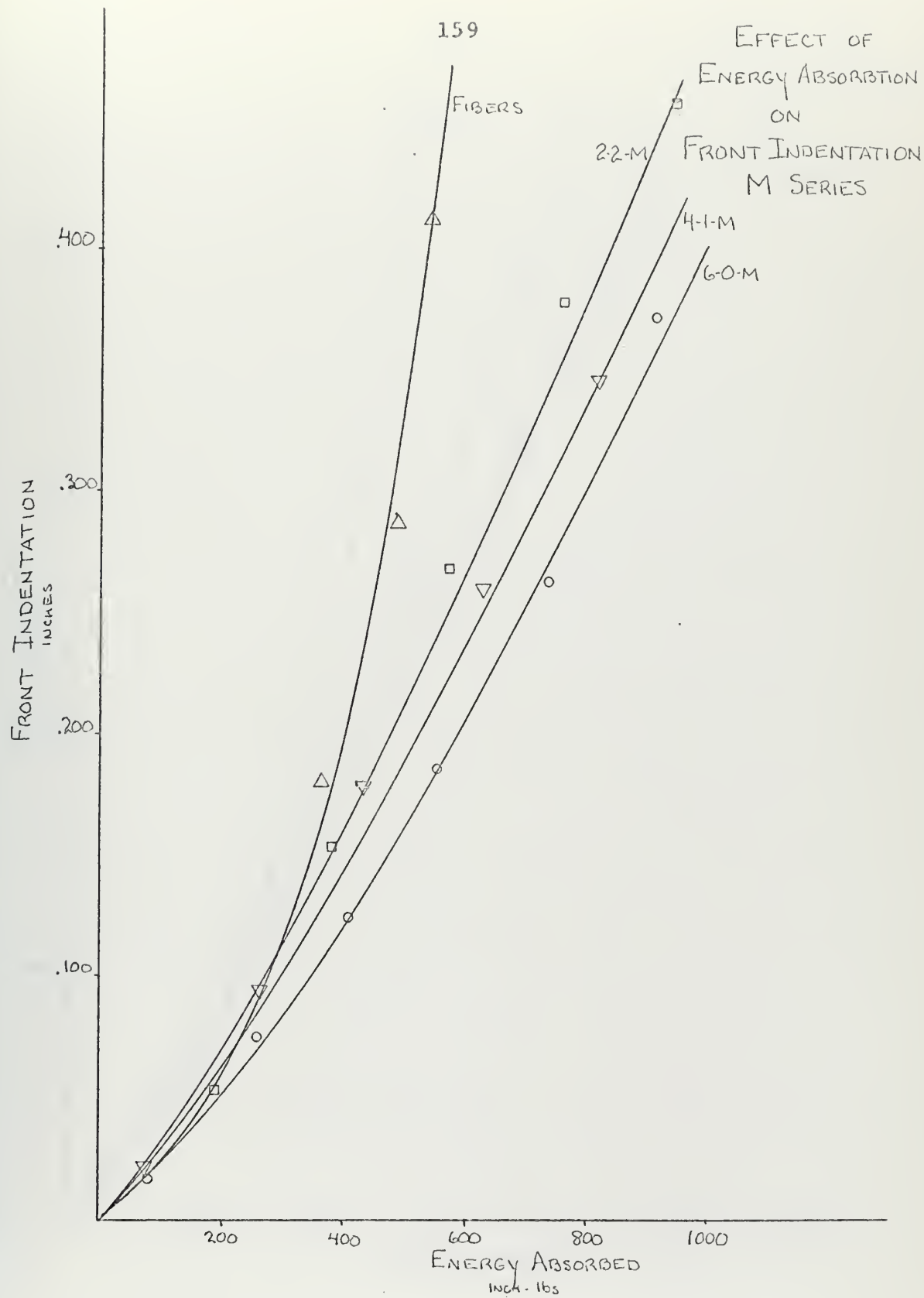


FIGURE 2



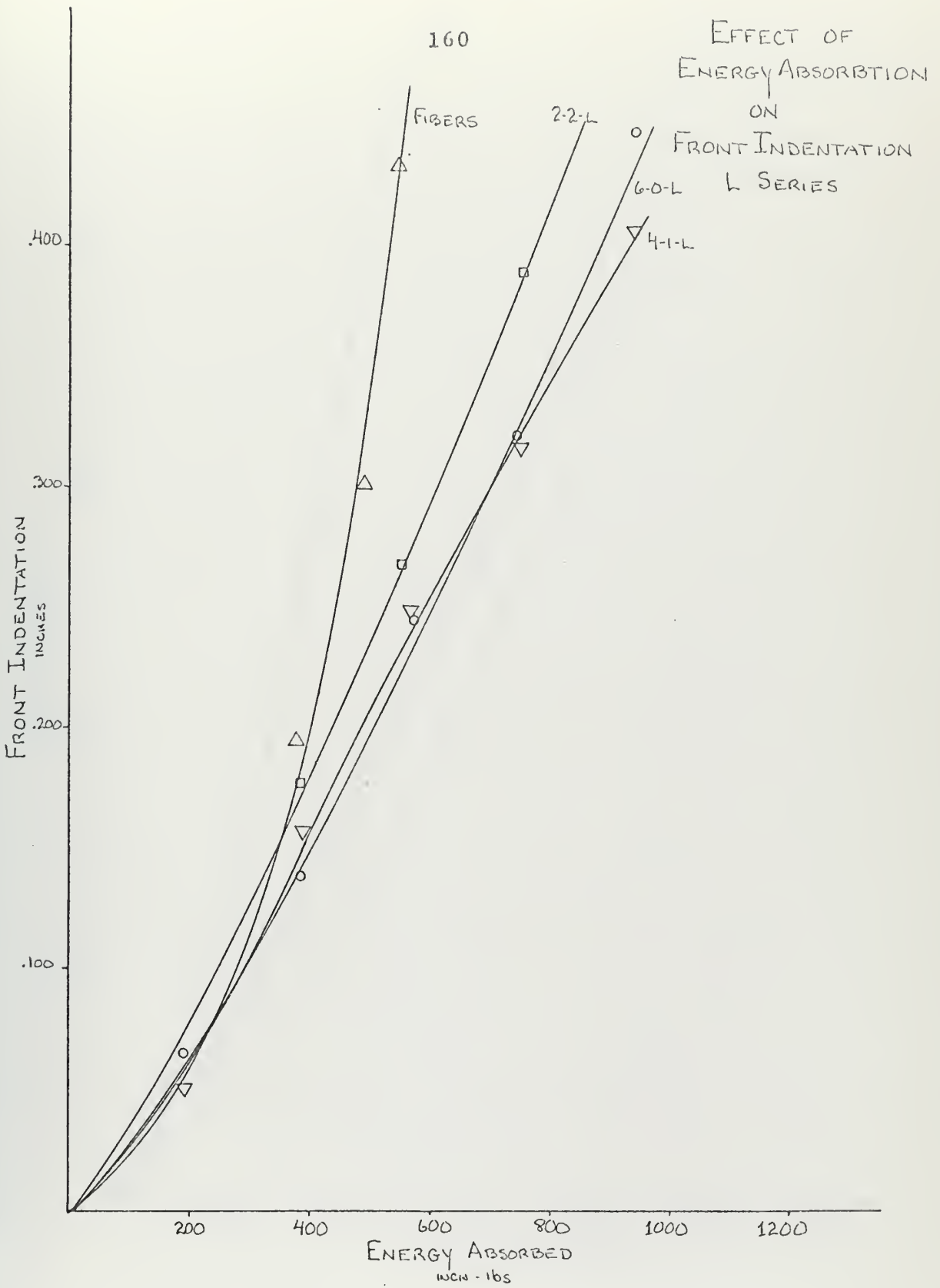


FIGURE 3



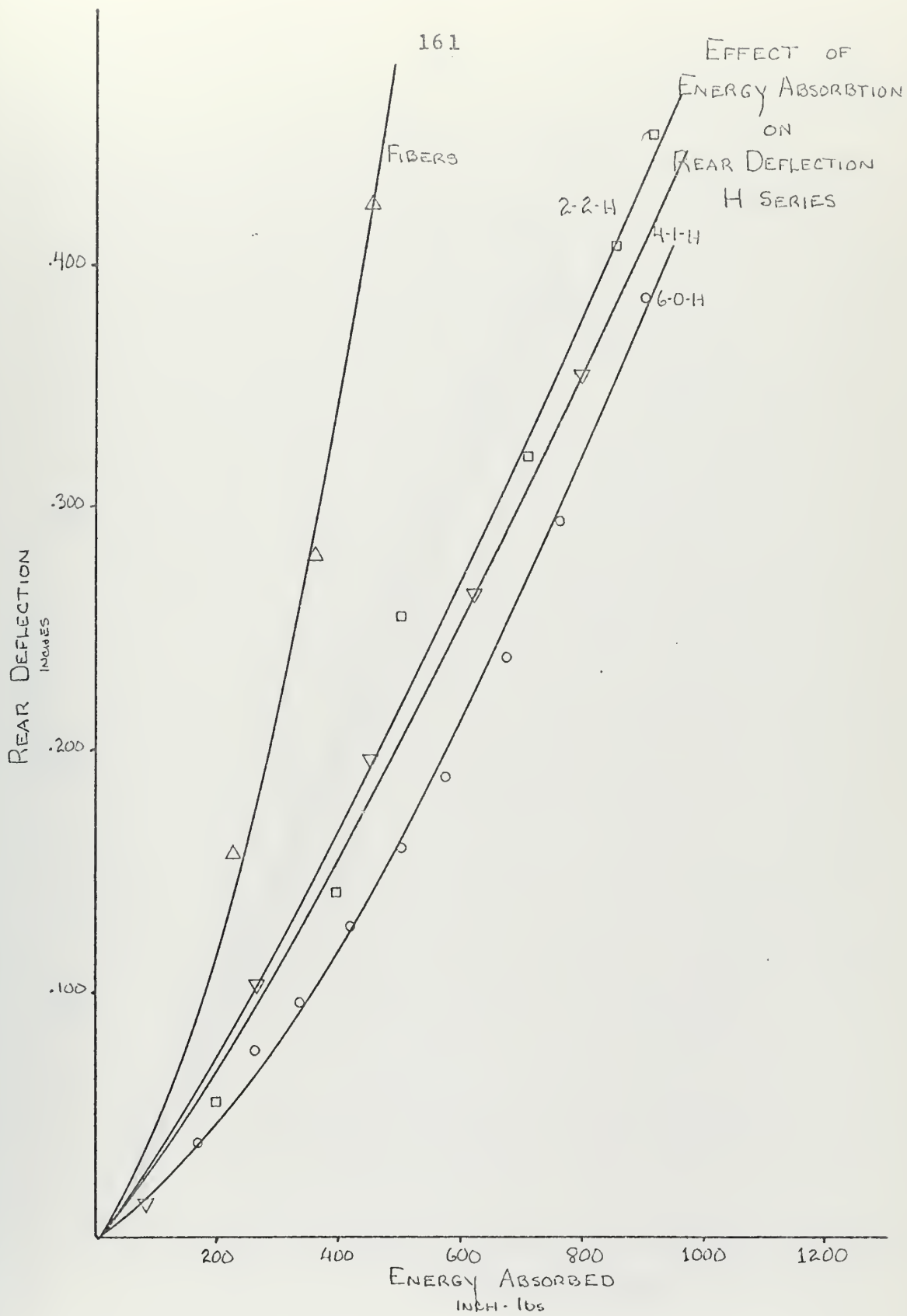


FIGURE 4





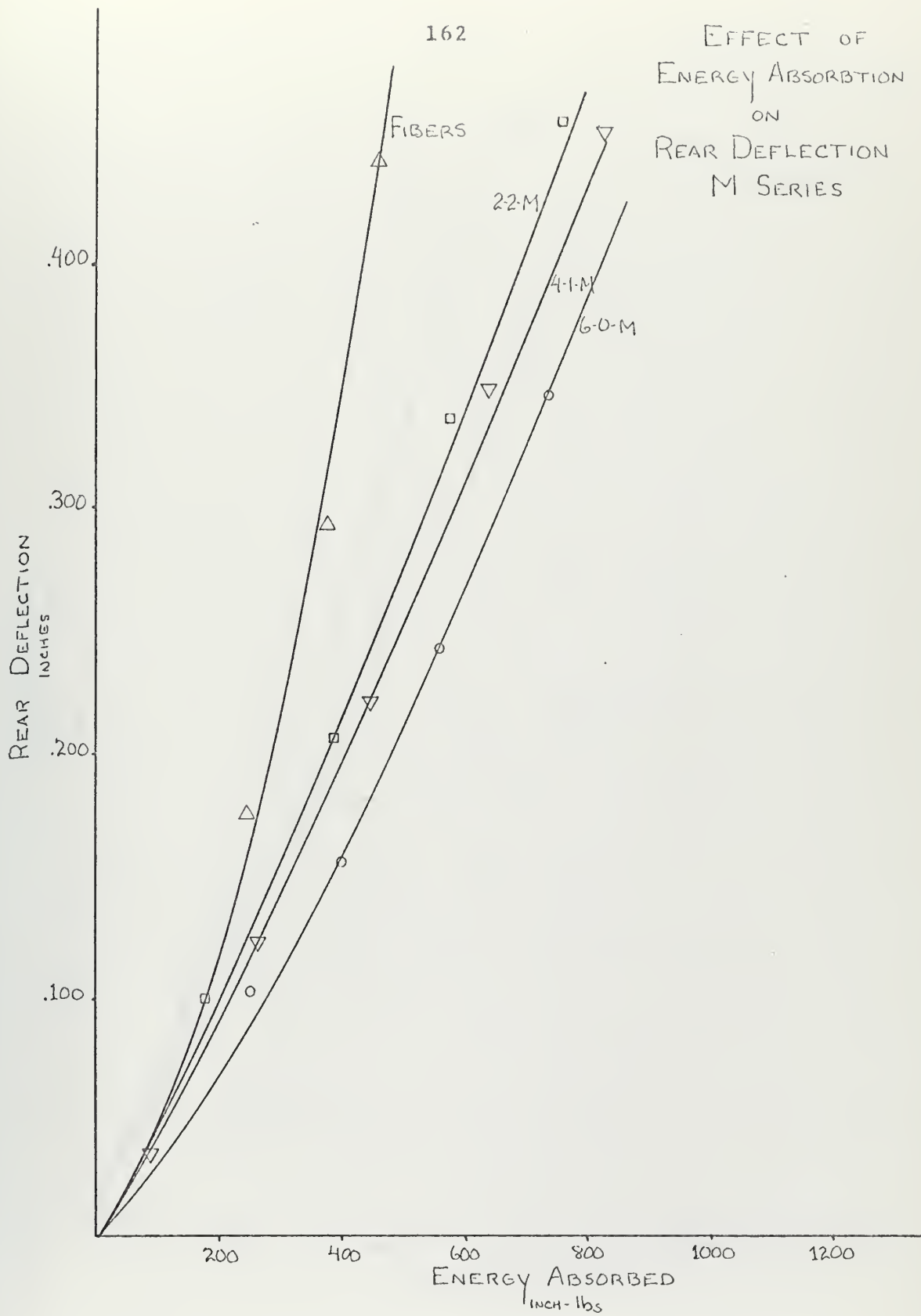


FIGURE 5



EFFECT OF  
ENERGY ABSORPTION  
ON  
REAR DEFLECTION  
L SERIES

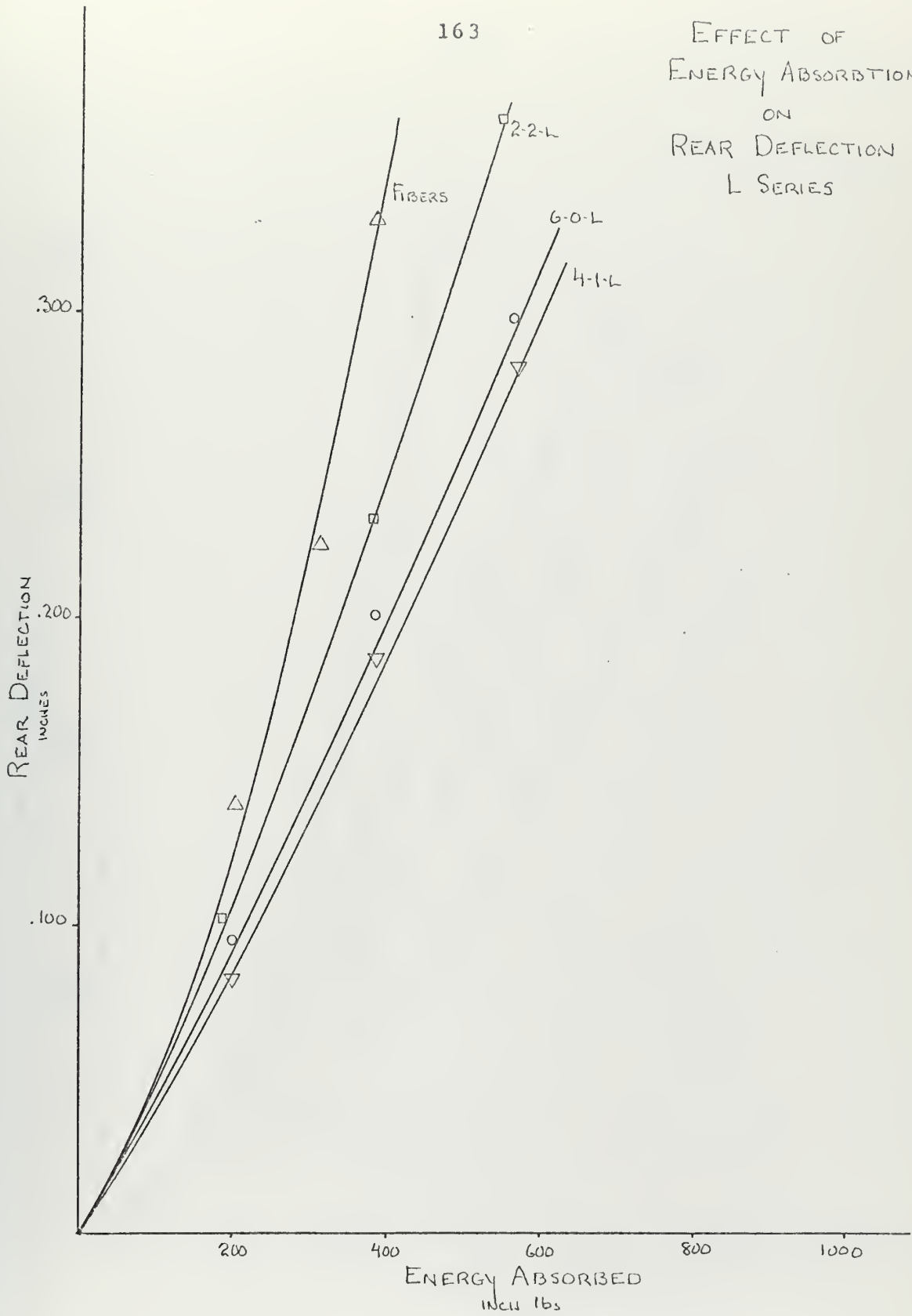


FIGURE 6



EFFECT OF  
ENERGY ABSORPTION  
ON  
FRONT INDENTATION  
G-O SERIES

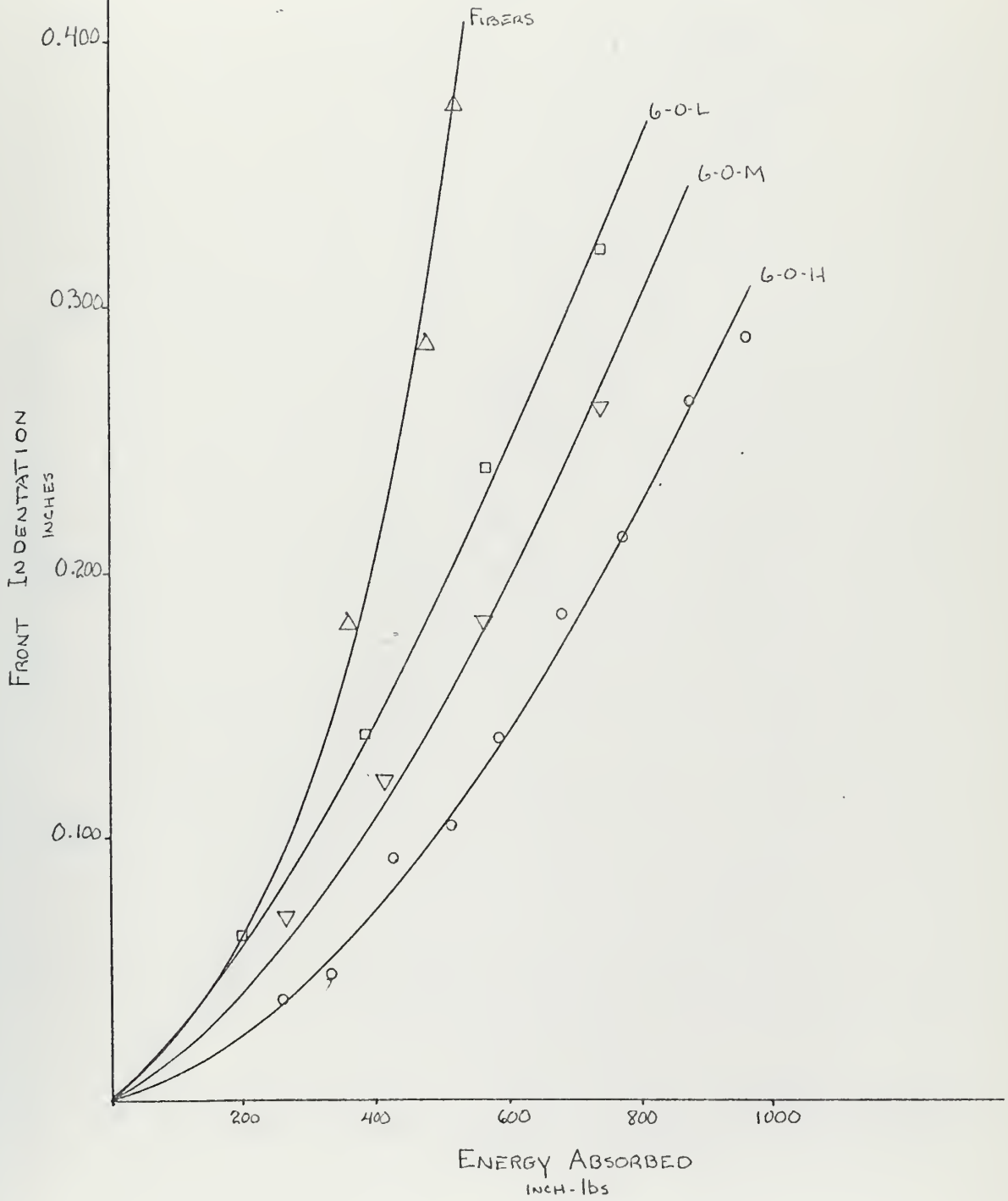


FIGURE 7



EFFECT OF  
ENERGY ABSORPTION  
ON  
FRONT INDENTATION  
4-1 SERIES

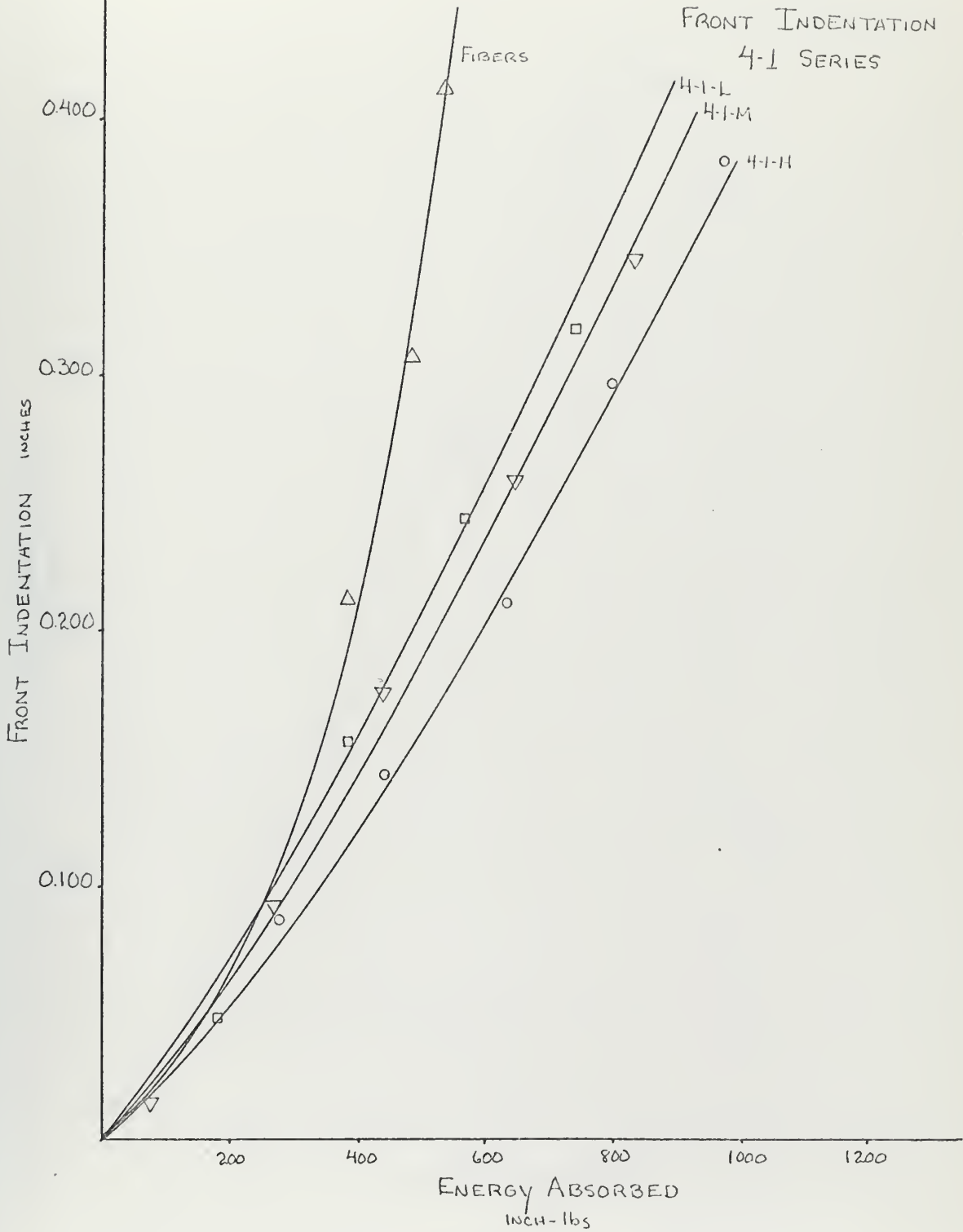


FIGURE 8





EFFECT OF  
ENERGY ABSORPTION  
ON  
FRONT INDENTATION  
2-2 SERIES

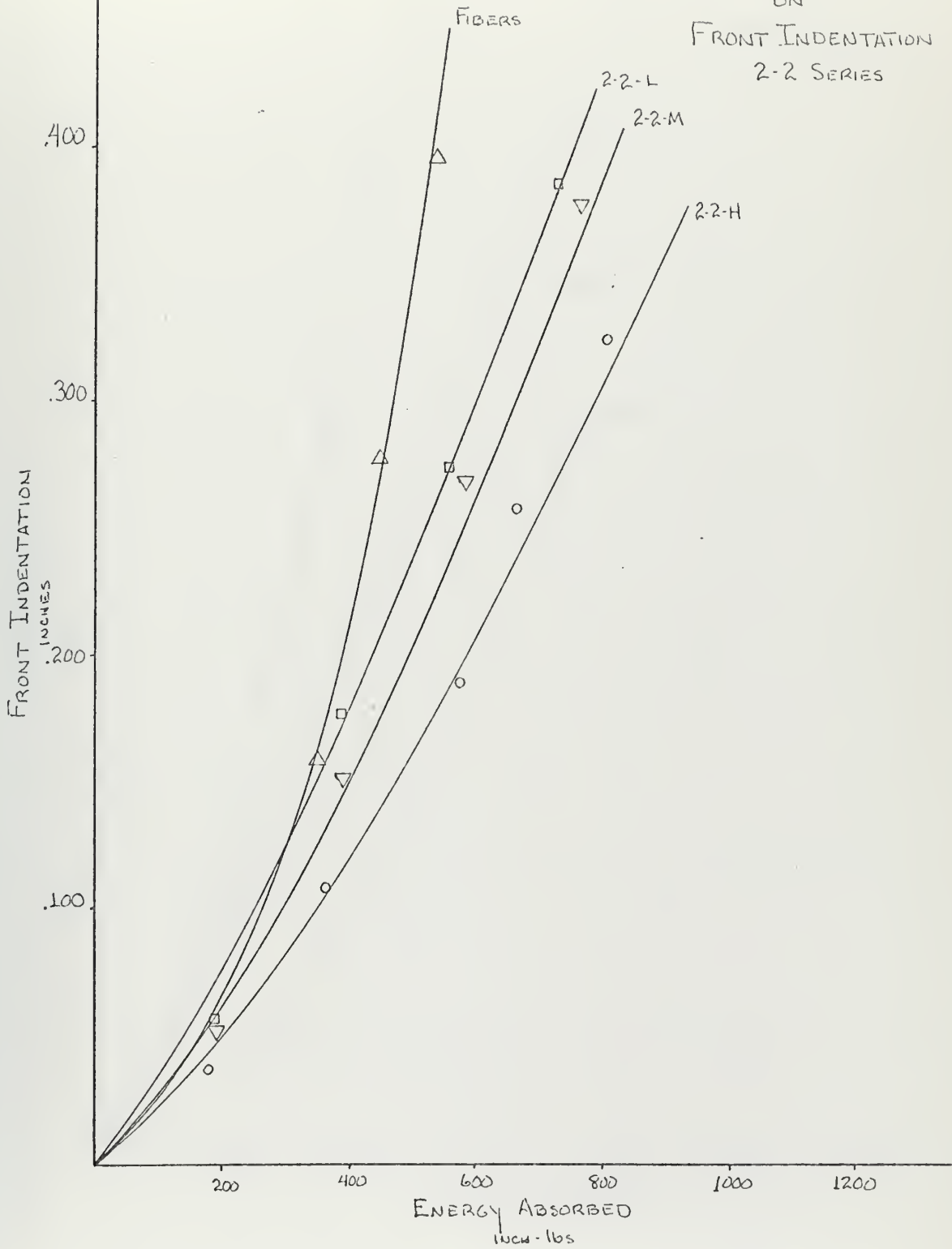


FIGURE 9



EFFECT OF  
ENERGY ABSORPTION  
ON  
REAR DEFLECTION  
G-O SERIES

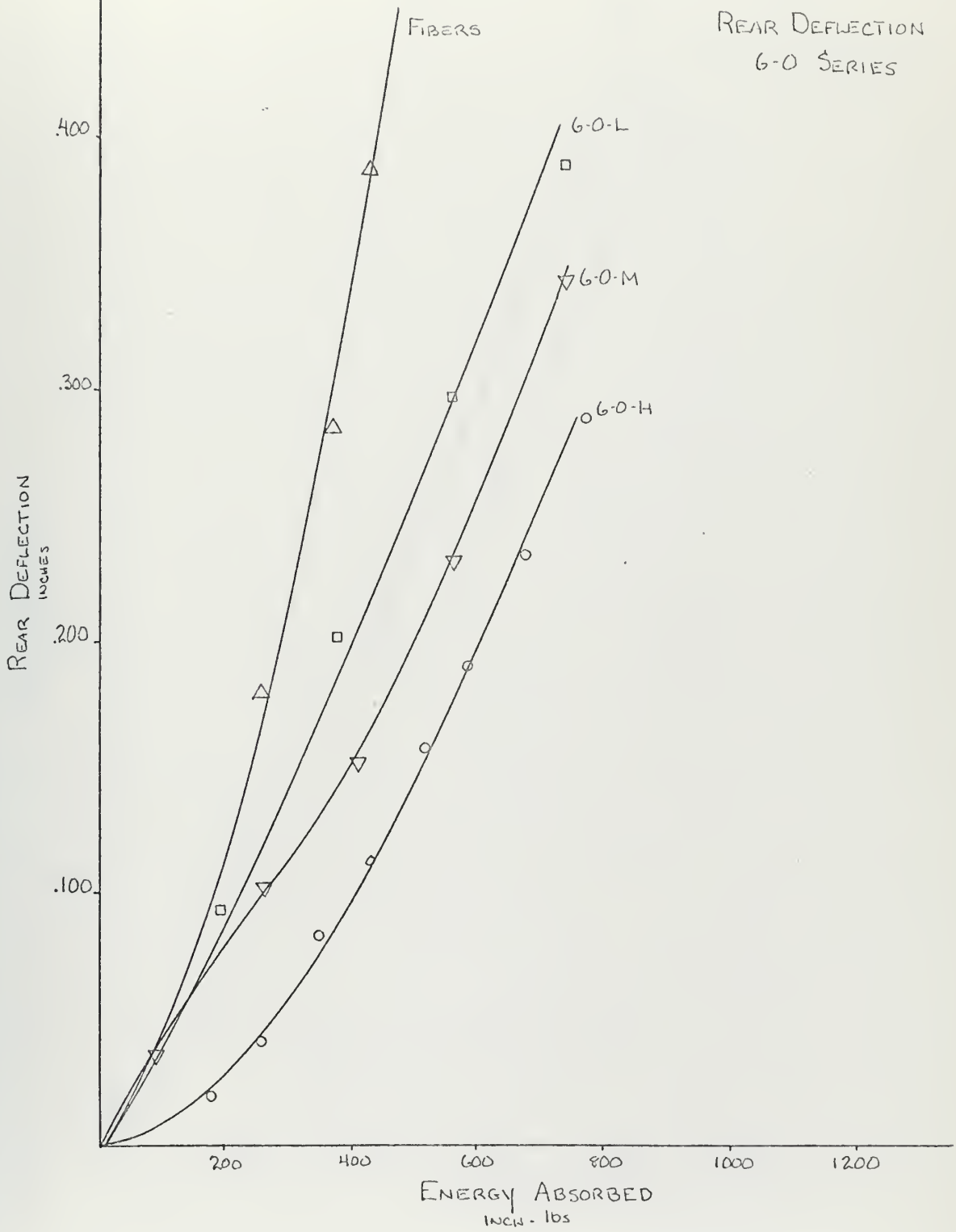


FIGURE 10



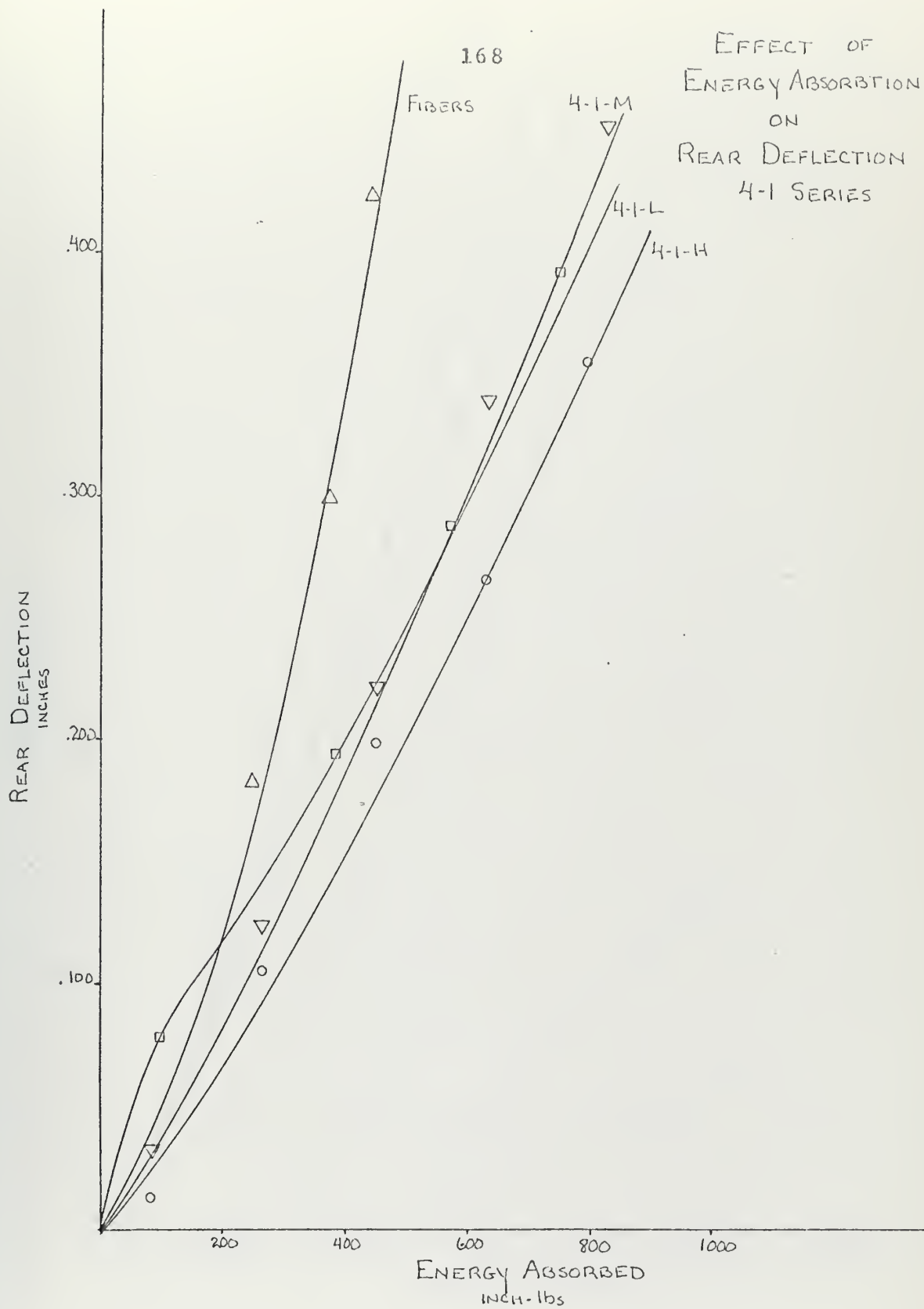


FIGURE 11



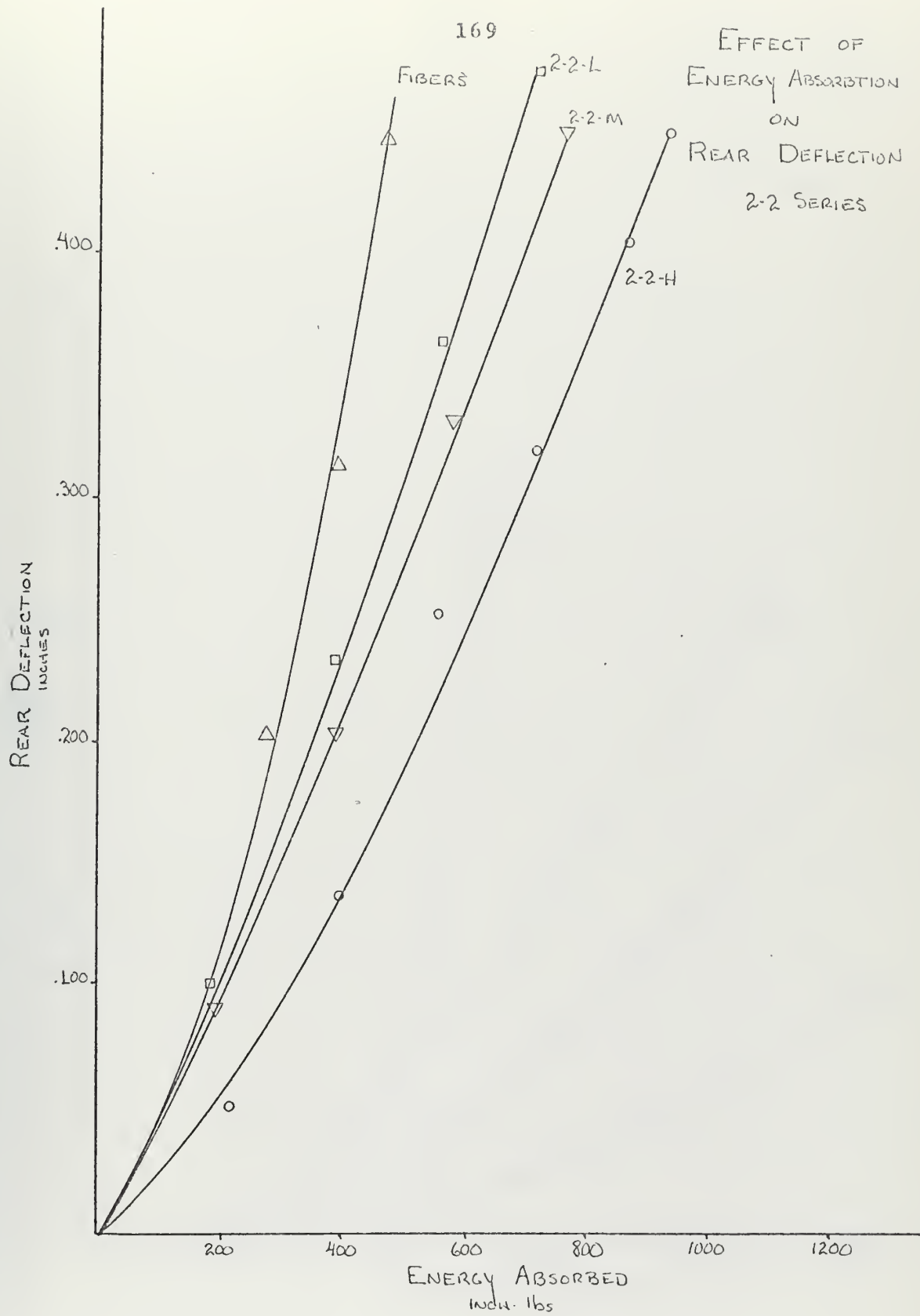


FIGURE 12





EFFECT OF  
ENERGY ABSORPTION  
ON  
FLOW RATE  
H SERIES

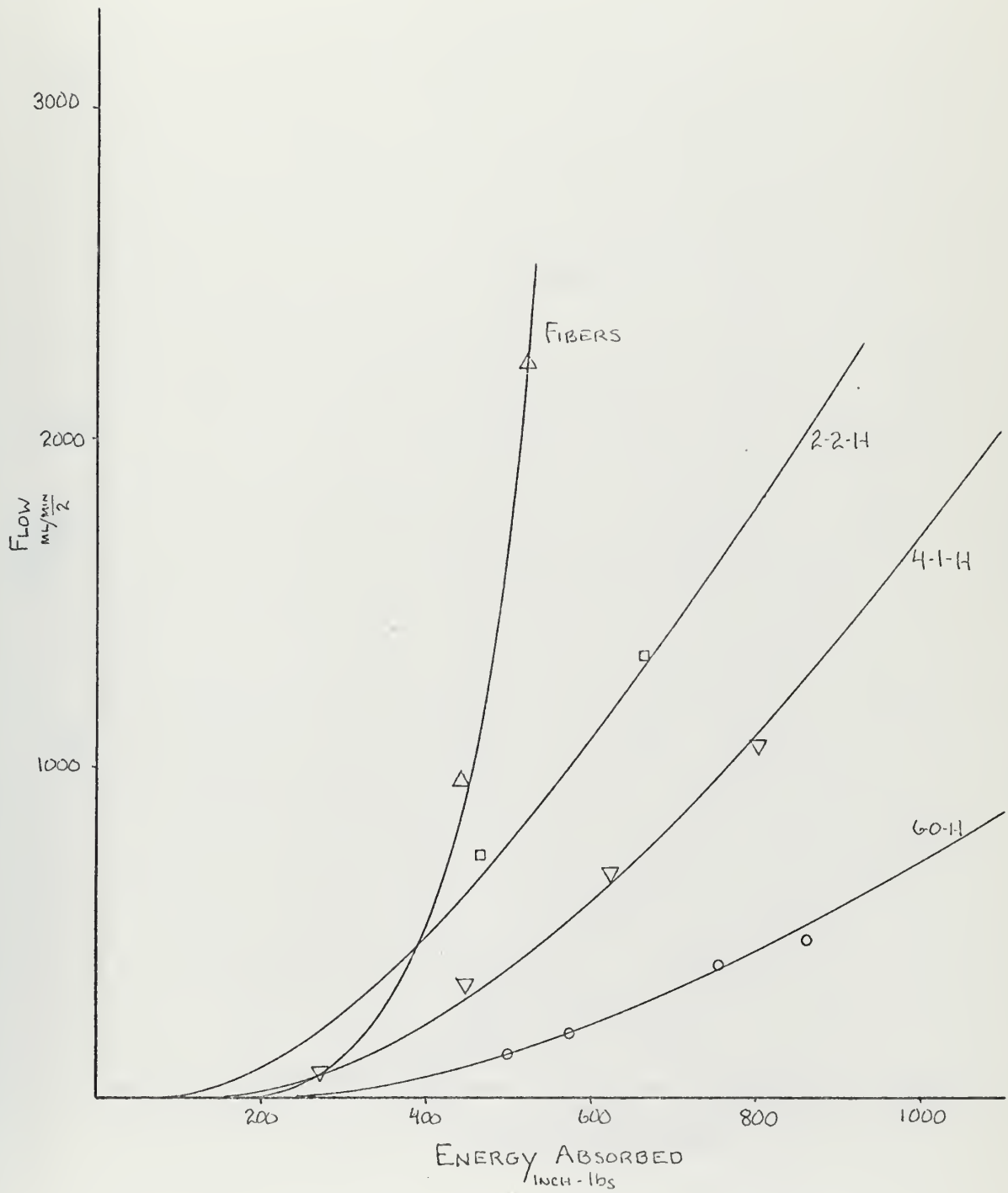


FIGURE 13



EFFECT OF  
ENERGY ABSORPTION  
ON  
FLOW RATE  
M SERIES

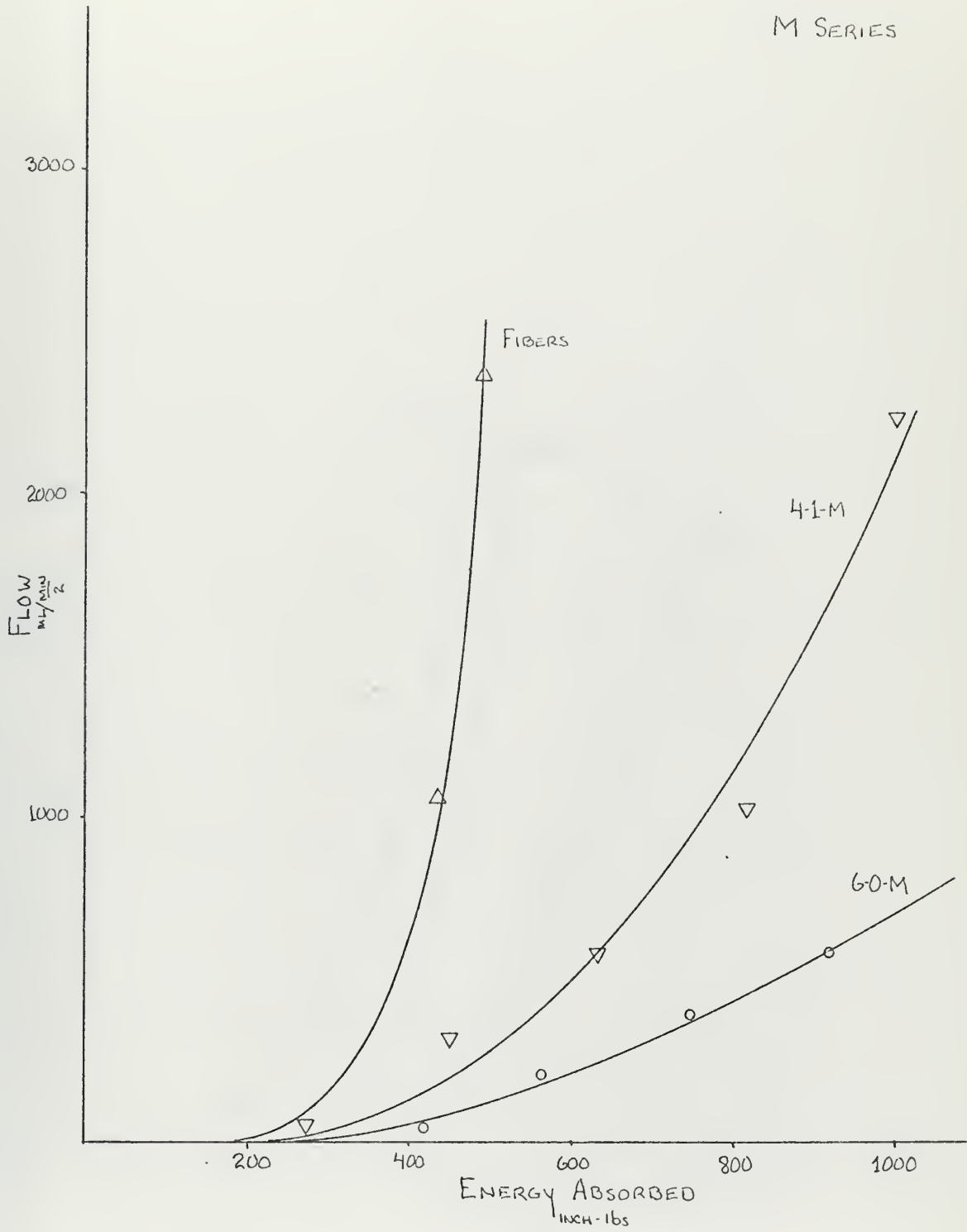


FIGURE 14



EFFECT OF  
ENERGY ABSORPTION  
ON  
FLOW RATE  
L SERIES

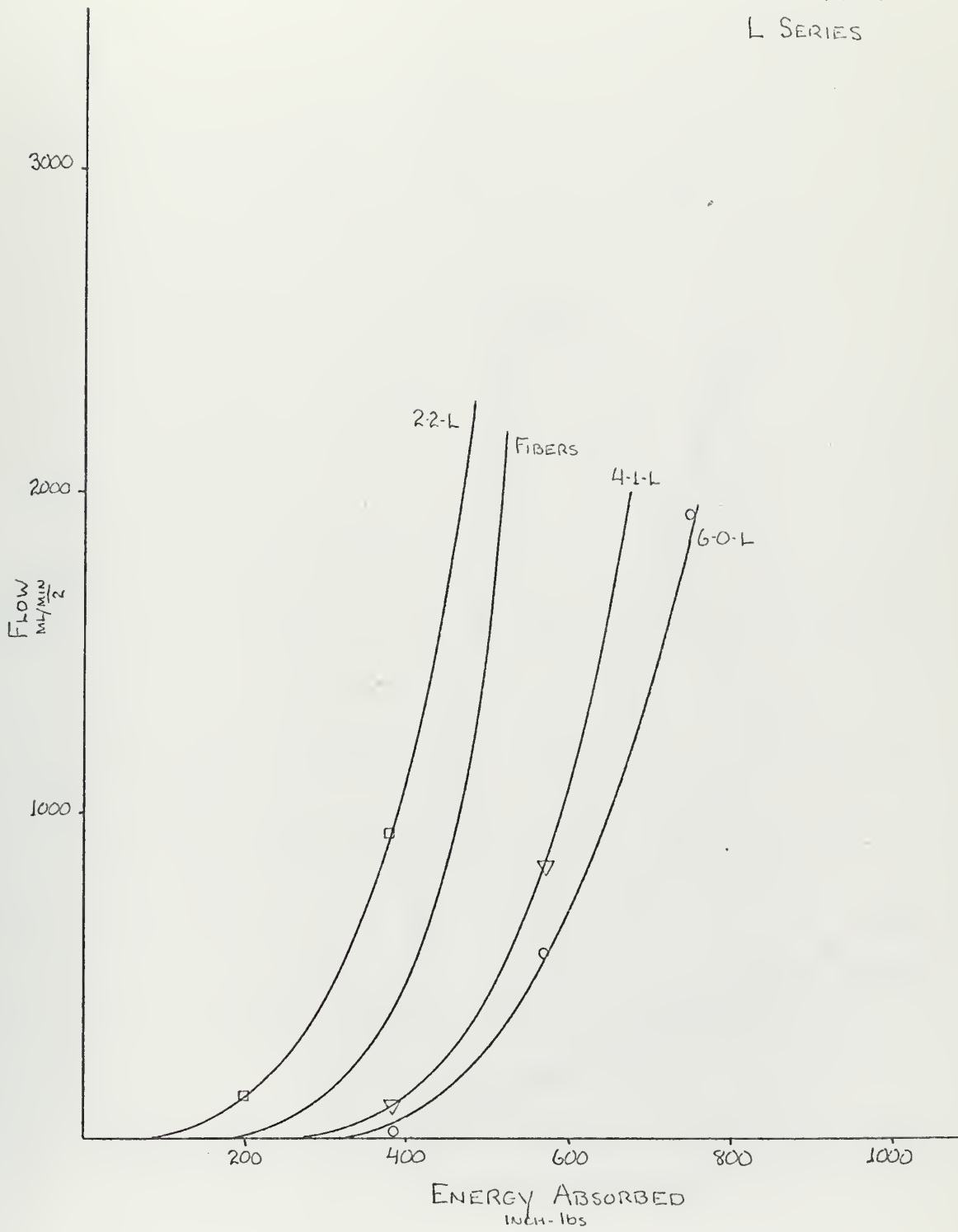


FIGURE 15



EFFECT OF  
ENERGY ABSORPTION  
ON  
FLOW RATE  
6.0 SERIES

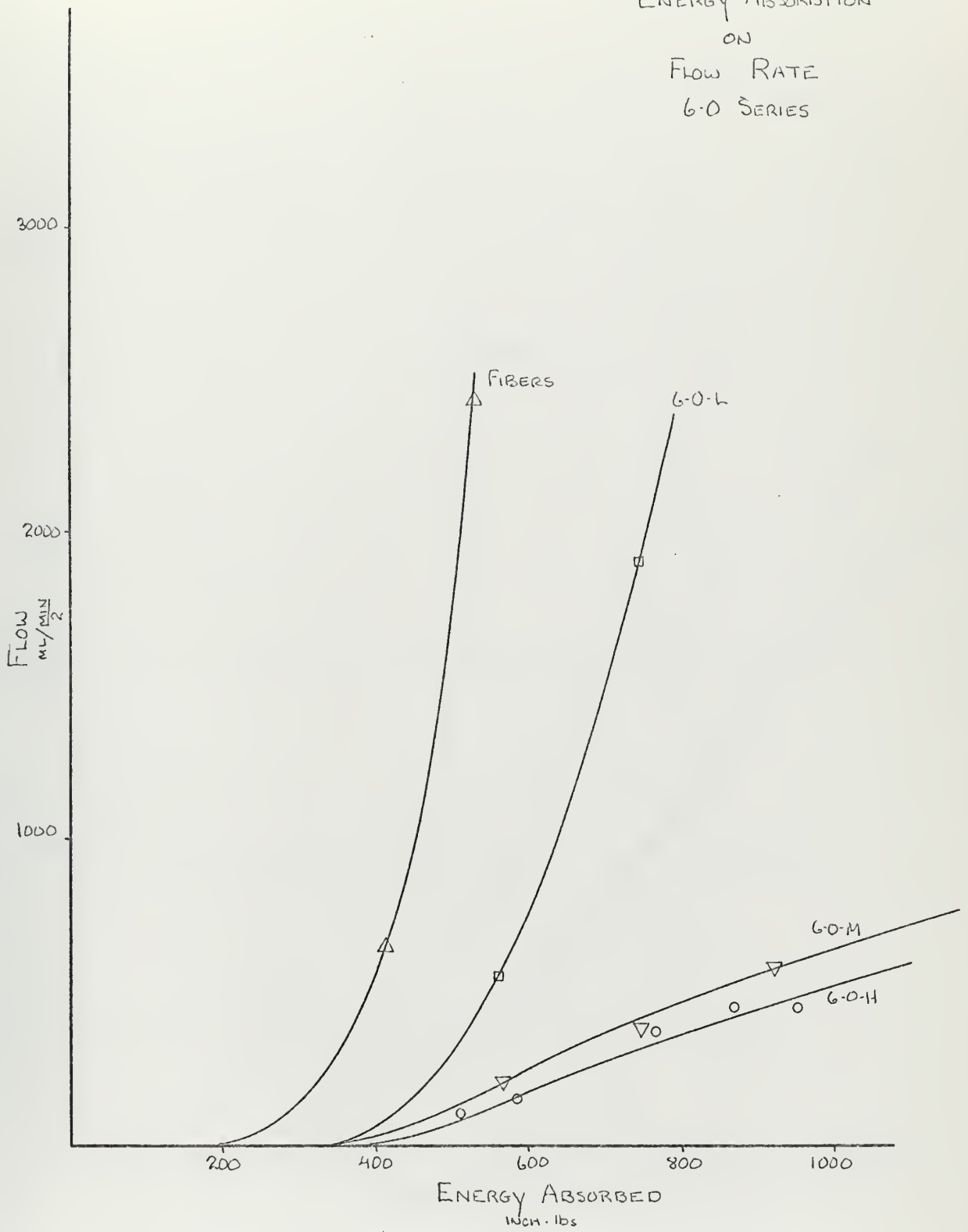


FIGURE 16





EFFECT OF  
ENERGY ABSORPTION  
ON  
FLOW RATE  
4-1 SERIES

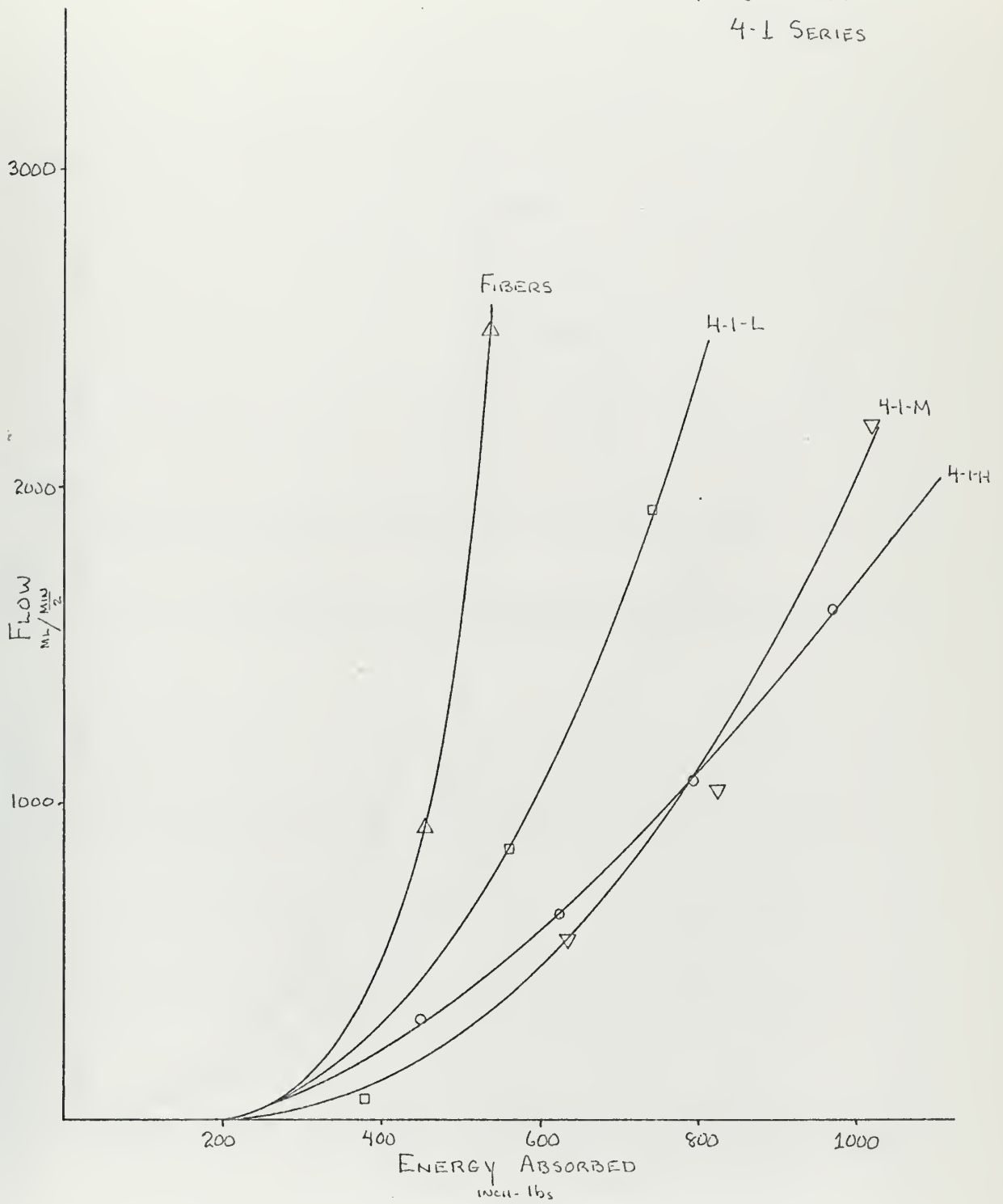


FIGURE 17



EFFECT OF  
ENERGY ABSORPTION  
ON  
FLOW RATE  
2-2 SERIES

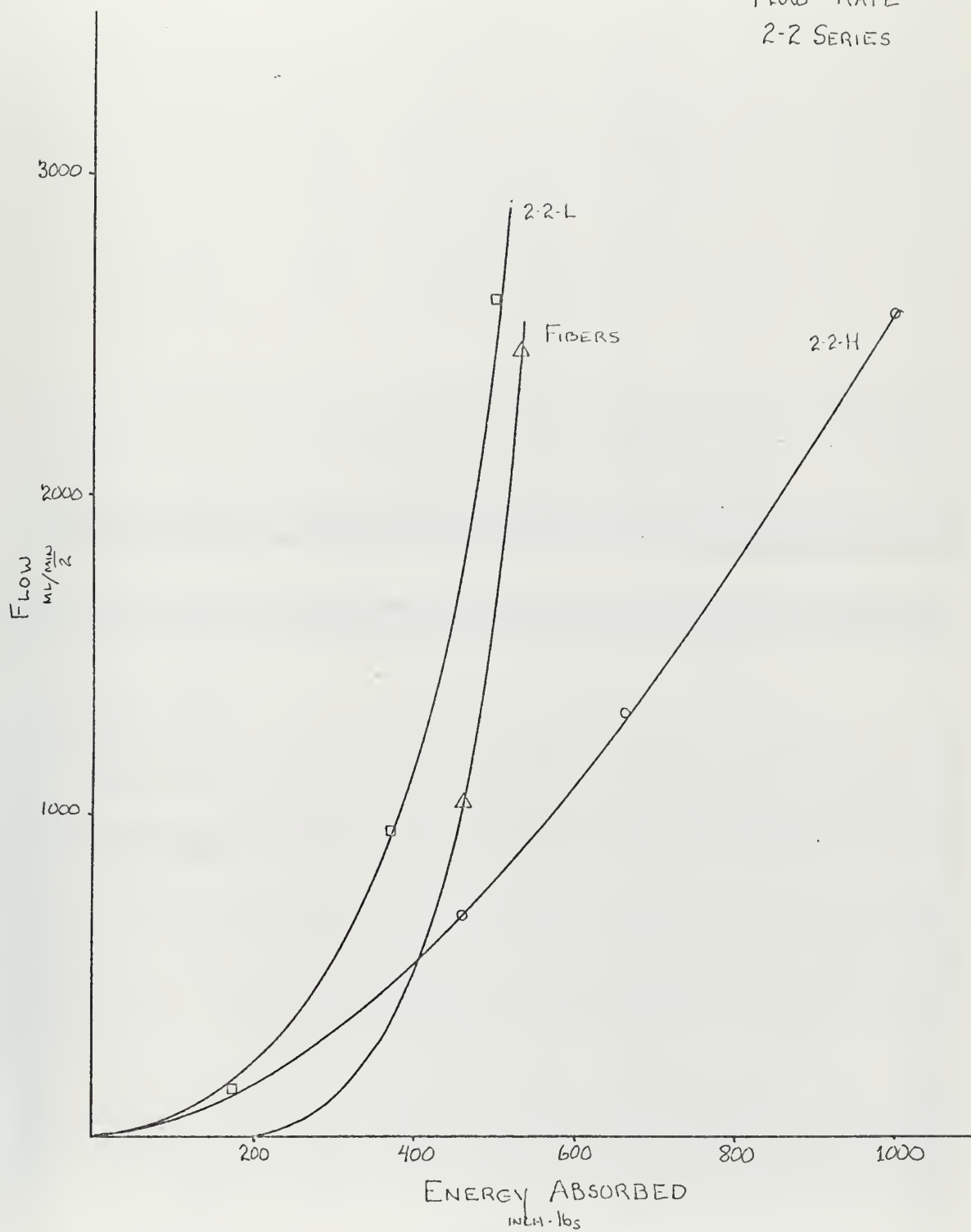


FIGURE 18



G-O-H

4-1-H



2-2-H

6-0-M





4-1-M

2-2-M



6-6-1

4-1-1



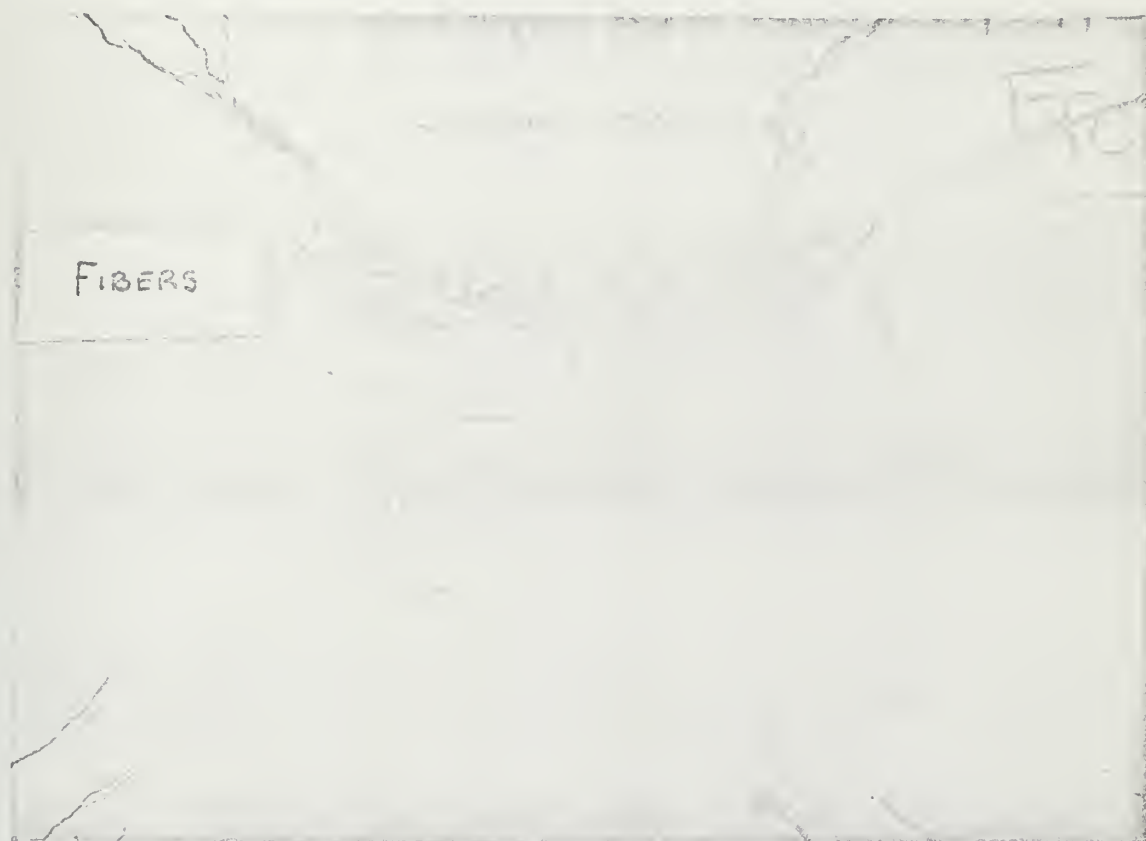
2-2-L



0-3-L











APPENDIX C



0.25" x 0.25" woven mesh	Ultimate Stress	Apparent Modulus	Average Apparent Modulus
High series	163,000	19.06 x 10 <sup>6</sup>	19.3 x 10 <sup>6</sup>
(ungalvanized)	159,500	19.6 x 10 <sup>6</sup>	
X Series	130,000	21.8 x 10 <sup>6</sup>	19.0 x 10 <sup>6</sup>
(galvanized)	126,500	19.3 x 10 <sup>6</sup>	
	134,000	16.8 x 10 <sup>6</sup>	
	127,000	17.9 x 10 <sup>6</sup>	
Medium series	119,500	17.8 x 10 <sup>6</sup>	17.4 x 10 <sup>6</sup>
(galvanized)	119,000	17.7 x 10 <sup>6</sup>	
	118,740	17.25 x 10 <sup>6</sup>	
Low series	56,900	7.72 x 10 <sup>6</sup>	7.3 x 10 <sup>6</sup>
(ungalvanized)	56,300	6.9 x 10 <sup>6</sup>	

1.0" x 1.0"  
welded mesh

Low series	57,700	19.35 x 10 <sup>6</sup>	20.8 x 10 <sup>6</sup>
	57,900	22.3 x 10 <sup>6</sup>	
	57,500	14.1 x 10 <sup>6</sup>	

0.016"  
fibers

low carbon

131,000

47

L/D

TABLE I



LOAD DEFLECTION  
CURVES

SERIES H WIRE MESH

9 WIRES

2" LENGTH

LOAD RATE 0.05"/MIN

184

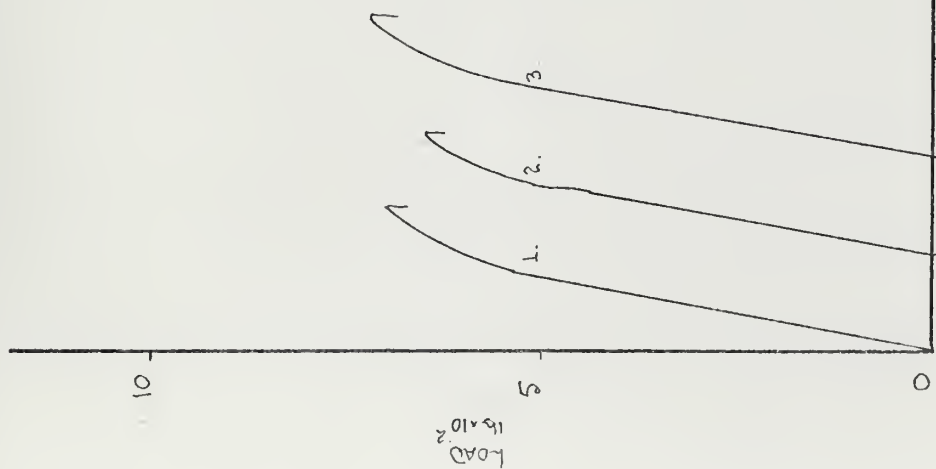


CHART DEFLECTION

$L_{WIRE} = 1 \text{ INCH}$

TO GET TRUE DEFLECTION, MULTIPLY BY  $1.25 \times 10^{-4}$

FIGURE 1



LOAD-DEFLECTION

CURVES

SERIES M WIRE MESH

9 WIRES

2" LENGTH

LOAD RATE 0.05"/min

185

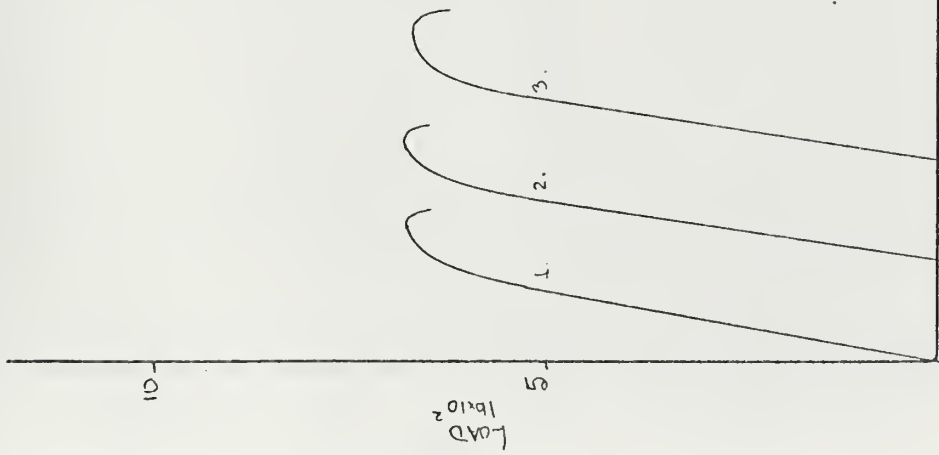


CHART DEFLECTION

1" = 1"

TO GET TRUE DEFLECTION, MULTIPLY BY  $1.25 \times 10^{-4}$

FIGURE 2





# LOAD-DEFLECTION

## CURVE

SERIES L WIRE MESH

9 WIRES

2" LENGTH

LOAD RATE 0.05"/min

186

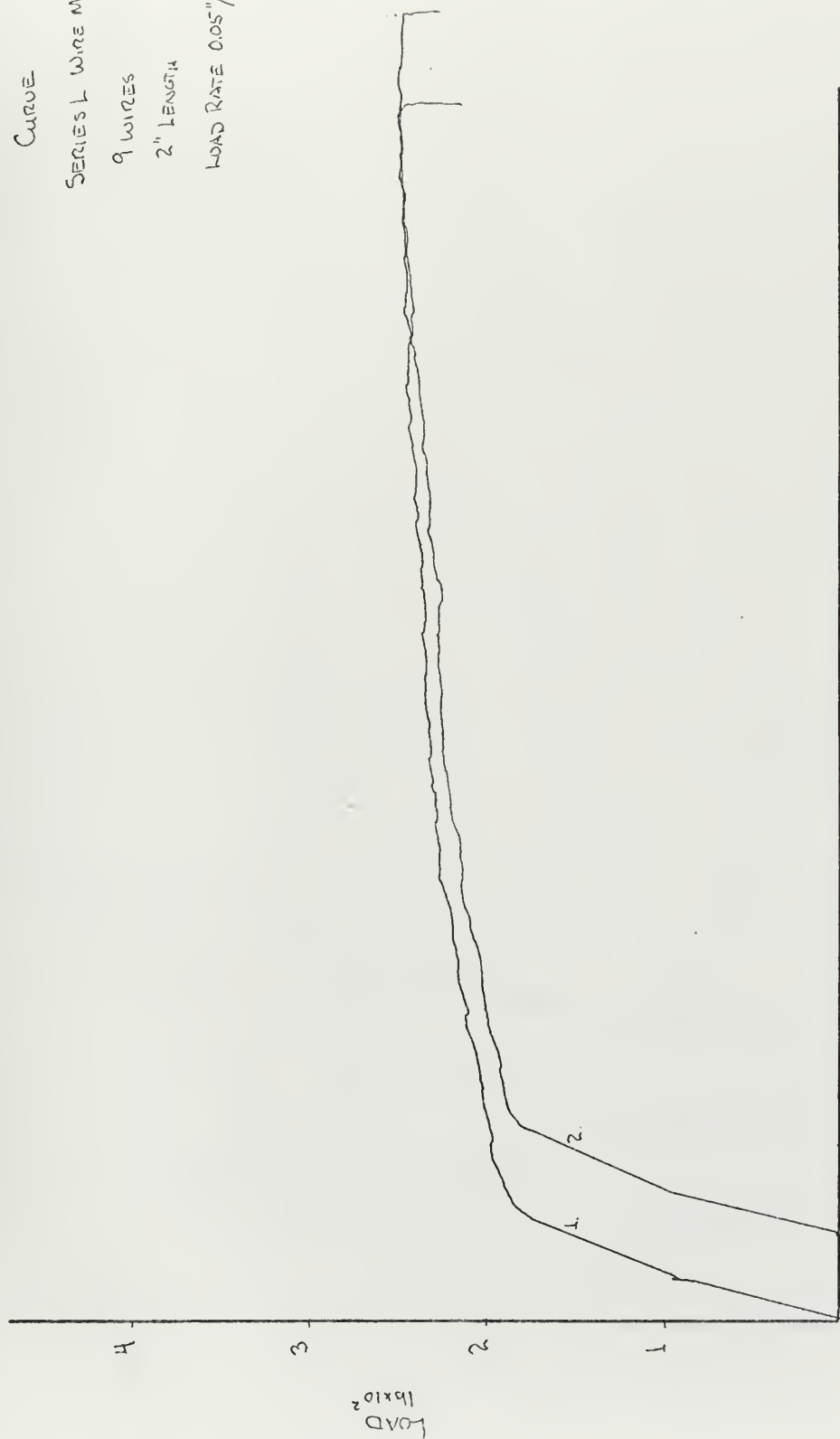


CHART DEFLECTION

1 INCH = 1 INCH

TO GET TRUE DEFLECTION, MULTIPLY BY  $1.25 \times 10^{-4}$

FIGURE 3



# LOAD DEFLECTION CURVES

SERIES X WIRE MESH

1. & 2. 11 WIRES

3 & 4. 10 WIRES

2" LENGTH

LOAD RATE 0.05"/MIN

187

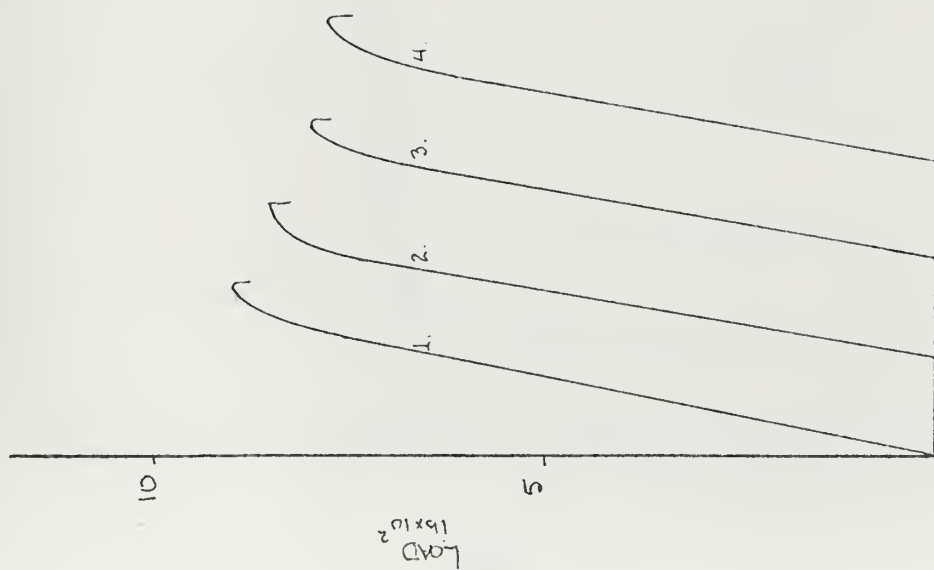


CHART DEFLECTION  
1" = 1"

TO GET TRUE DEFLECTION, MULTIPLY BY  $1.25 \times 10^{-4}$

FIGURE 4



LOAD-DEFLECTION  
CURVES  
1.0" x 1.0" WELDED MESH  
1 WIRE  
2" LENGTH  
LOAD RATE .1"/min



CHART DEFLECTION  
1" = 1"

TO GET TRUE DEFLECTION, MULTIPLY BY  $1.25 \times 10^{-4}$

FIGURE 5



APPENDIX D





190

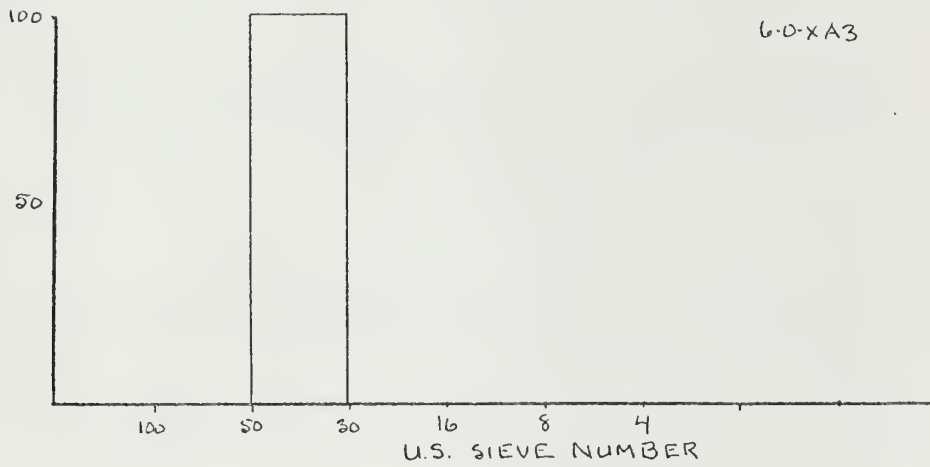
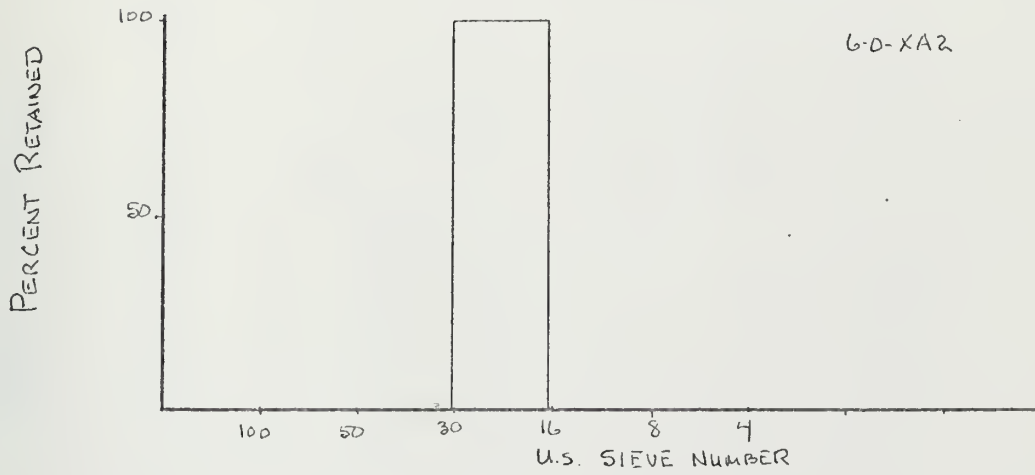
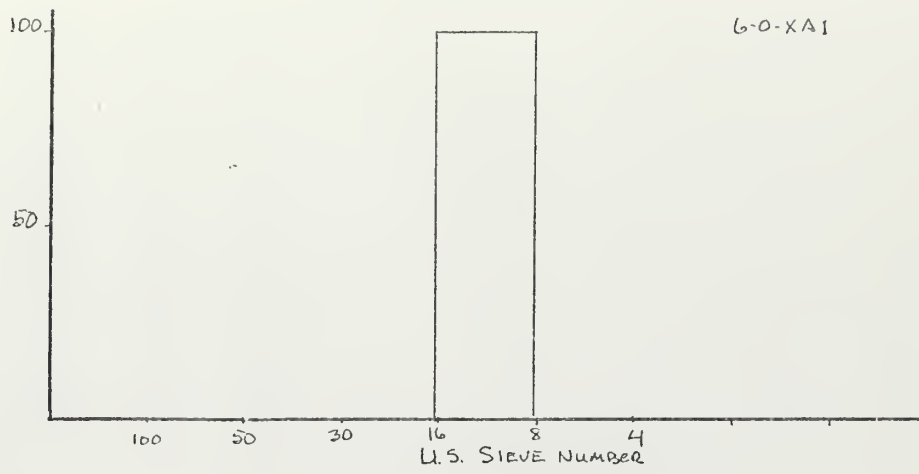


FIGURE 1 SAND GRADING CHART



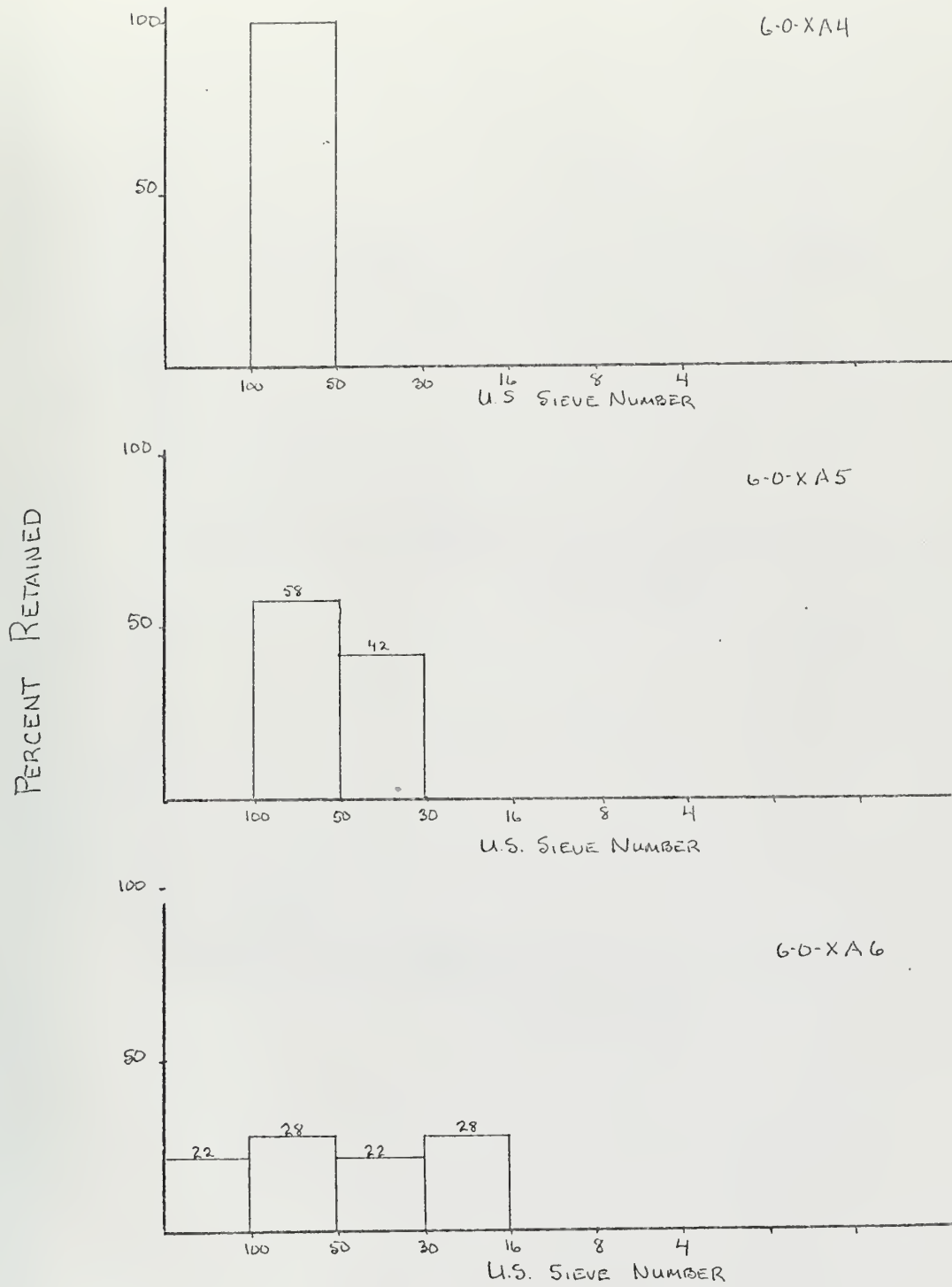


FIGURE 2 SAND GRADING CHART



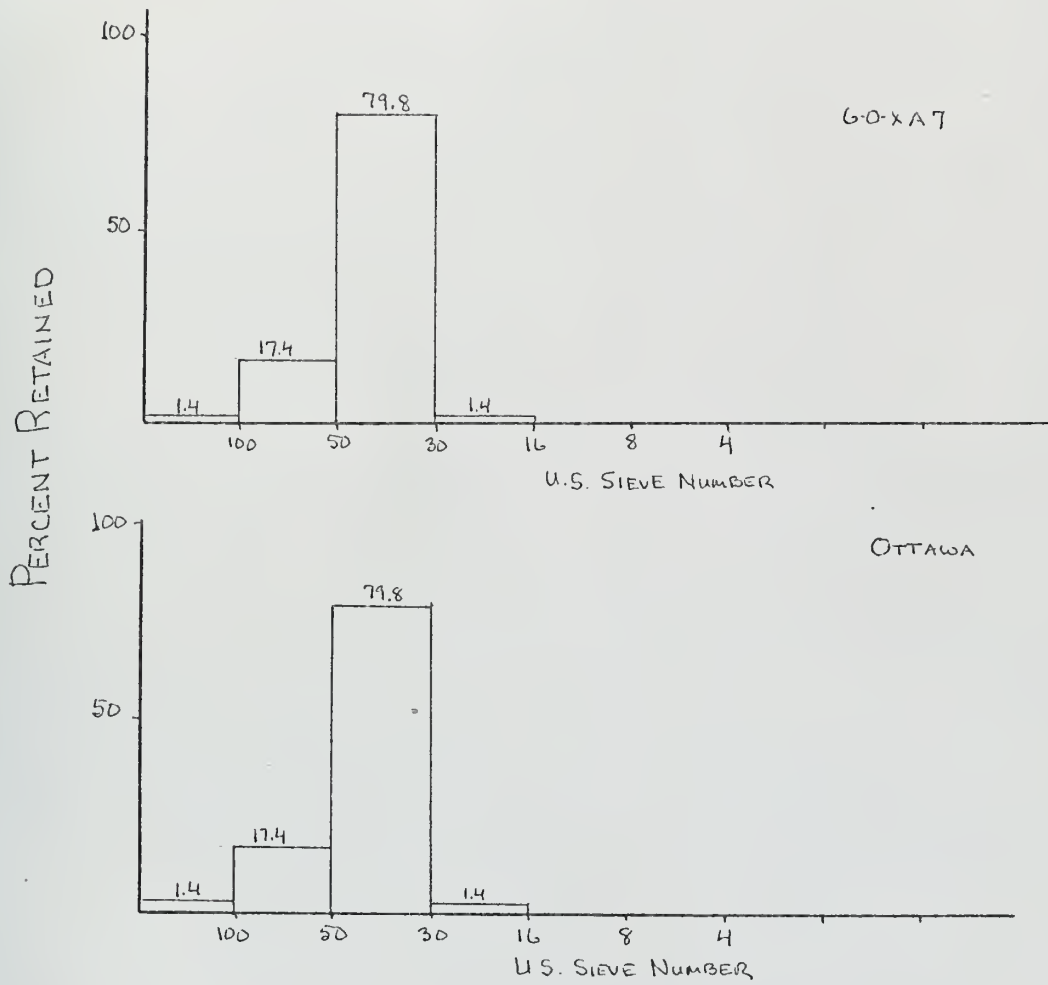


FIGURE 3 SAND GRADING CHART



11 DEC 73

21488

Thesis  
K396

Key

118516

Impact resistance of  
ferro-cement plates.

10 SEP 70  
11 DEC 73

DISPLAY  
21488

Thesis  
K396

Key

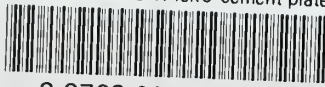
118516

Impact resistance of  
ferro-cement plates.



thesK396

Impact resistance of ferro-cement plates



3 2768 001 03227 9

DUDLEY KNOX LIBRARY